DASA-RSS3318

R621

Technical Report

STRENGTH AND BEHAVIOR OF RESTRAINED REINFORCED CONCRETE SLABS UNDER STATIC AND DYNAMIC LOADINGS

April 1969

Sponsored by
DEFENSE ATOMIC SUPPORT AGENCY

NAVAL CIVIL ENGINEERING LABORATORY
Port Hueneme, California

STRENGTH AND BEHAVIOR OF RESTRAINED REINFORCED CONCRETE SLABS UNDER STATIC AND DYNAMIC LOADINGS

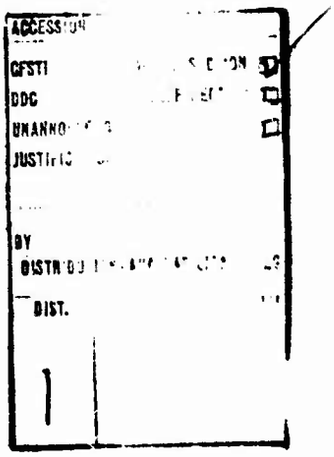

Technical Report R-621

Y-F008-08-02-123, DASA-RSS3318

by

W. A. Keenan

ABSTRACT

Results are reported for a theoretical and experimental study of the resistance and behavior of reinforced concrete slabs under static and dynamic loadings. The scope is restricted to square slabs, clamped and longitudinally restrained along all edges, under uniform lateral pressure. The study deals with the entire range of behavior from elastic through tensile membrane action. The experimental tests are limited to long-duration dynamic loads, but the theory considers very short durations.

The experimental study involved nine reinforced concrete slabs loaded in the NCEL slab loader: six under a uniform static pressure, and three under dynamic loads of long duration. The clear span of each slab was 72 inches; the span-to-thickness ratios were 12.0, 15.2, and 24. Steel reinforcement ranged from zero to 1.33%. Arrangement of reinforcement was identical in each face except for one slab which had only positive steel along the edges and over the unloaded surface.

In all slabs, tension cracks first became visible at a resistance corresponding to over 70% of Johansen's yield line resistance. The slabs failed initially in a flexural mode, followed by total collapse at a much greater deflection. Collapse corresponded to rupture of reinforcement in tension, large cracks on the unloaded face, and disintegration of concrete along the edges and diagonals of the slab. In the case of dynamic loading, collapse included tearing portions of the slab from its support and/or blasting blocks of concrete free from the reinforcing mesh. The thinner slabs deflected more than 2.5 times their thickness under both static and dynamic loading.

The theoretical study deals with a square slab, restrained against rotation and longitudinal movement at the edges. The study covers the static resistance at various stages of behavior, failure criteria, size and extent of missile fragments from dynamic loads, and design recommendations. An analytical method is

developed to predict the static resistance, deflection, and longitudinal restraining thrust at ultimate failure. The method considers a plane quadrant of an assumed collapse mechanism and uses equilibrium of forces, compatibility of deformations, and the stress-strain characteristics of the steel and concrete. A parametric study of longitudinally restrained slabs is presented using this method. The results show the effects of the reinforcing index, arrangement of steel, ultimate concrete strain and concrete strength on the resistance, deflection, and membrane forces at ultimate flexural failure for variations in the span-thickness ratio.

It was found that the resistance and behavior of longitudinally restrained square slabs are predictable and that such a slab, if properly designed, can resist dynamic loads effectively and more economically than a similar slab with no longitudinal edge restraint.

CONTENTS

INTRODUCTION

Objectives

The major objectives of this study are (1) to develop design criteria for the resistance and deflection of slabs with boundary conditions which induce significant membrane forces, and (2) to extend knowledge of the response of slabs under dynamic load.

Scope

A theory is presented for the static ultimate flexural resistance and corresponding center deflection of longitudinally restrained square slabs. The theory is followed by the results of experimental tests of slabs under static and dynamic uniform pressure. Both the theory and tests are limited to uniformly loaded square slabs, clamped and longitudinally restrained along all edges.

The theory takes into account the compressive membrane forces induced in a slab by full or partial longitudinal restraint at the edges. The various parameters included span-thickness ratio, reinforcement ratio, ultimate strength and crushing strain of the concrete, yield strength of reinforcement, and amount of longitudinal movement at the edges of the slab.

The experimental tests involved nine reinforced concrete slabs loaded in the NCEL slab loader: six slabs under a uniform static pressure, and three under dynamic pressures of long duration. The loaded area of all slabs was 72 inches square with all edges clamped and longitudinally restrained. The major parameters varied in the tests were span-thickness ratio (12 to 24), reinforcement ratio (0 to 1.33%), and type of loading (static versus dynamic pressure). An orthogonal arrangement of reinforcement was identical in each face except for one slab which had only positive steel along the edges and over the loaded surface. One slab had no reinforcement. Measurements included transverse load, deflections at the sixth point and center, steel and concrete strains at the edges and center, and midspan acceleration (dynamic tests).

Background

The approach to blast-resistant design of reinforced concrete slabs is to design the slab so that the maximum deflection under the blast load is less than some specified limit deflection. In this approach the designer needs to know (1) the *flexural resistance* of slabs, (2) the *acceptable limit deflection* of slabs, and (3) the *response* of slabs under dynamic loads. Several investigators have studied the flexural resistance of reinforced concrete slabs under static loading.[1-5] These studies show that the simple yield line theory[2] gives a conservative estimate of the ultimate flexural resistance even though the theory is considered an upper-bound solution. The degree of conservatism was found to depend upon the boundary conditions of the slab. For example, Johansen[2] found the theory is especially good for slabs with boundary conditions which allow a collapse mechanism to form in which membrane forces are insignificant. However, Wood,[4] Park,[5] MIT,[6] and others found that the theory grossly underestimates the flexural resistance of slabs with boundary conditions which induce significant compressive membrane forces. Such forces develop in slabs restrained at their edges against longitudinal movement. Sufficient restraint is often provided by surrounding panels or stiff walls and by support friction in the case of simply supported slabs with span-depth ratios less than about five.[7] Thus, the yield line theory is a safe practical method for predicting the ultimate flexural resistance of longitudinally unrestrained slabs but is too conservative for longitudinally restrained slabs.

A design method is needed which takes advantage of the additional flexural resistance inherent in slabs with boundary conditions which induce significant membrane forces. The need is especially important in the design of slabs to resist long-duration dynamic loads. For this type of loading, resistance is much more important than ductility; increasing resistance will increase the dynamic load capacity of a slab much more than if, instead, the ductility of the slab were increased by the same percentage. Equally important, compressive membrane forces can significantly enhance the shear resistance of the slab cross section. For very high overpressure levels there is a practical limit as to how much shear steel can be placed in a slab. This might be solved by designing boundary conditions which induce membrane forces. In fact, the high values of $v/\sqrt{f'_c}$ reported for static loads on deep slabs[7] may be caused by compressive membrane forces induced in the slab by friction at the supports.

There is a lack of information on the acceptable limit deflection of slabs. Knowledge of the limit deflection is particularly important for the case of very-short-duration dynamic loads where total strain energy capacity of the slab determines the dynamic load capacity. Generally, this limiting

deflection corresponds to failure criteria associated with a stage of behavior such as inelastic behavior, loss of airtight integrity of the slab, emission of concrete missile fragments, or imminent collapse. Experimental data is needed to establish criteria to aid the designer in selecting an acceptable limiting deflection for any of these failure criteria.

Having defined the resistance function for a slab, the designer needs to know the response of the slab under dynamic loads. Several investigators[8] have developed procedures for predicting the response of slabs, but the accuracy of these procedures has not been confirmed by experimental tests. A few dynamic tests have been conducted recently.[9] In an earlier investigation, a limited number of small-scale slabs were tested but the results are misleading and inconclusive; the machines used to apply the dynamic loads were not capable of applying the load fast enough relative to the fundamental period of vibration of the slabs to cause a true dynamic response. Consequently, the slabs "saw" the load simply as a fast "static" load. Therefore, for the study reported herein, a special testing device was built to determine the true dynamic response of slabs.

THEORETICAL STUDY OF LONGITUDINALLY RESTRAINED SLAB

The yield line theory accredited to A. Ingerslev[10] and extended by K. W. Johansen,[2] is a method for predicting the ultimate flexural resistance of reinforced concrete slabs. The theory assumes that an increasing static load on a slab causes a concentration of strain in the reinforcing steel and concrete along lines of maximum moment. These lines, referred to as yield lines, form and spread into a pattern which divides the slab into segments. Near failure, the elastic deformations of each segment are assumed negligible with respect to the plastic deformations at the yield lines. Consequently, all curvatures in the slab at failure are assumed to be concentrated at the yield lines. These lines are the axis of rotation for the movements of each segment. Each segment is assumed to be a plane surface. The slab segments deflect to form a collapse mechanism.

For a given collapse mechanism, the resistance of the slab can be calculated by considering the equilibrium of an individual segment of the mechanism. The segment must be in equilibrium under the applied static load, the shear along the support line, and the resisting forces along each yield line. In other words, ***the ultimate flexural resistance is limited by the forces which the cross section along each yield line can resist before material failure of the section.***

The actual forces acting on the cross section along the yield lines depend upon the boundary conditions of the slab. For example, if the edges of the slab are free to translate, moment, but not in-plane thrust, develops along the hinge lines. However, if the edges are restrained against longitudinal movement, both thrust *and* moment act on sections along the yield lines. These thrust forces affect the equilibrium of the segment. More importantly, these thrust forces significantly increase the moment resistance of the slab cross section which in turn significantly increases the ultimate flexural resistance of the slab. The exact increase depends upon (1) *the magnitude of the thrust* and (2) *the interaction between the thrust and moment resistance of the reinforced concrete section.* A failure interaction diagram[11] is a convenient way to describe this interaction.

Failure Interaction Diagram

A failure interaction diagram[11] is an envelope curve of all combinations of thrust and moment which constitute material failure of a given reinforced concrete section. Material failure is generally defined by an extreme fiber strain in the concrete equal to some preselected limiting strain. In other words, the envelope curve shows the effects of in-plane thrust forces in a slab on the ultimate moment resistance of sections along the hinge lines. An idealized interaction diagram is shown in Figure 1.

A failure interaction diagram is constructed by first assuming a stress-strain relationship for the reinforcement and concrete. In this report, the assumed stress-strain relationship for the reinforcement is the idealized curve shown in Figure 2. The properties of both tension and compression steel are assumed to be identical under tensile and compressive stresses. The elastic and plastic range of behavior are idealized by two straight lines. The strain hardening range of behavior is neglected.

The stress-strain relationship assumed for the concrete in compression is shown in Figure 3. The concrete is assumed to have no tensile strength. The diagram is that derived by Hognestad[12] from tests on short plain concrete columns subject to combined bending and axial load. The concrete is assumed to carry compressive stress out to ϵ_u, the crushing strain. This is the value of strain at the extreme fiber of all hinge sections corresponding to initial formation of the collapse mechanism. The modulus of elasticity of the concrete is the value recommended by the ACI Building Code.[13]

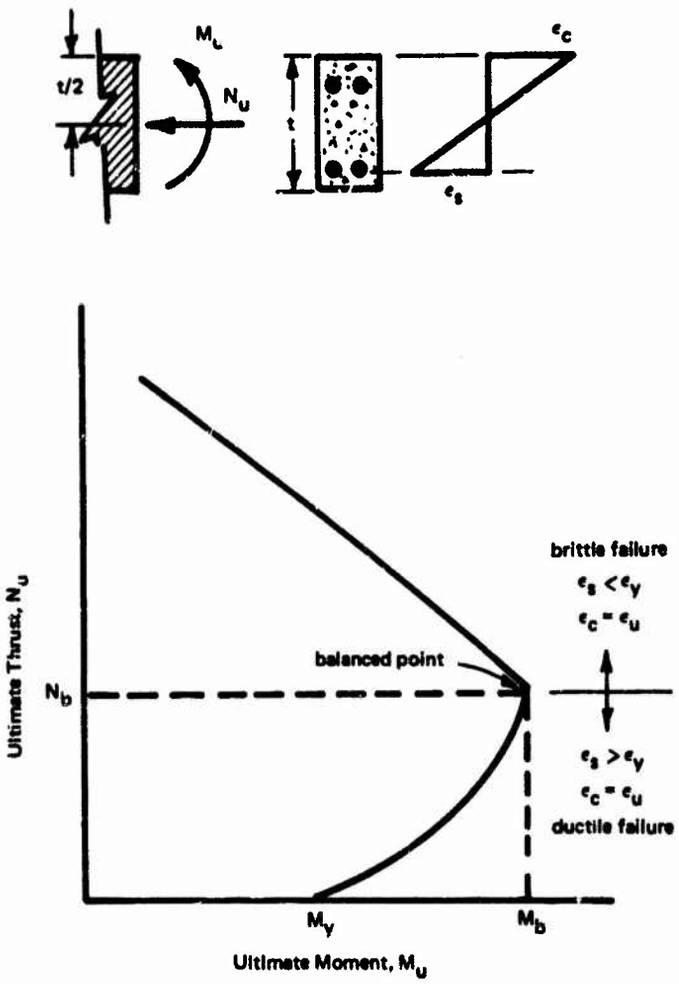

Figure 1. Idealized failure interaction diagram for a reinforced concrete section.

After material properties have been defined, the coordinates (M_u, N_u) on the interaction diagram are calculated by assuming a compatible linear strain distribution over the depth of the section. For an assumed strain distribution, the corresponding forces in the reinforcement and stress block for the concrete are calculated using Figures 2 and 3, respectively. Finally, the thrust, N_u, and moment, M_u, are computed for static equilibrium of the section. In this report, all moments are related to mid-thickness (t/2) of the section, not to the plastic centroid. The advantage of this procedure later becomes evident when thrust is considered in the equilibrium of a slab segment. This process of assuming various compatible strain distributions and computing M_u and N_u is continued until enough points have been calculated to define the failure envelope curve.

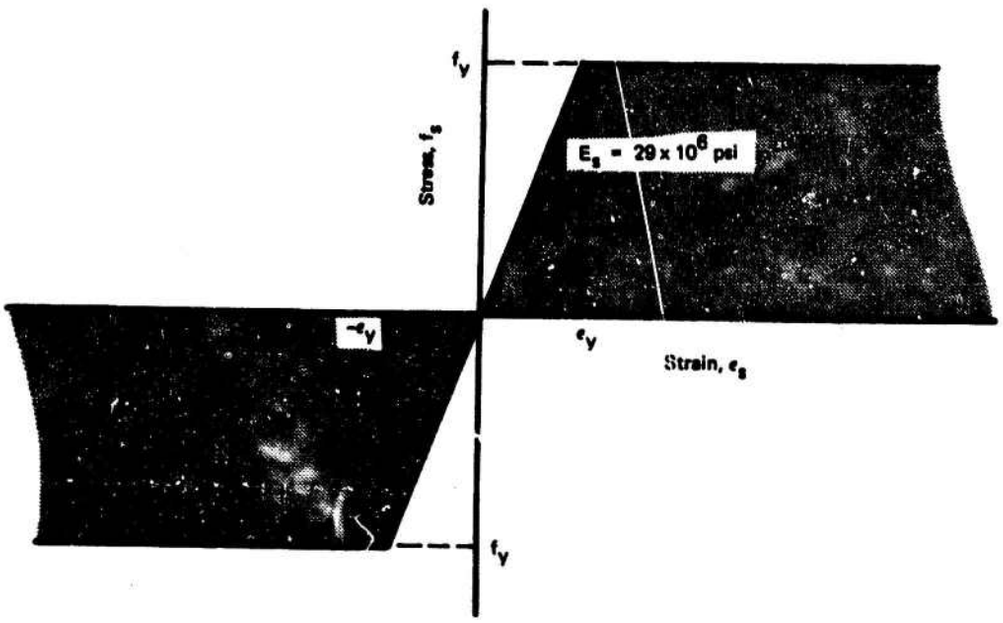

Figure 2. Idealized stress-strain relationship for steel.

The point on the failure envelope curve corresponding to a sharp break in the curve (Figure 1) is referred to as the balanced point. This point represents the combination of thrust, N_b, herein referred to as the balanced thrust, and balanced moment, M_b; acting together these produce simultaneously crushing of the concrete at the extreme fiber and yielding of the tension reinforcement. If the membrane thrust on a section along a hinge line of the slab is less than the balanced thrust, the tension steel yields before the concrete crushes. Such a failure is characterized by considerable rotation capacity (ductility) of the section. The rotation capacity is generally sufficient to assure complete formation of a flexural collapse mechanism. If N_u at failure of the section is greater than N_b, crushing of the concrete precedes yielding of the tension reinforcement. Such failures are generally characterized by a sudden, brittle type of failure with limited rotation capacity of the section. The collapse mechanism may form suddenly or only partially with excessive disintegration of concrete along the hinge lines followed by a sudden drop in load-carrying capacity. Equally important, the disintegrated concrete is a source of concrete missile fragments under dynamic loading. This subject is treated at greater length in the section entitled *Concrete Missile Fragments.*

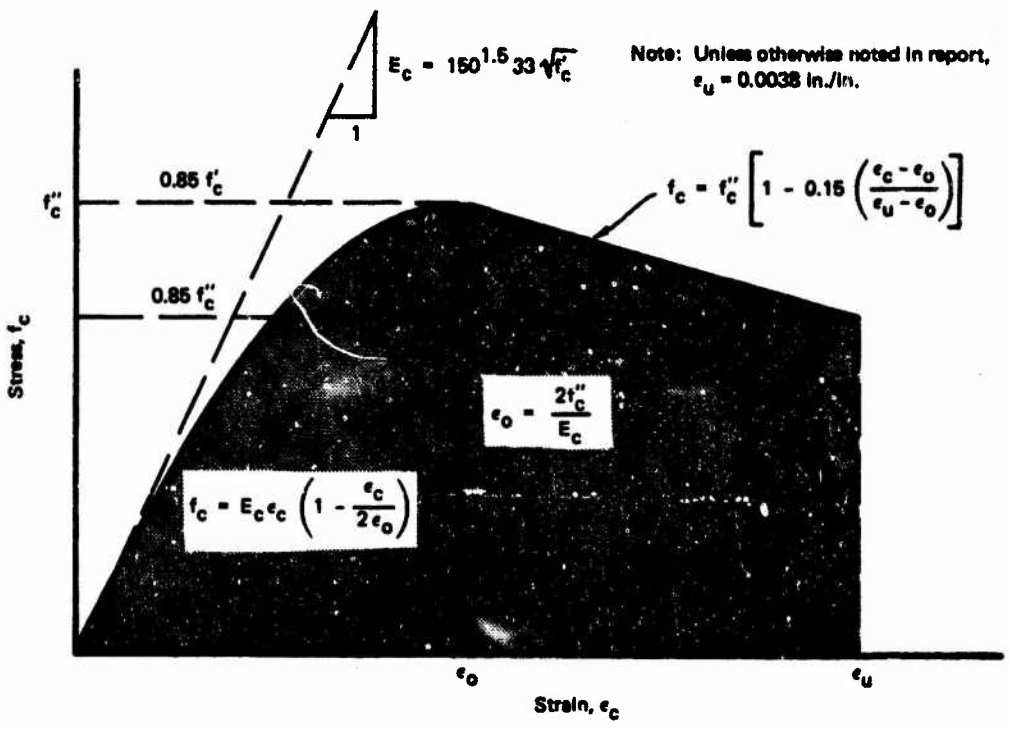

Figure 3. Idealized stress-strain relationship for concrete.

The effect of the crushing strain of the concrete, ϵ_u, on the shape of the failure envelope is shown in Figure 4. Note that the envelope curve is almost unaffected by the crushing strain of the concrete except for thrusts near the balance point. ***The balanced thrust, N_b, increases with the limiting strain capacity of the concrete.*** The ultimate moment resistance of the section is essentially unaffected by the limiting concrete strain for any thrust less than about 80% of the balanced thrust corresponding to $\epsilon_u = 0.0038$.

The effects of steel percentage on the shape of the interaction curve are shown in Figures 5a and 5b. For a section with equal amounts of tension and compression steel, an increase of steel percentage does not change the balanced thrust but does increase the moment resistance of the section. However, for a section with no compression steel, increasing the steel percentage decreases the balanced thrust (Figure 5a). At a steel percentage, p_b, corresponding to the balanced steel percentage, $N_b = 0$. For this case, any amount of compressive thrust induced in the slab will produce a brittle failure at sections along the hinge lines.

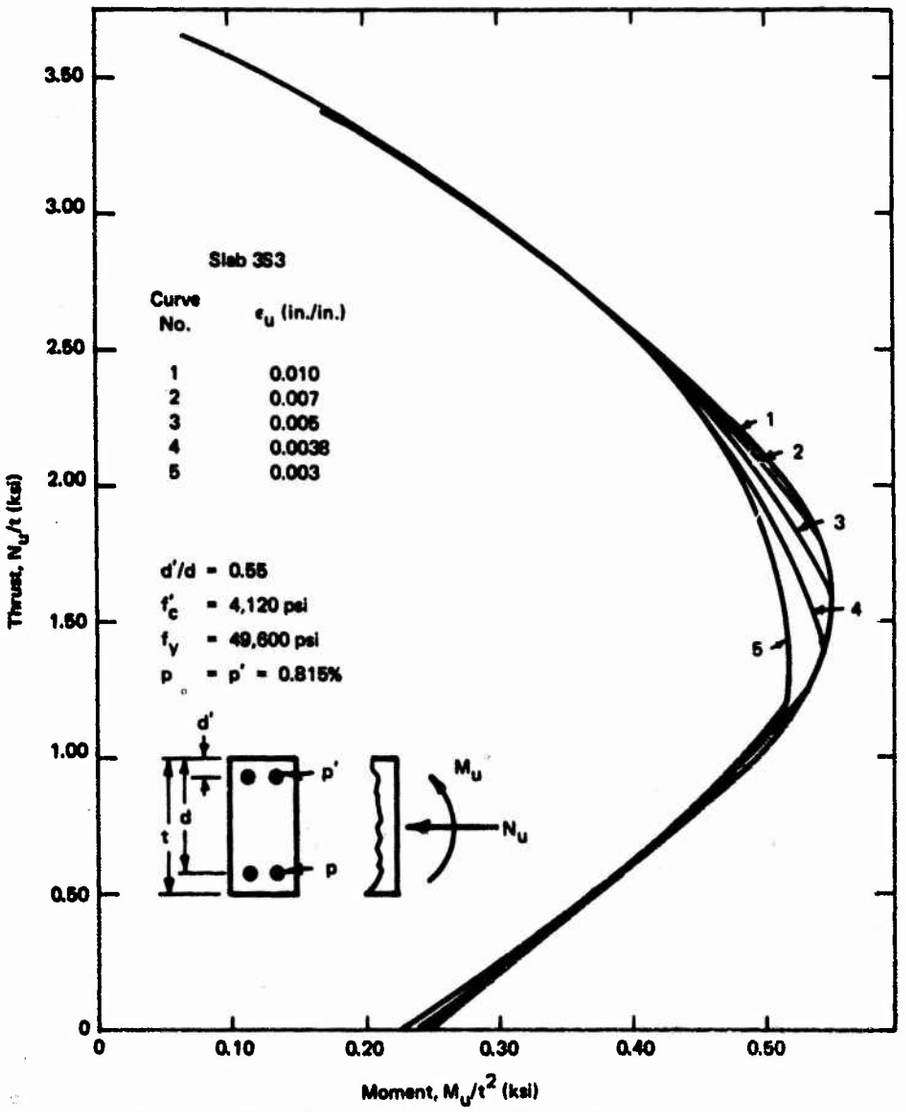

Figure 4. Effect of ultimate concrete strain on shape of interaction curve.

In summary, the properties of the slab cross section should be proportioned to assure that the maximum in-plane thrust induced by longitudinal edge restraint is less than N_b in order to (1) prevent a sudden brittle type of failure; (2) minimize a source of concrete missile fragments; and (3) guarantee that sections along the yield lines have sufficient rotation capacity to develop fully the flexural collapse mechanism. How the section should be proportioned, of course, depends upon the magnitude of the thrust induced in the longitudinally restrained slab when the collapse mechanism forms. This is the topic of the next section.

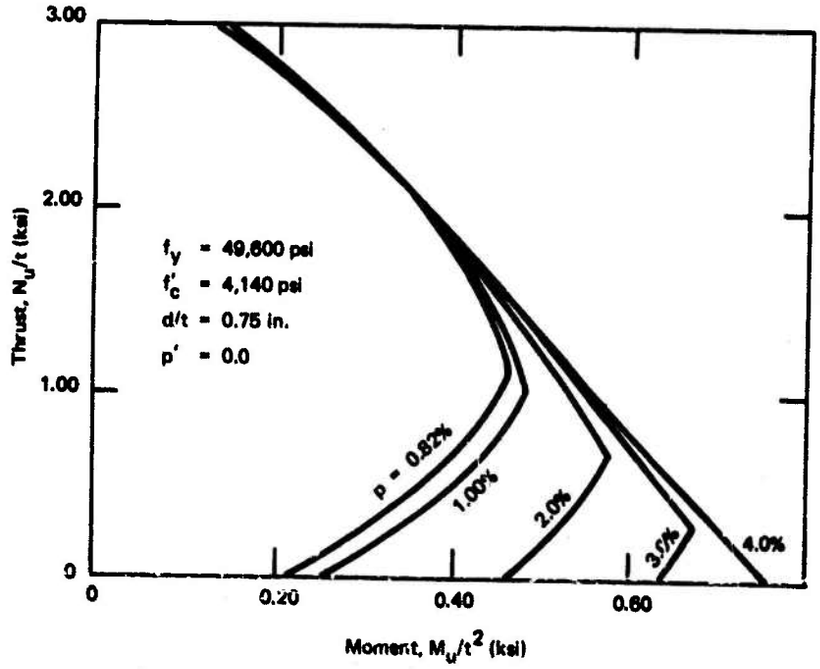

Figure 5a. Effect of tensile steel percentage on shape of interaction diagram for section without compression steel.

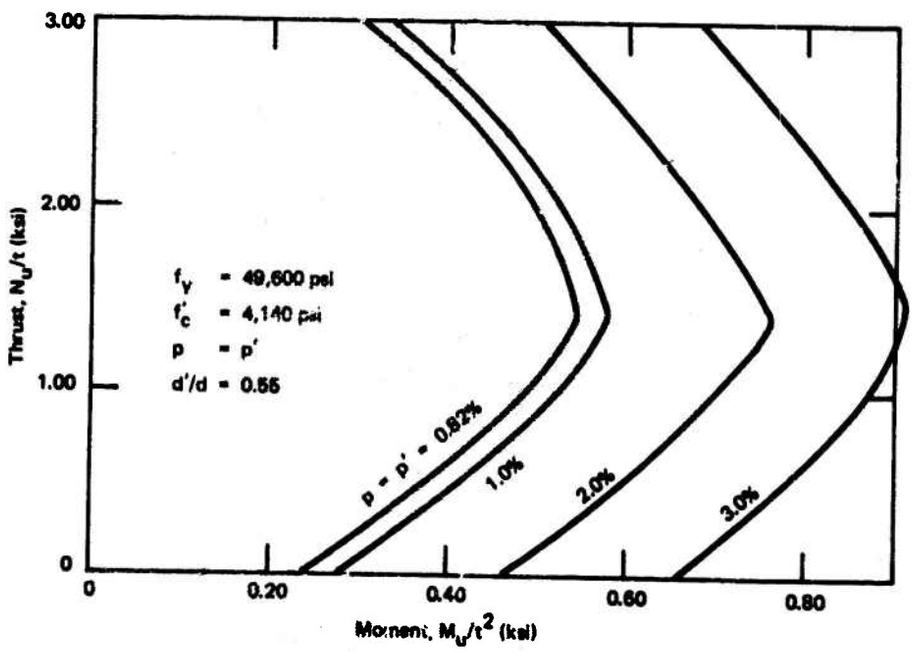

Figure 5b. Effect of equal amounts of tensile and compression steel on shape of interaction diagram.

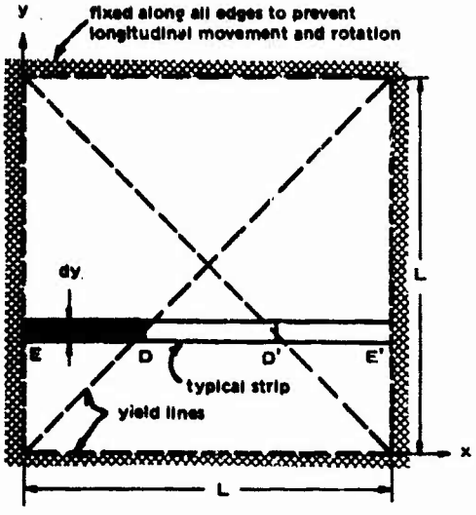

Figure 6. Plan view of collapse mechanism for square slab.

Ultimate Thrust

A clamped slab with edges restrained against longitudinal movement is considered subject to a uniform static load, q_u, in Figure 6. A yield line pattern or collapse mechanism has formed which divides the slab into four equal quadrants. Each quadrant of the mechanism is assumed to be a *plane surface*. This assumption requires the yield lines between quadrants to be straight lines which extend into the corners of the slab; i.e., corner fans are neglected. The yield line pattern for such a slab is illustrated by the heavy dashed lines in Figure 6.

The slab mechanism is assumed to be composed of strips oriented in the x and y directions (Figure 6). A strip in either direction has the same thickness as the slab and contains only the steel in that direction. Park[5] refers to the slab composed of such strips as the "equivalent slab." The yield sections of the strips are at right angles to the direction of the strip, and the torsional moments acting on these sections are assumed equal to zero.

The static load capacity or static ultimate resistance can now be expressed as the sum of the load carried by each individual strip. Each strip load, in turn, can be expressed in terms of the deflection, strains, and section properties of the strip by considering the stress-strain properties of the concrete and steel, equilibrium of forces, and geometric restraints.

Consider the typical strip, EDD'E', with plastic hinges *just* formed at sections E, D, D', and E' (Figure 6). The deflected shape of the strip is shown in Figure 7. Assume the strip is rigid with all axial and flexural strains concentrated at sections E, D, D', and E'. Under a vertical deflection, u, of the center portion of the strip, DD', the concrete *begins* to crush simultaneously at all hinge sections.

The forces acting on strip ED at this stage of behavior are shown in Figure 8. In addition to moment, membrane or in-plane thrust forces are induced by full or partial restraint at the ends of the strip against in-plane movement. Considering the equilibrium of horizontal forces acting on the strip ED

$$N_{ud} = N_{ue} = N_u$$

The subscripts d and e refer to sections of the strip at the diagonal and the edge of the slab, respectively. The subscript u refers to the ultimate stage of behavior; i.e., initial crushing of the extreme fiber of the concrete at each hinge section.

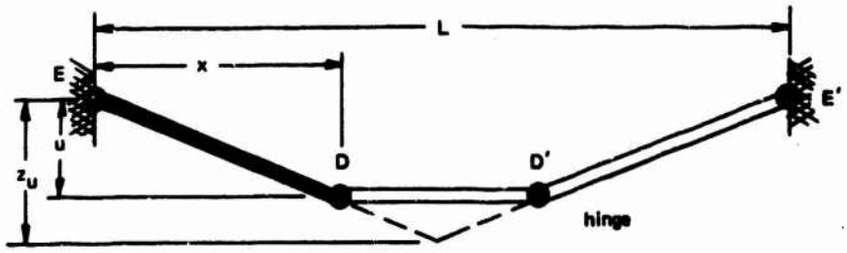

Figure 7. Deflected shape of typical strip.

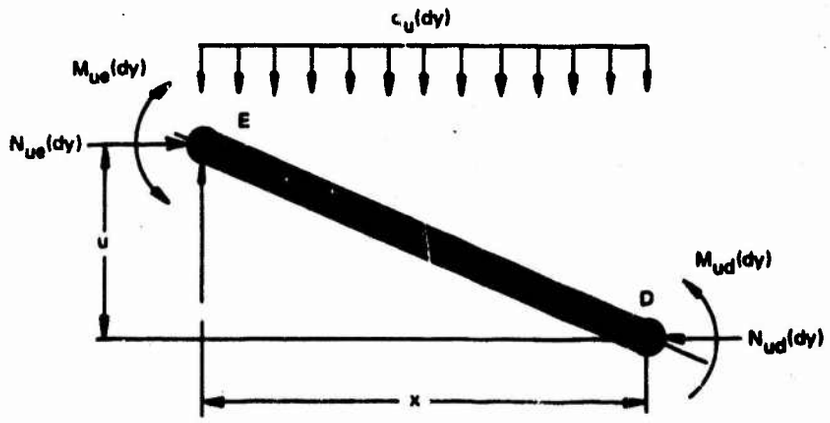

Figure 8. Forces on strip E D.

The lateral restraining forces, N_{ud} and N_{ue}, depend on the state of strain and properties of the cross section at points D and E. It is assumed that the strain on these sections varies linearly through the depth of the section; plane sections before bending are assumed to remain plane after bending. Such a strain distribution is shown on sections D and E in Figures 9 and 10, respectively. The strain at the extreme fiber of the

concrete is assumed equal to ϵ_u, the crushing strain of the concrete. Assume the crushing strain is reached simultaneously at sections D and E. The resulting stress distributions based on the assumed stress-strain relationships for the steel (Figure 2) and concrete (Figure 3) are also shown. Considering the horizontal equilibrium of forces in Figure 9, the thrust on section D required to initiate crushing of the concrete in terms of the stresses and properties of the cross section, is

$$N_{ud} = k_1 f''_c c_d - p_d d_d f_{sd} + p'_d d_d f'_{sd}$$

$$\frac{N_{ud}}{t f''_c} = \frac{k_1 c_d}{t} - \left(\frac{p_d f_{sd} - p'_d f'_{sd}}{f''_c} \right) \frac{d_d}{t}$$

or

$$\frac{N_{ud}}{t f''_c} = \frac{k_1 c_d}{t} - \bar{q}_d \left(\frac{d_d}{t} \right) \tag{1}$$

where

$$\bar{q}_d = \left(\frac{p_d f_{sd} - p'_d f'_{sd}}{f''_c} \right) \tag{1a}$$

Similarly, the thrust on the section E required to initiate crushing of the concrete is

$$\frac{N_{ue}}{t f''_c} = \frac{k_1 c_e}{t} - \bar{q}_e \left(\frac{d_e}{t} \right) \tag{2}$$

where

$$\bar{q}_e = \left(\frac{p_e f_{se} - p'_e f'_{se}}{f''_c} \right) \tag{2a}$$

Portion ED of the typical strip EDD'E' is enlarged in Figure 11 to relate the depths to the neutral axis, c_e and c_d, to the geometry of the strip under the vertical deflection, u. This deflection results from the rigid body displacement of the plane quadrant of the collapse mechanism containing strip ED. The strip geometry is similar to that assumed by Park[5] for similar analysis.

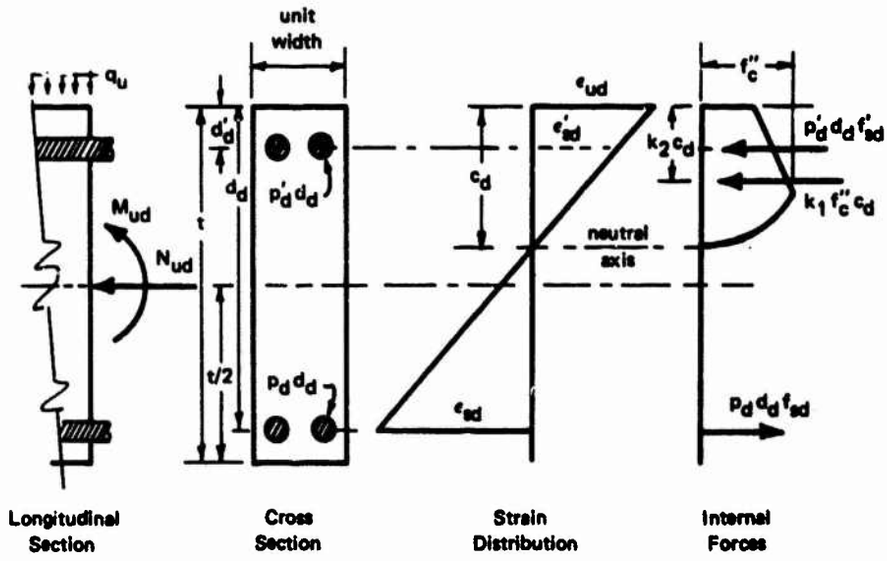

Figure 9. Conditions at section D of strip ED.

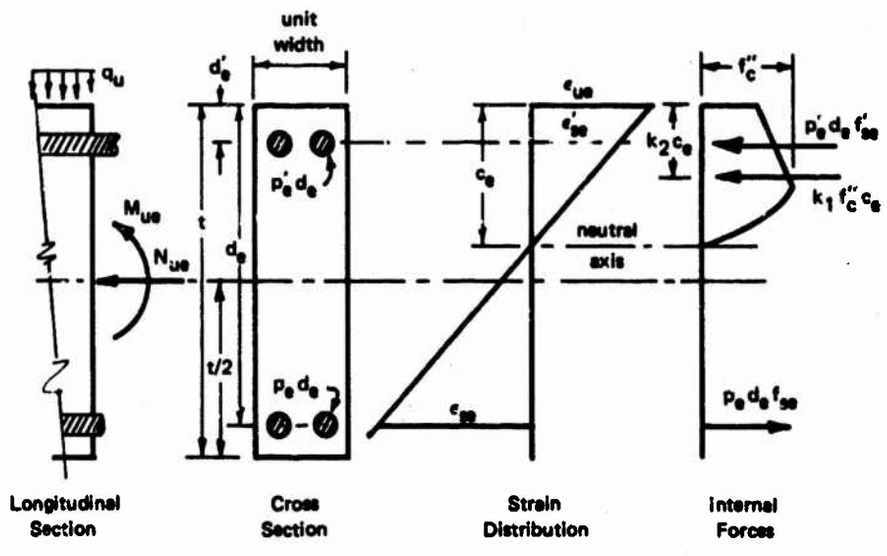

Figure 10. Conditions at section E of strip ED.

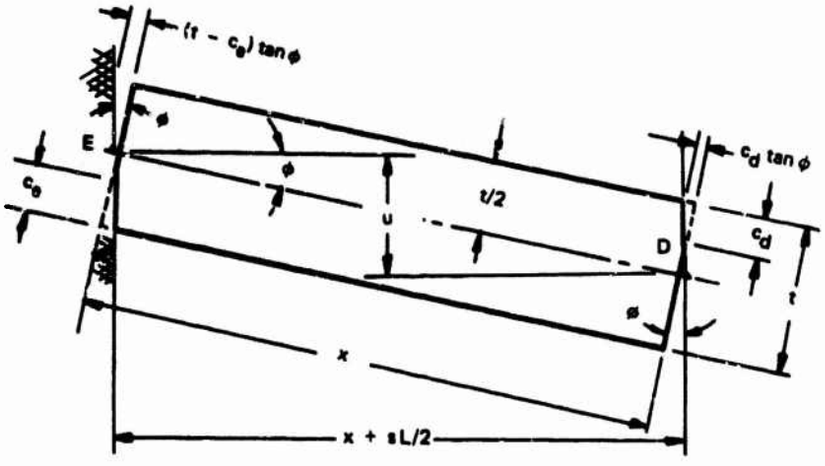

Figure 11. Geometric restraints for strip ED.

The effect of partial restraint against in-plane movement at the supports is considered in Figure 11. The support lines at points E and E' (Figure 7) of strip EDD'E' are assumed to move outward a distance equal to sL/2. This longitudinal movement increases the original distance between supports from L to L(1 + s). From the geometry of the strip (Figure 11),

$$\left(x + \frac{sL}{2}\right) \sec\phi = x + (t - c_e)\tan\phi - c_d \tan\phi$$

Since ϕ is small, the above expression reduces to

$$\frac{c_d + c_e}{t} = 1 - \frac{u}{2t} - \frac{sLx}{2ut} \qquad (3)$$

From the geometry of the deflected shape in Figure 7,

$$u = 2z_u\left(\frac{x}{L}\right) \qquad x \leq L/2 \qquad (4a)$$

Therefore, $$\frac{c_d + c_e}{t} = 1 - \left(\frac{z_u}{t}\right)\left(\frac{x}{L}\right) - \frac{s}{4\left(\frac{z_u}{t}\right)}\left(\frac{L}{t}\right)^2 \qquad (4)$$

Combining Equations 1 through 4, the depths to the neutral axis are

$$\frac{k_1 c_d}{t} = \frac{1}{2}\left\{\left[1 - \left(\frac{z_u}{t}\right)\left(\frac{x}{L}\right) - \frac{s}{4\left(\frac{z_u}{t}\right)}\left(\frac{L}{t}\right)^2\right]k_1 - \bar{q}_e\frac{d_e}{t} + \bar{q}_d\frac{d_d}{t}\right\} \quad (5)$$

$$\frac{k_1 c_e}{t} = \frac{1}{2}\left\{\left[1 - \left(\frac{z_u}{t}\right)\left(\frac{x}{L}\right) - \frac{s}{4\left(\frac{z_u}{t}\right)}\left(\frac{L}{t}\right)^2\right]k_1 + \bar{q}_e\frac{d_e}{t} - \bar{q}_d\frac{d_d}{t}\right\} \quad (6)$$

Substituting Equation 5 into Equation 2 and noting that $N_{ue} = N_u$, the thrust developed at the ends of any strip is

$$\frac{N_u}{t f''_c} = \frac{1}{2}\left\{\left[1 - \left(\frac{z_u}{t}\right)\left(\frac{x}{L}\right) - \frac{s}{4\left(\frac{z_u}{t}\right)}\left(\frac{L}{t}\right)^2\right]k_1 - \bar{q}_e\frac{d_e}{t} - \bar{q}_d\frac{d_d}{t}\right\} \quad (7)$$

To evaluate N_u from Equation 7, it is necessary to know the values of $\bar{q}_e$ and $\bar{q}_d$ which depend upon the steel stresses, f_{se}, f'_{se}, f_{sd}, and f'_{sd}. The value of these stresses in turn depends on the value of the balanced thrust for the cross sections **E** and **D**.

The balanced thrust depends on the properties of the cross section. It is the point on the failure interaction diagram where initial yielding of the tension steel occurs simultaneously with crushing of the concrete. For any thrust on the cross section *less* than the balanced thrust, the tension steel is yielding ($f_s = f_y$) when the strain in the extreme fiber of the concrete reaches ϵ_u (see Figure 1).

Referring to the strain distribution in Figures 9 and 10, the positions of the neutral axis at each hinge section for $\epsilon_{sd} = \epsilon_y$ and $\epsilon_{se} = \epsilon_y$ are

$$\frac{c_{bd}}{t} = \left[\frac{\epsilon_u}{\epsilon_u + (f_y/E_s)}\right]\frac{d_d}{t} \quad (8)$$

and

$$\frac{c_{be}}{t} = \left[\frac{\epsilon_u}{\epsilon_u + (f_y/E_s)}\right]\frac{d_e}{t} \quad (9)$$

The subscript **b** refers to the balanced condition. Substituting Equations 8 and 9 into Equations 1 and 2, respectively, and noting that $f_{sd} = f_{se} = f'_{sd} = f'_{se} = f_y$, the balanced thrusts for each end of the slab strip are

$$\frac{N_{bd}}{t f''_c} = \left\{ k_1 \left[\frac{\epsilon_u}{\epsilon_u + (f_y/E_s)} \right] - q_d \right\} \frac{d_d}{t} \qquad (10)$$

and

$$\frac{N_{be}}{t f''_c} = \left\{ k_1 \left[\frac{\epsilon_u}{\epsilon_u + (f_y/E_s)} \right] - q_e \right\} \frac{d_e}{t} \qquad (11)$$

where

$$q_d = (p_d - p'_d) \frac{f_y}{f''_c} \qquad (10a)$$

$$q_e = (p_e - p'_e) \frac{f_y}{f''_c} \qquad (11a)$$

The values q_d and q_e are referred to as the reinforcing index for sections of the strip at points **D** and **E**, respectively.

For the special case of a strip with $q_e = q_d = q$, i.e. identical sections at each end of the strip, Equations 10 and 11 reduce to

$$\frac{N_b}{t f''_c} = \left\{ k_1 \left[\frac{\epsilon_u}{\epsilon_u + (f_y/E_s)} \right] - q \right\} \frac{d}{t} \qquad (12)$$

where

$$q = (p - p') \frac{f_y}{f''_c} \qquad (12a)$$

For the case of a tension failure at both ends of strip **D E**, the thrust at initial crushing of the concrete (Equation 7) can now be stated in terms of the following criteria:

$$\frac{N_u}{t f''_c} = \frac{1}{2} \left\{ \left[1 - \left(\frac{z_u}{t}\right)\left(\frac{x}{L}\right) - \frac{s}{4\left(\frac{z_u}{t}\right)} \left(\frac{L}{t}\right)^2 \right] k_1 - q_e \frac{d_e}{t} - q_d \frac{d_d}{t} \right\} \qquad (13)$$

provided

$$\left.\begin{aligned} \frac{N_u}{N_{bd}} &< 1 \\ \frac{N_u}{N_{be}} &< 1 \end{aligned}\right\} \qquad (13a)$$

A compression failure will occur at one or both ends of the strip if Equation 13a is not satisfied. The failure will be brittle, allowing a relatively small rotation at the hinge lines and a possible failure before the collapse mechanism is fully developed. This effect of thrust on the rotation capacity of a concrete section is clearly illustrated in a paper by Pfrang.[11] The criteria given by Equation 13a should not be violated in the design of longitudinally restrained slabs.

For the special case of a strip with $q_e = q_d = q$, Equation 13 reduces to

$$\frac{N_u}{tf''_c} = \frac{1}{2}\left\{\left[1 - \left(\frac{z_u}{t}\right)\left(\frac{x}{L}\right) - \frac{s}{4\left(\frac{z_u}{t}\right)}\left(\frac{L}{t}\right)^2\right]k_1 - 2q\frac{d}{t}\right\} \qquad (14)$$

provided $N_u/N_b < 1$.

For $q_e = q_d$, the ratio of the ultimate thrust at a corner of the slab (Equation 14 with $x/L = 0$) to the balanced thrust (Equation 12) is plotted in Figure 12. The thrust ratio is shown as a function of the reinforcement ratio, $p - p'$. Note that the ratio N_u/N_b never exceeds the value 1.0 for the range of steel and concrete strengths considered. For $(p - p') < 2.5\%$, $0.8 < N_u/N_b < 1.0$. The steel ratio corresponding to the point on each curve where $N_u/N_b = 0$ is the balanced steel ratio, $(p - p')_b$. Any steel ratio greater than $(p - p')_b$ will produce an over-reinforced section. The balanced thrust will be less than zero ($N_b < 0$), and any amount of thrust on the section will produce crushing of the concrete before the tension steel yields.

The ultimate thrust at the center of the slab for span-thickness ratios of 10, 15, and 20 is shown in Figure 13. For $q_e = q_d$, the ratio of the ultimate thrust at the center of the slab (Equation 14 with $x/L = 1/2$) to the balanced thrust (Equation 12) is plotted in Figure 13. It should be noted that the ratio N_u/N_b never exceeds 1.0 but tends toward this value with increasing steel strengths (f_y), and decreasing steel ratios $(p - p')$ and span-thickness ratios (L/t). For the range of span-thickness ratios considered ($10 < L/t < 20$), $0.6 < N_u/N_b < 1.0$ for $(p - p') < 1.5\%$.

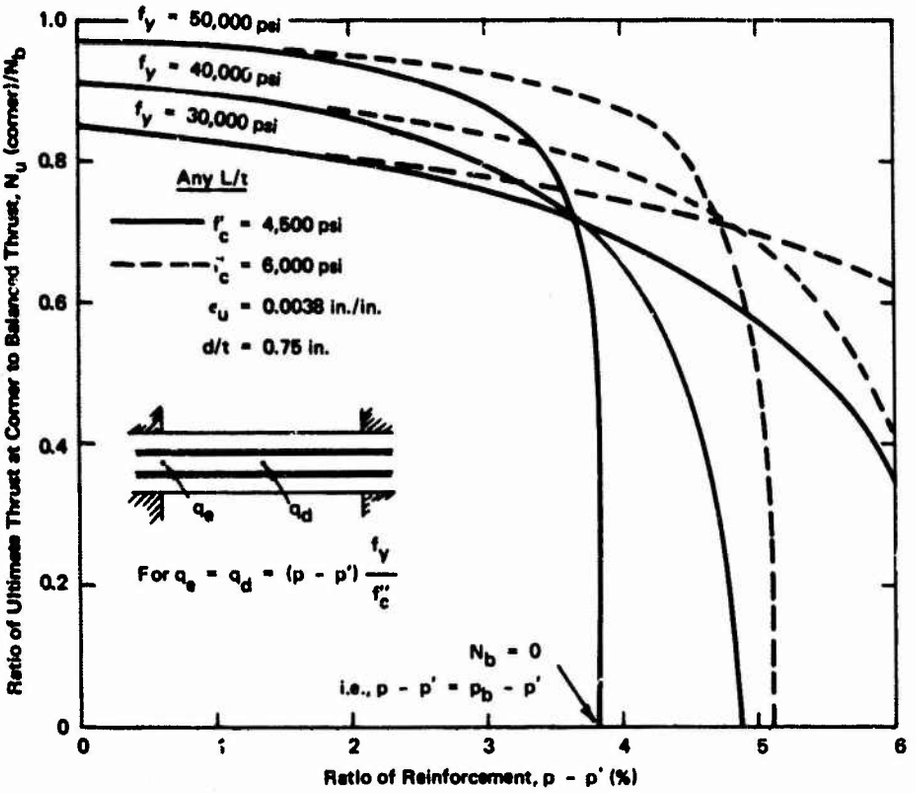

Figure 12. Effect of $p - p'$ and f_y on thrust ratio at corner.

To plot the curves shown in Figures 12 and 13, the values of k_1 and z_u/t were required in the equations. The value of the coefficient k_1 was that recommended by Hognestad[12] (Figure 14). The value for the ultimate deflection, z_u, was obtained from expressions derived in the following section.

Ultimate Deflection

The ultimate deflection, z_u, is the central deflection of the slab at initial formation of the flexural collapse mechanism. In other words, z_u *is the deflection required to develop the crushing strain of the concrete,* ϵ_u, *along the hinge lines.* The value of z_u is necessary to evaluate expressions for thrusts, moments, and slab resistance at ultimate flexural failure. From the strip geometry in Figure 11,

$$\tan\phi = \frac{x\,\epsilon_u}{2c_e} = \frac{u}{x + (s\,L/2)}$$

From Figure 7, at $x = L/2$, $u = z_u$. Substituting these values in the above expression,

$$\frac{z_u}{t} = \frac{\epsilon_u t}{8 c_e} \left(\frac{L}{t}\right)^2 (1 + s)$$

Substituting the expression for c_e given by Equation 6 into the above expression, letting $x = L/2$, and rearranging terms,

$$\left(\frac{z_u}{t}\right)^2 - 2\left(1 + \bar{q}_e \frac{d_e}{tk_1} - \bar{q}_d \frac{d_d}{tk_1}\right)\frac{z_u}{t} + \frac{1}{2}\left(\frac{L}{t}\right)^2\left[s(1 + \epsilon_u) + \epsilon_u\right] = 0$$

For $N_u/N_b \leq 1$,

$$\left(\frac{z_u}{t}\right)^2 - 2\left(1 + q_e \frac{d_e}{tk_1} - q_d \frac{d_d}{tk_1}\right)\frac{z_u}{t} + \frac{1}{2}\left(\frac{L}{t}\right)^2\left[s(1 + \epsilon_u) + \epsilon_u\right] = 0$$

Therefore, the central deflection required to crush the concrete along the hinge lines is

$$\frac{z_u}{t} = \left(1 + q_e \frac{d_e}{tk_1} - q_d \frac{d_d}{tk_1}\right) - \sqrt{\left(1 + q_e \frac{d_e}{tk_1} - q_d \frac{a_d}{tk_1}\right)^2 - \frac{1}{2}\left(\frac{L}{t}\right)^2\left[s(1 + \epsilon_u) + \epsilon_u\right]} \quad (15)$$

where $q_e = (p_e - p_e')\frac{f_y}{f_c''}$

$$q_d = (p_d - p_d')\frac{f_y}{f_c''}$$

Equation 15 shows that the central deflection of the slab required to produce crushing of the concrete and initiate the collapse mechanism depends on (1) the properties of the cross section at each end of the strip; (2) the crushing strain of the concrete; (3) the span-thickness ratio of the slab; (4) the amount of longitudinal movement at the supports; and (5) the depth to the tension steel in the slab relative to the slab thickness.

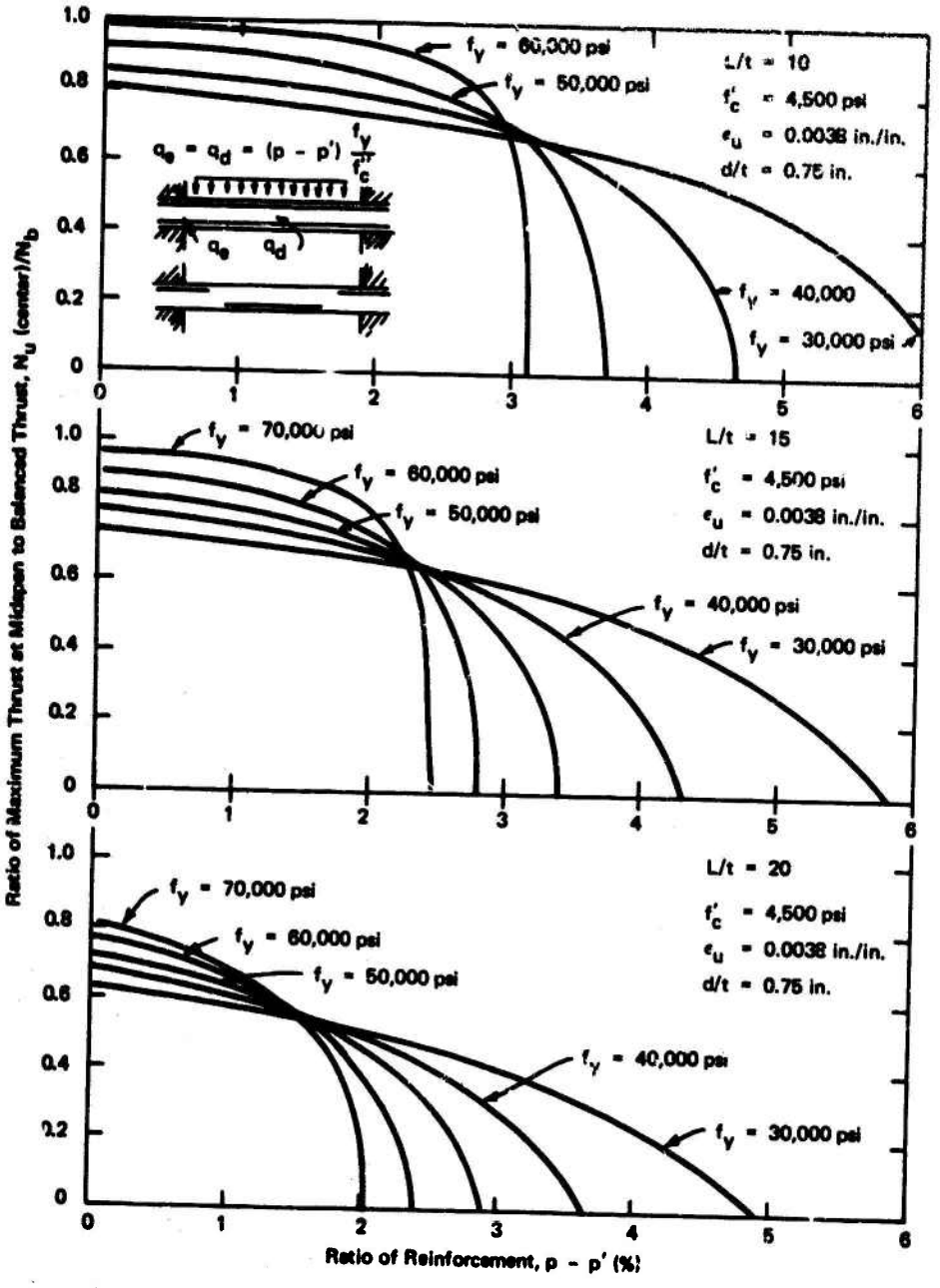

Figure 13. Effect of p - p′ and f_y on thrust ratio at midspan for L/t = 10, 15, 20.

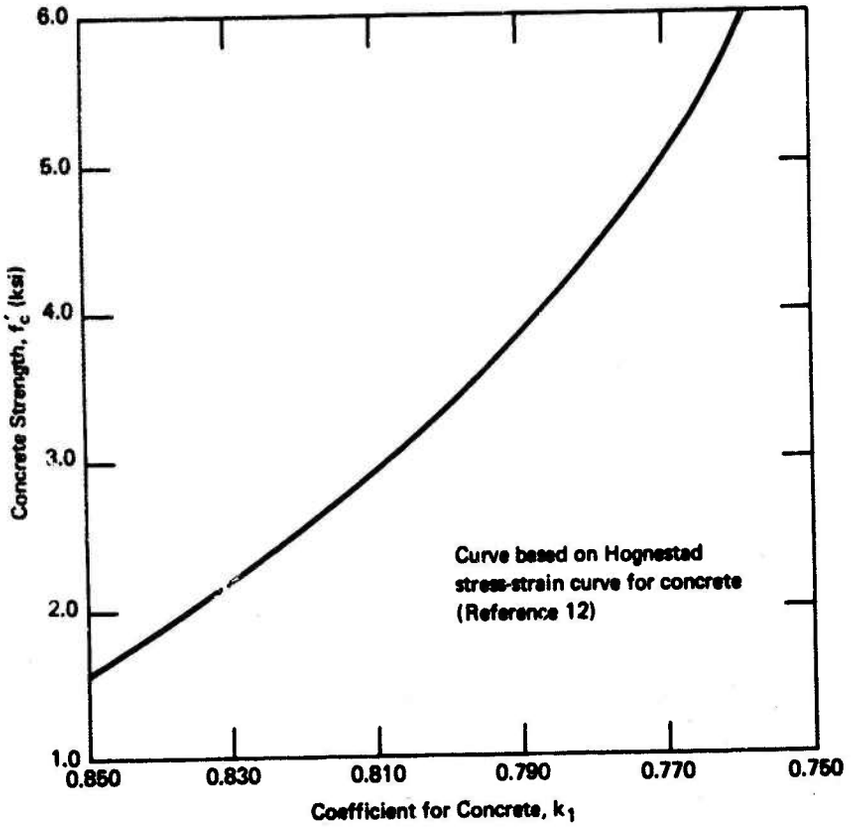

Figure 14. Coefficient for average stress in concrete, k_1.

For the special case of a strip with $q_e = q_d$, Equation 15 reduces to

$$\frac{z_u}{t} = 1 - \sqrt{1 - \frac{1}{2}\left(\frac{L}{t}\right)^2 \left[s(1+\epsilon_u) + \epsilon_u\right]} \qquad (16)$$

Equation 16 with $s = 0$ is plotted in Figure 15. Note that for a given crushing strain for the concrete, z_u/t increases with span-thickness ratio. For $\epsilon_u = 0.0038$, z_u/t exceeds 0.5 for L/t greater than 20. Figure 15 also shows curves for the special case of a slab reinforced with one layer of steel near the unloaded face and extending into the supports. This arrangement of steel was used in longitudinally restrained slabs tested by MIT.[6]

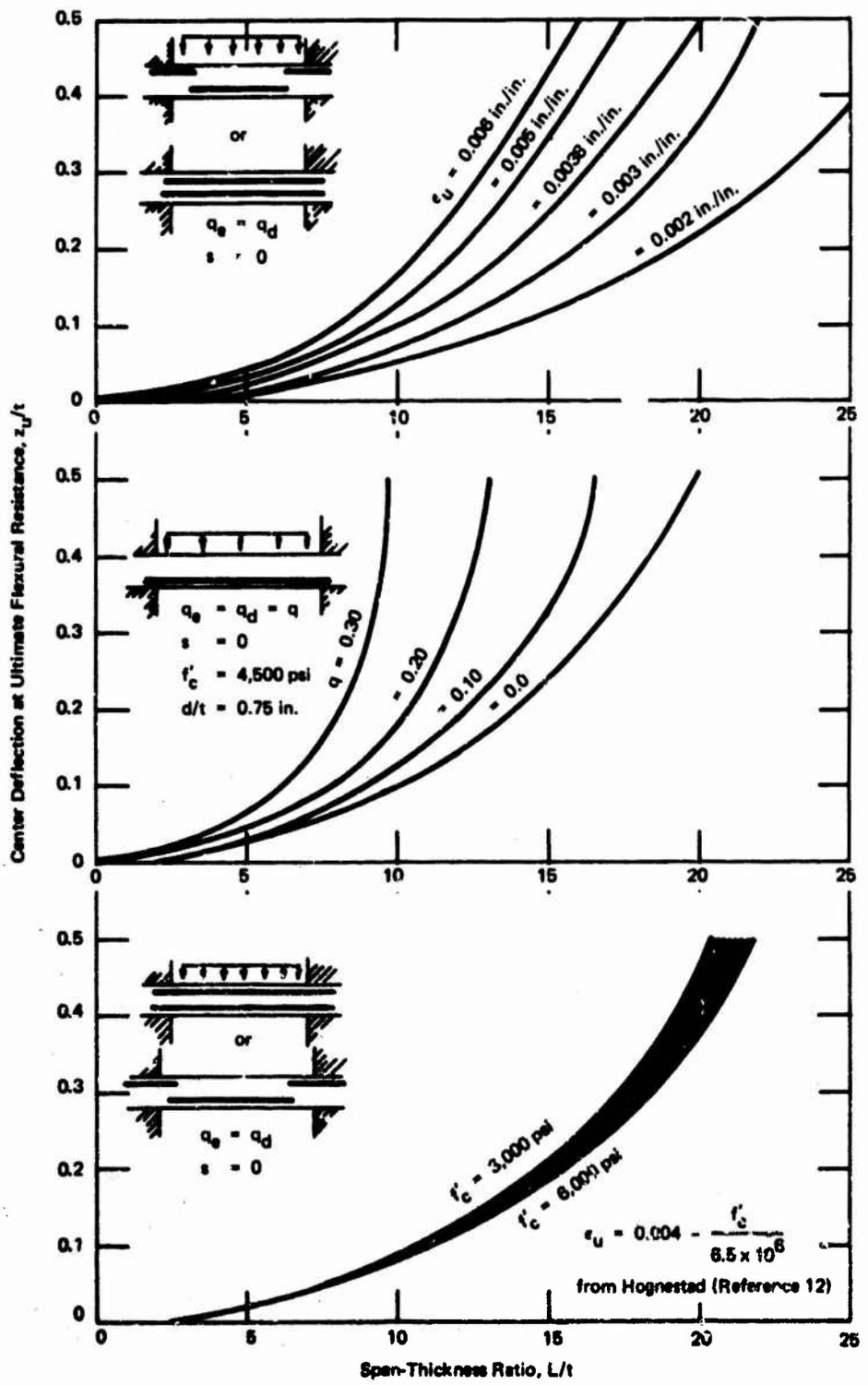

Figure 15. Effects of reinforcing index, arrangement of steel, ultimate concrete strain, and concrete strength on ultimate deflection of fully restrained slab for various span-thickness ratios.

Equation 16 is also plotted in Figure 16 with $s = 0$. It shows the effect of longitudinal movement at the supports on the central deflection at crushing of concrete as a function of span-thickness ratio. Curves are plotted for crushing strains equal to 0.0038 and 0.006 in./in. Note that for a given span-thickness ratio (L/t) the ultimate deflection (z_u/t) increases with the edge movement, s, and concrete crushing strain, ϵ_u. For example, if L/t = 16, then $z_u/t = 0.28$ when the slab edges are fully jammed ($s = 0$). However, if the edges are only partially restrained, so that the lateral movement at the support line is 0.24 inch, then z_u/t increases to 0.50 for a 10-foot span ($s = 0.002$). Thus, the greater the edge movement, the greater the central deflection when the flexural collapse mechanism forms. This increase in central deflection has the effect of decreasing the thrust at the center and corners of the slab (see Equation 14), which, in turn, decreases the moment resistance of sections along the hinge lines.

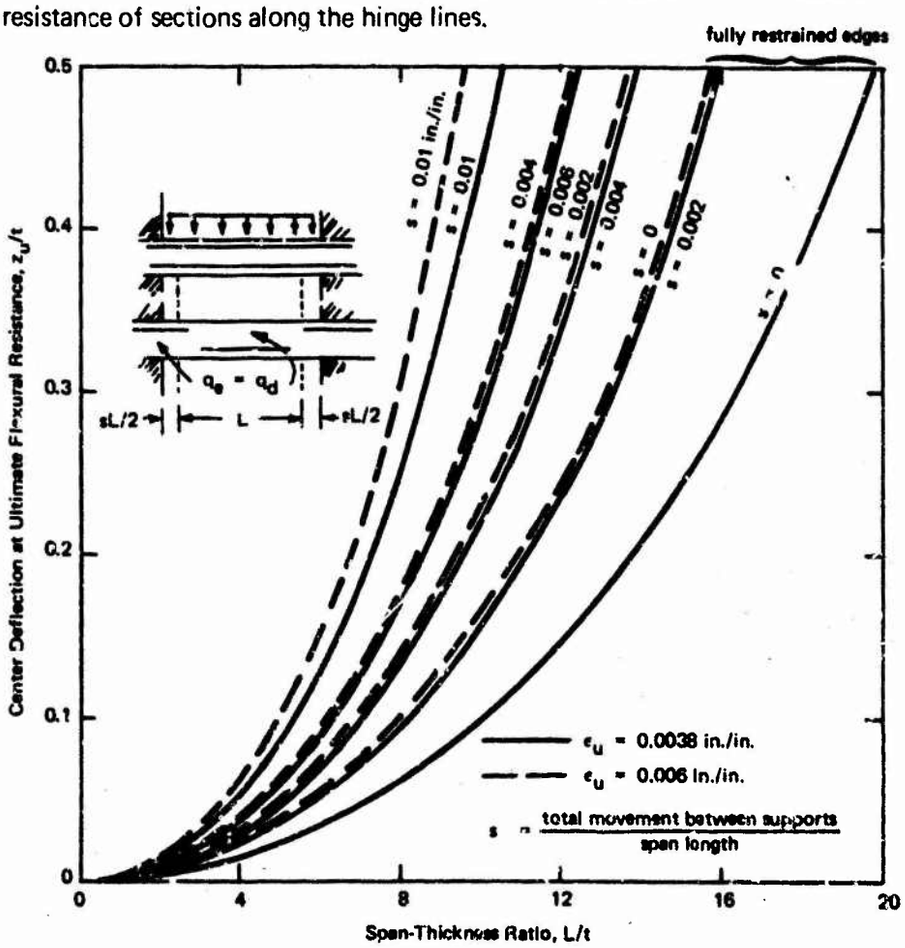

Figure 16. Effect of movement at supports on deflection at ultimate flexural resistance for various span-thickness ratios.

Ultimate Flexural Resistance

The ultimate flexural resistance is calculated by considering the equilibrium of a typical slab strip (Figure 8).

$$\frac{1}{2} q_u x^2 (dy) = M_{ud} (dy) + M_{ue} (dy) - N_u u (dy)$$

For the square slab shown in Figure 6, $x = y$ at all points along a diagonal, and $u = 2 z_u x/L$ (Equation 4a). Substituting these relations into the above equation and summing the contribution of each strip over a segment of the collapse mechanism,

$$2 \int_0^{L/2} \left(\frac{q_u x^2}{2} \right) dx = 2 \int_0^{L/2} \left[M_{ud} + M_{ue} - 2 N_u \left(\frac{z_u}{L} \right) x \right] dx$$

Substituting the expression for N_u (Equation 7) and integrating,

$$\frac{q_u L^2}{24} = \frac{2}{L} \int_0^{L/2} (M_{ud})\, dx + \frac{2}{L} \int_0^{L/2} (M_{ue})\, dx - \left(\frac{z_u}{t} \right) \frac{t}{6} \left[2 N_u (L/2) + N_u (0) \right] \quad (17a)$$

where $N_u(0)$ = ultimate thrust at the corner of slab (Equation 7 for $x = 0$).

$N_u(L/2)$ = ultimate thrust at center of slab (Equation 7 for $x = L/2$).

Both M_{ud} and M_{ue} are nonlinear in x, yielding an awkward expression for

$$\int_0^{L/2} (M_{ud})\, dx \quad \text{and} \quad \int_0^{L/2} (M_{ue})\, dx$$

However, a simple expression which proves to be a good approximation for each integral is

$$\left.\begin{aligned} \frac{2}{L} \int_0^{L/2} (M_{ud})\, dx &= (\bar{M}_{ud}) \frac{L}{2} \\ \frac{2}{L} \int_0^{L/2} (M_{ue})\, dx &= (\bar{M}_{ue}) \frac{L}{2} \end{aligned}\right\} \quad (17b)$$

where $\bar{M}_{ud}$ = the ultimate moment resistance about mid-thickness of sections along the diagonal produced by the *average* thrust acting across the span, $[N(L/2) + N(0)]/2$.

$\bar{M}_{ue}$ = the ultimate moment resistance about mid-thickness of sections along the edge produced by the *average* thrust acting across the span, $[N(L/2) + N(0)]/2$.

The errors in these approximations (Equation 17b) are

$$(\text{Error})_d = \int_0^{L/2} (M_{ud})\,dx - (\bar{M}_{ud})\,\frac{L}{2}$$

$$(\text{Error})_e = \int_0^{L/2} (M_{ue})\,dx - (\bar{M}_{ue})\,\frac{L}{2}$$

The error depends on the ultimate thrust at the center and corner of the slab relative to the balanced thrust for the section. Since the thrust is linear in x, three conditions are possible. These conditions are shown in Figure 17 for a typical interaction diagram. The error in the approximation is equal to the shaded area. Note that the error is negligible for case 1 [$N_u(0)/N_b < 1$, $N_u(L/2)/N_b < 1$]. This case always exists for slabs with identical sections along the edge and diagonal ($q_e = q_d$), at least for the range of material strengths and steel ratios shown in Figures 12 and 13. The error is greatest for case 2 and least for case 3 (Figure 17). For every case, the error decreases as the thrust distribution along the hinge line becomes uniform [$N(0) - N(L/2) \rightarrow 0$]. Careful inspection of Figures 12 and 13 shows that thrust becomes more uniform with smaller span-thickness ratios.

The ultimate flexural resistance of a longitudinally restrained square slab can now be stated from Equation 17a using the approximation of Equation 17b.

$$q_u = \frac{24}{L^2}\left\{\bar{M}_{ud} + \bar{M}_{ue} - \left(\frac{z_u}{t}\right)\frac{t}{6}\left[2N_u(L/2) + N_u(0)\right]\right\} \qquad (17)$$

where z_u/t = ultimate deflection (Equation 15).

$N_u(L/2)$ = ultimate thrust at $x = L/2$ (Equation 13), lb/in.

$N_u(0)$ = ultimate thrust at $x = 0$ (Equation 13), lb/in.

$\bar{M}_{ud}$ = ultimate moment resistance about mid-thickness of a section along a diagonal due to a thrust equal to $(1/2)[N_u(L/2) + N_u(0)]$, in.-lb/in.

$\bar{M}_{ue}$ = ultimate moment resistance about mid-thickness of a section along an edge due to a thrust equal to $(1/2)[N_u(L/2) + N_u(0)]$, in.-lb/in.

The quantities $\bar{M}_{ud}$ and $\bar{M}_{ue}$ are taken from the failure interaction diagram for typical sections along the diagonal and edge of the slab, respectively.

For a slab with no longitudinal edge restraint, the thrust is equal to zero; i.e., $N_u(L/2) = N_u(0) = 0$. Therefore, Equation 17 reduces to the flexural resistance given by the yield line theory:

$$q_y = \frac{24}{L^2}(M_{yd} + M_{ye}) \qquad (18)$$

where M_{yd} = ultimate moment resistance at mid-thickness of a section along a diagonal for zero thrust, in.-lb/in.

M_{ye} = ultimate moment resistance at mid-thickness of a section along an edge for zero thrust, in.-lb/in.

The enhancement in ultimate flexural resistance due to longitudinal edge restraint is the ratio of the resistances given by Equations 17 and 18 (q_u/q_y). This ratio is plotted in Figure 18 for the sectional properties noted. These properties are assumed identical along both the diagonal and edge of the slab. For a given cross section, the enhancement in ultimate flexural resistance decreases with increasing edge movement and span-thickness ratio. The lines for a constant s are essentially parallel for $L/t \leq 18$. For $L/t > 18$ the lines diverge. This divergence stems from the value of the second term in Equation 15; for $\epsilon_u = 0.0038$, this term is the square root of a negative quantity for $L/t > 18$. Therefore, the curves in Figure 18 are based on $z_u/t = 0.42$ for $L/t > 18$. This is a reasonable assumption based on test results reported later.

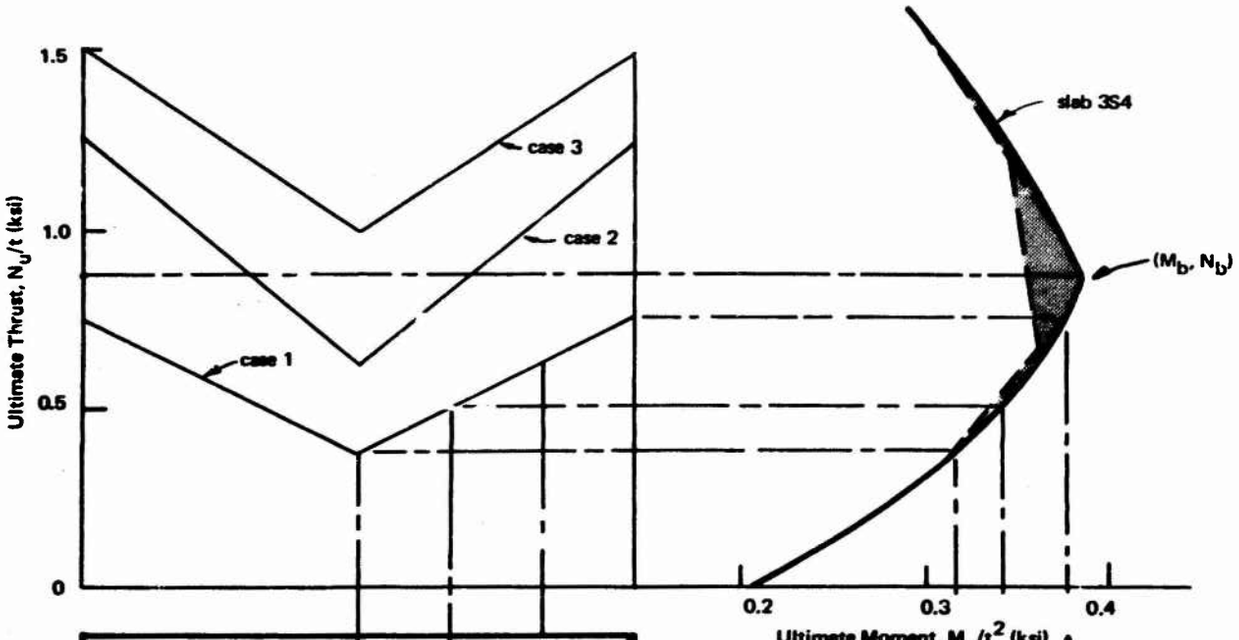

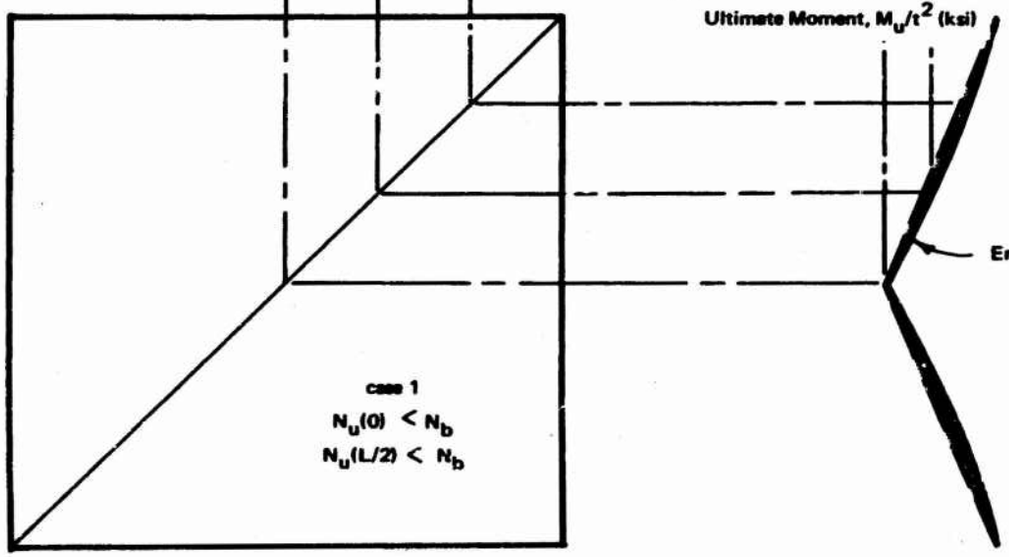

Error = $\int_0^{L/2} (M_{ue})\,dx - (\bar{M}_{ue})\frac{L}{2} \approx 0$

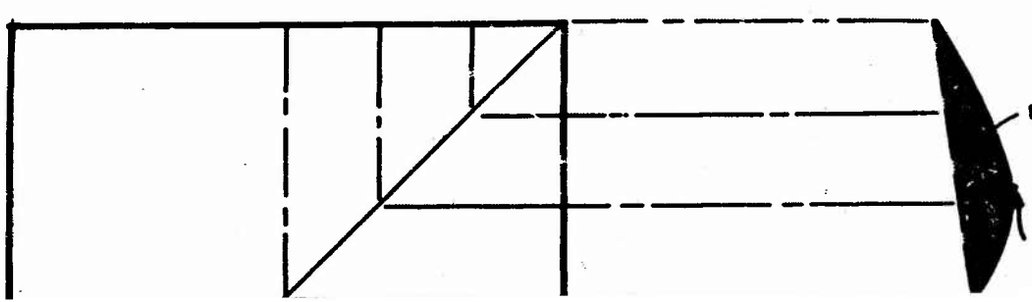

Error = $\int_0^{L/2} (M_{ue})\,dx - (\bar{M}_{ue})\frac{L}{2}$ = small

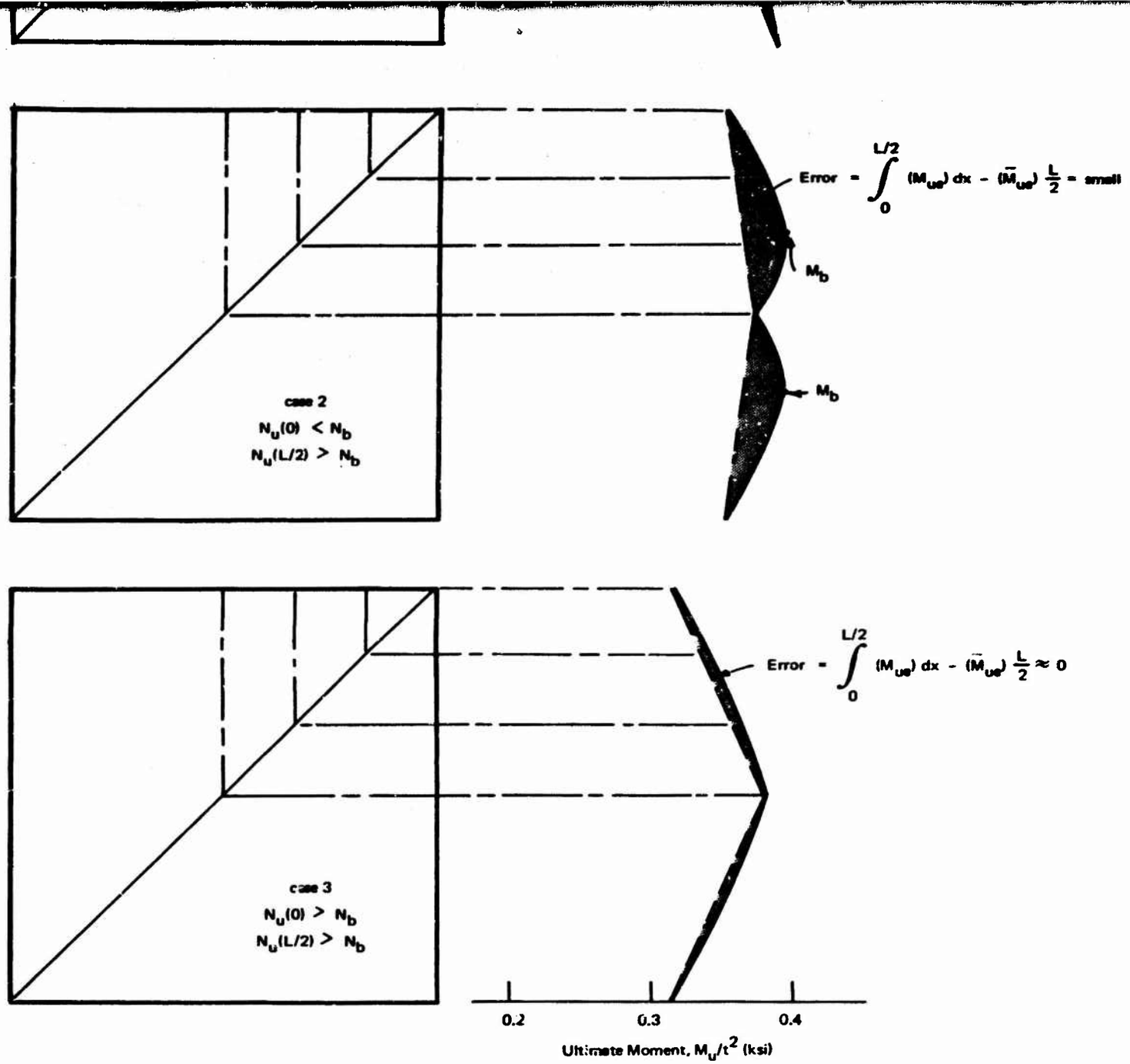

Figure 17. Effect of ultimate thrust on distribution of ultimate moment resistance.

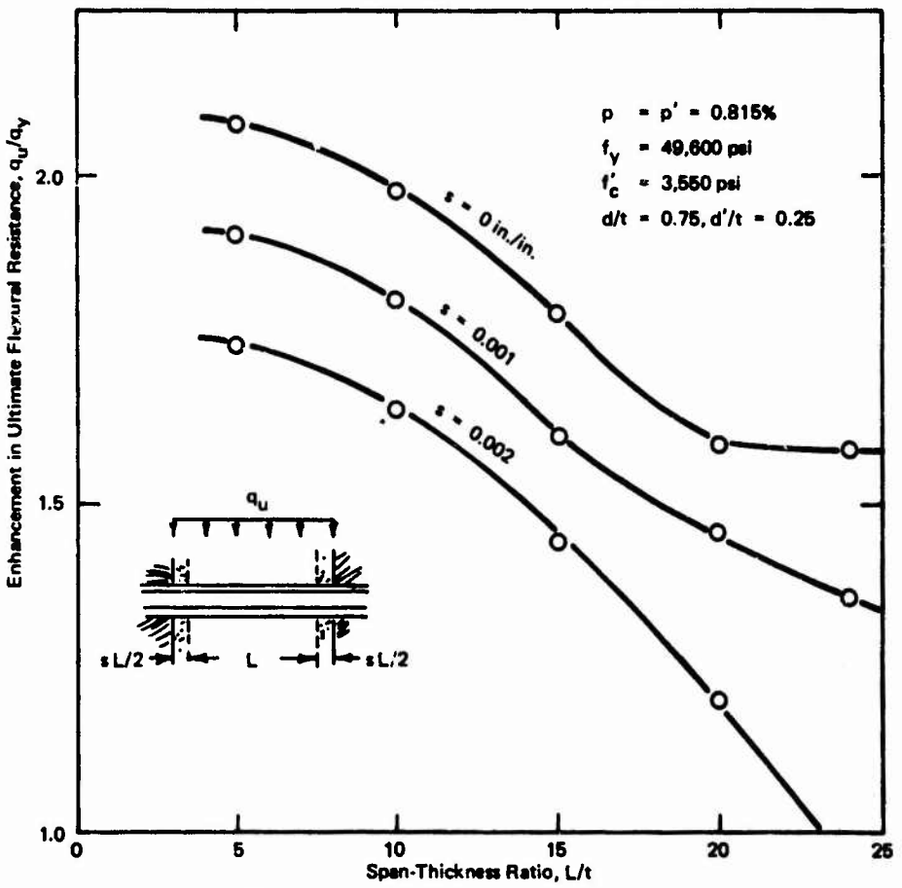

Figure 18. Effect of edge movement on ultimate flexural resistance.

The effect of the steel ratio on the enhancement factor, q_u/q_y, for various span-thickness ratios is shown in Figure 19. The curves, although based on a given steel and concrete strength, illustrate three important conclusions:

1. The enhancement factor, q_u/q_y, increases with decreasing steel ratios. The enhancement factor is infinite for $p = 0$ (since $q_y = 0$) and approaches unity as p approaches p_b, the balanced steel ratio.

2. The effect of compression steel, p', on the enhancement factor depends upon the tensile steel ratio, p. For small amounts of tensile steel ($p < 0.7\%$), the enhancement factor decreases as p'/p increases. For larger amounts of tensile steel ($p > 0.7\%$), the enhancement factor increases as p'/p increases. This observation is important for design since slabs often

have small amounts of tensile steel ($p < 1\%$). Thus, the importance of compression steel increases as the tensile steel ratio approaches the balanced steel ratio.

3. For a given cross section, the enhancement factor increases as the span-thickness ratio, **L/t**, decreases.

EXPERIMENTAL STUDY

Loading Machine

The slabs were tested in the NCEL slab loader (Figure 20). The slab loader is designed to apply a uniform pressure to the surface of a slab specimen. It will accommodate slabs with a clear span of 6 feet and produce static or dynamic pressures up to 300 psi.

The slab loader is a reinforced concrete open-top box with a steel-lined cavity. The slab specimen is fastened to the top face of the box with anchor bolts located around the perimeter of the loader.

Loads are applied to the "bottom" face of the slab by generating pressure in the cavity of the slab loader. Static loads are generated by pumping water under hydrostatic pressure into the cavity. Dynamic loads are applied to the slab by generating expanding gases in the cavity from the simultaneous detonation of four separate charges of PETN Primacord. The peak dynamic pressure is controlled by the amount of Primacord; the decay time can be controlled by two pipes which vent the gases from the cavity to the atmosphere. A detailed description of the slab loader and the principle of generating static and dynamic loads is described in Appendix A.

Slab Specimens

Description. Nine slabs involving five different cross sections were loaded to failure. The slab dimensions and arrangement of the reinforcement are shown in Figure 21; other details are described in Table 1. All slabs were square with an overall length of 8 feet 4 inches and a clear span of 6 feet. Slab thicknesses were 3, 4.75, and 6 inches which correspond to a span-thickness ratio of 24, 15.2, and 12, respectively.

The slabs were designated by a combination of numbers and letters, such as 3S1. The first number designates the total thickness of the slab. The letter indicates how the slab was loaded: **S**, static load; **D**, dynamic load. The second number designates the slab number. Some slabs were loaded more than once, in which case an additional "dash" number was added to the slab designation to indicate the cycle of loading. For example, 4.75D1-4 means 4-3/4-inch-thick slab, dynamic load, slab No. 1, fourth cycle of loading.

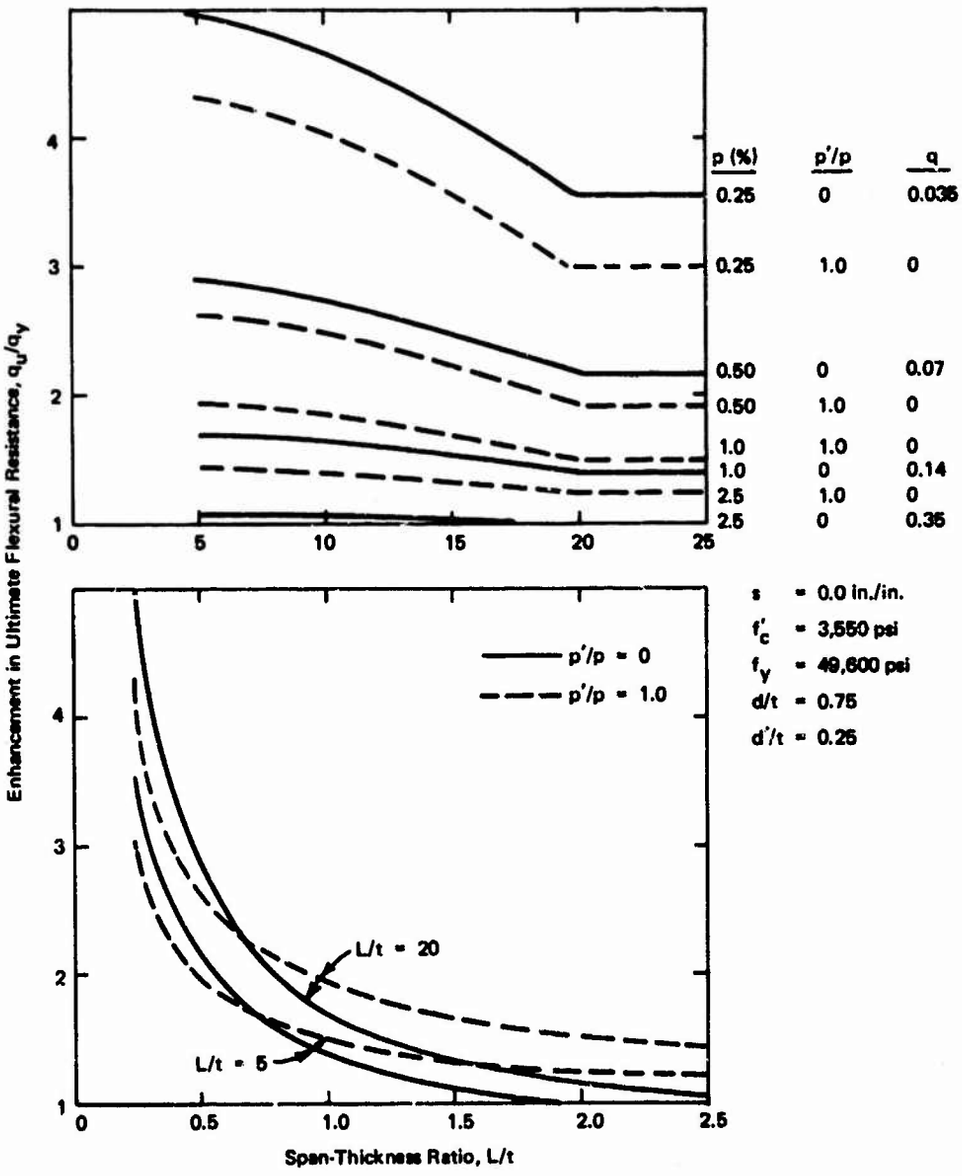

Figure 19. Effect of steel percentage on ultimate flexural resistance.

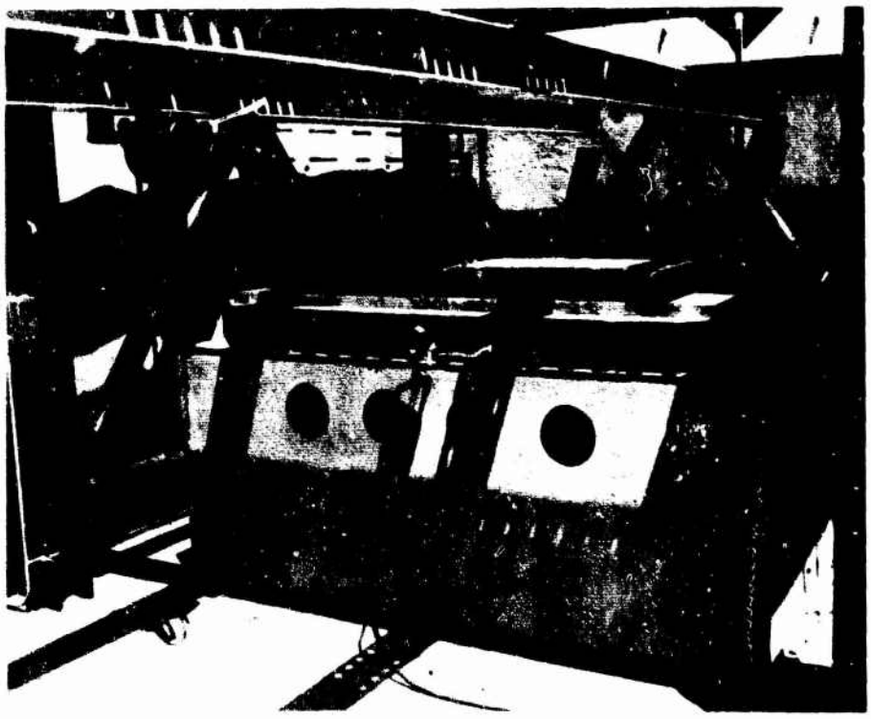

Figure 20. NCEL slab loader.

Longitudi reinforcement consisted of an orthogonal set of uniformly spaced bars in each face of the slab; total amount of reinforcement in each face varied between 0 and 1.33%. All bars were continuous throughout the length of the slab and extended into the supports. Over the supports, the bars were securely hooked around longitudinal bars spanning the other direction. For slabs of each thickness, the size and spacing of bars in each face were identical with two exceptions. One slab, 3S2, had no reinforcement and another slab, 3S4, had only tension reinforcement. The tension steel in slab 3S4 was placed over the whole of the loaded area of the slab but was terminated 2 inches from the support line; the tension steel over the supports was hooked near the edge of the slab and extended 16 inches into the slab from the support line (see Figure 21). The reinforcement for each slab was designed to provide enough steel to assure that the tensile membrane load capacity (corresponding to rupture of the bars) was greater than the compressive membrane load capacity.

Table 1. Slab Details

Slab No.	Test Age (days)	Concrete Strength, f'_c (psi)	Slab Dimensions				Longitudinal Reinforcement						
			Slab Thickness, t (in.)	Clear Span, L (in.)	Span Ratio, L/t	Mean Depth, d (in.)	Bar		Strength		Steel Ratio (each d		
							Size No.	Space, s (in.)	Yield, f_y (ksi)	Ultimate, f_u (ksi)	Edge		
											p_e (%)	p'_e (%)	p_i (%
3S1	35	3,550	3.0	72	24.0	2.25	3	6	49.6	67.0	0.815	0.815	0.8
3S2	35	4,140	3.0	72	24.0	–	–	–	–	–	0.0	0.0	0.0
3S3	36	4,120	3.0	72	24.0	2.25	3	6	49.6	67.0	0.815	0.815	0.8
3S4	39	3,295	3.0	72	24.0	2.25	3	6	49.6	67.0	0.815	0.0	0.8
3D1	40	3,795	3.0	72	24.0	2.25	3	6	49.6	67.0	0.815	0.815	0.8
4.75S1	47	3,165	4.75	72	15.2	3.75	4	6	47.4	70.0	0.889	0.889	0.8
4.75D1	66	3,320	4.75	72	15.2	3.75	4	6	47.4	70.0	0.889	0.889	0.8
4.75D2	110	3,595	4.75	72	15.2	3.75	4	6	47.4	70.0	0.889	0.889	0.8
6S1	36	3,615	6.0	72	12.0	5.00	4	3	47.4	70.0	1.33	1.33	1.3

* 9-gage wire

Table 1. Slab Details

Longitudinal Reinforcement								Shear Reinforcement				
Bar		Strength		Steel Ratio (each direction)				Bar		Strength		Steel Ratio, p_v (%)
Size No.	Space, s (in.)	Yield, f_y (ksi)	Ultimate, f_u (ksi)	Edge		Midspan		Size No.	Space, s (in.)	Yield, f_y (ksi)	Ultimate, f_u (ksi)	
				p_e (%)	p'_e (%)	p_d (%)	p'_d (%)					
3	6	49.6	67.0	0.815	0.815	0.815	0.815	9*	1.5	37.5	52.3	0.19
–	–	–	–	0.0	0.0	0.0	0.0	–	–	–	–	0.0
3	6	49.6	67.0	0.815	0.815	0.815	0.815	9*	1.5	37.5	52.3	0.19
3	6	49.6	67.0	0.815	0.0	0.815	0.0	9*	1.5	37.5	52.3	0.19
3	6	49.6	67.0	0.815	0.815	0.815	0.815	9*	1.5	37.5	52.3	0.19
4	6	47.4	70.0	0.889	0.889	0.889	0.889	2	2.0	40.0	64.5	0.42
4	6	47.4	70.0	0.889	0.889	0.889	0.889	2	2.0	40.0	64.5	0.42
4	6	47.4	70.0	0.889	0.889	0.889	0.889	2	2.0	40.0	64.5	0.42
4	3	47.4	70.0	1.33	1.33	1.33	1.33	2	1.0	40.0	64.5	1.67

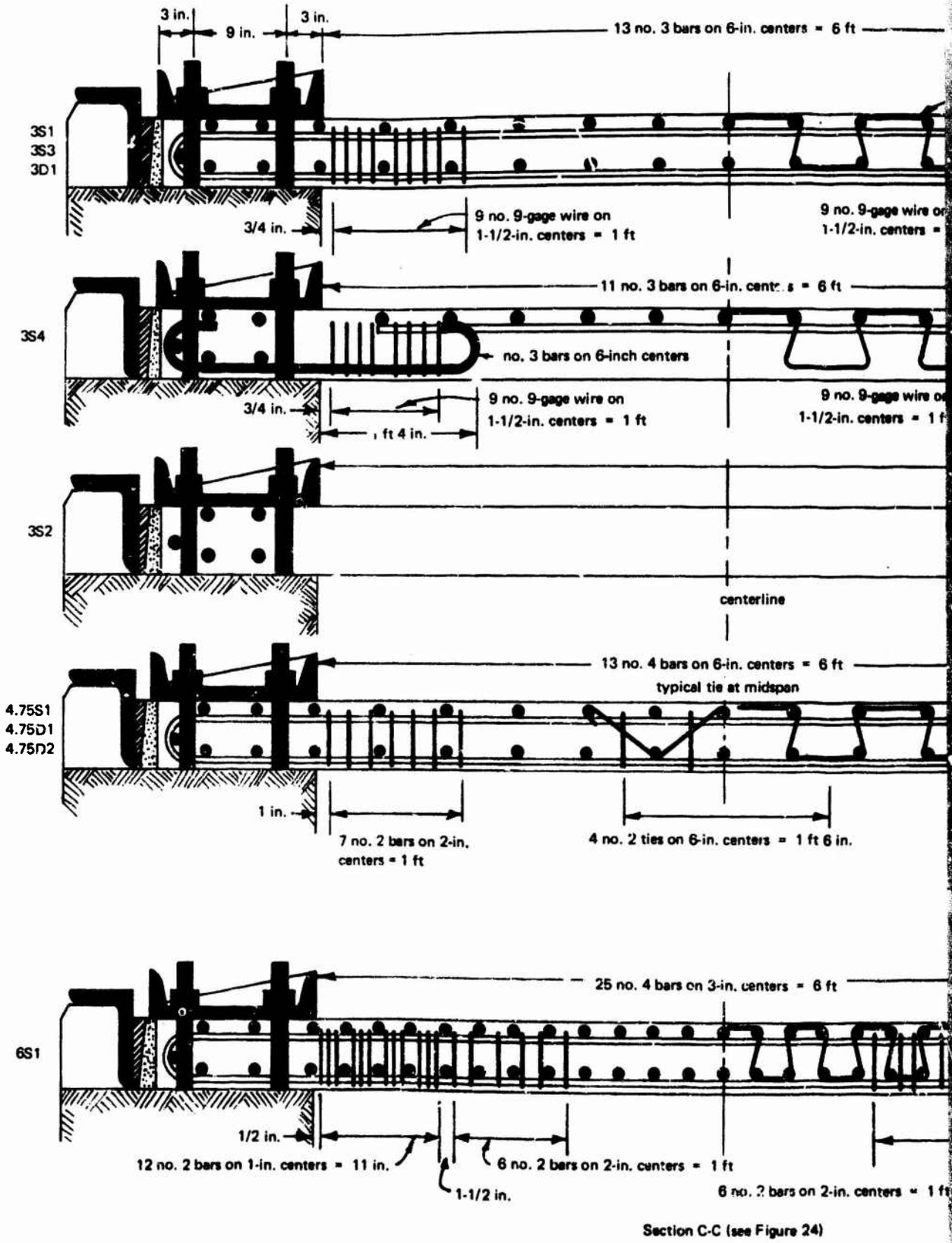

Figure 21. Slab deta

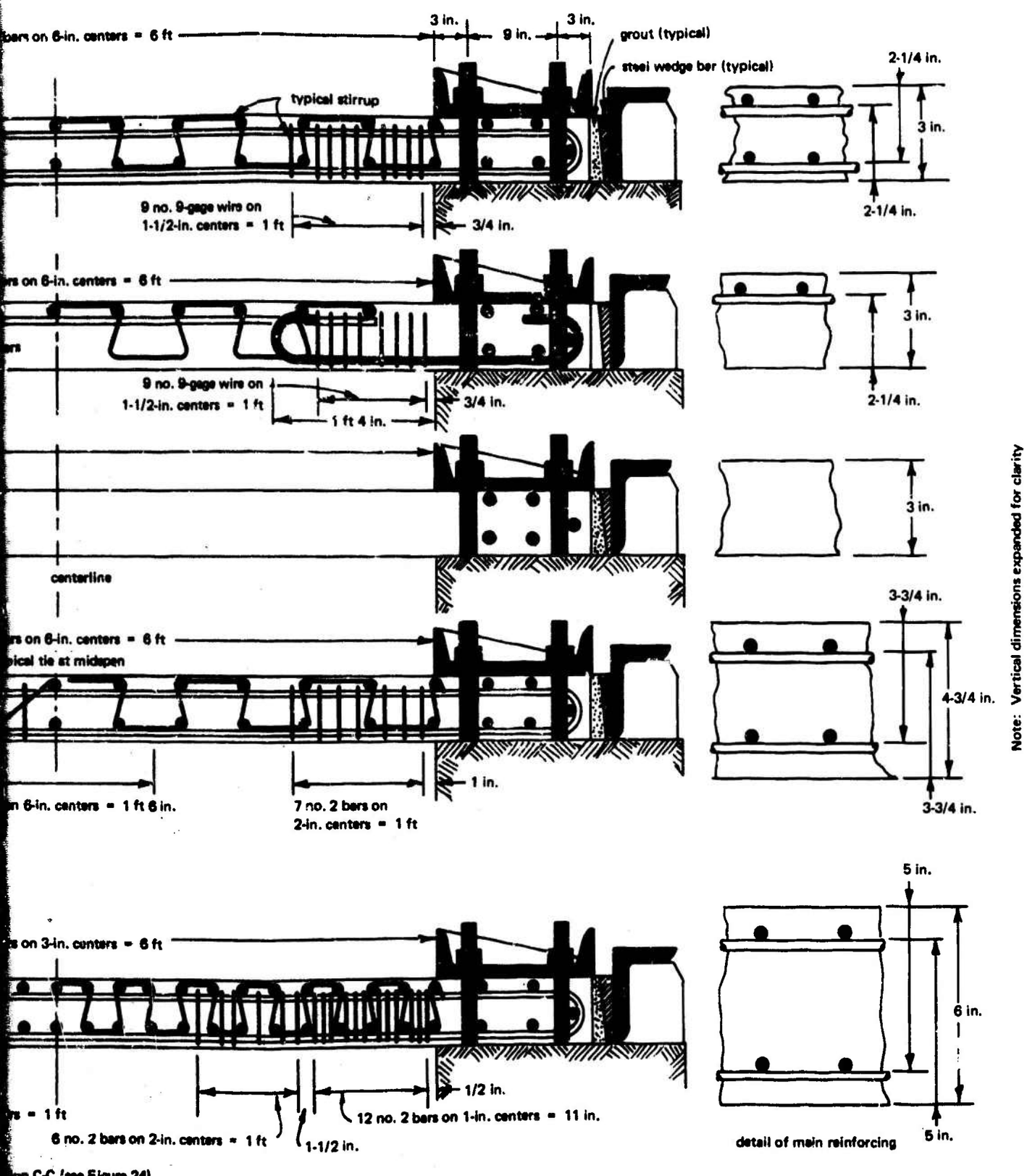

Note: Vertical dimensions expanded for clarity

Figure 21. Slab details.

Stirrup details near the supports are shown in Figure 21 and Table 1. Each stirrup extended the full length of the slab. It consisted of one continuous bar, tightly wrapped in a zigzag fashion around the top and bottom longitudinal bars. The ends of the stirrups were hooked and securely anchored to longitudinal bars over the supports (Figure 21). The stirrups were designed to carry the shear in excess of $4\sqrt{f'_c}$ and were assumed to be 100% effective. The critical section for shear was assumed to be located a distance **d**/2 from the periphery of the loaded area. This procedure conforms in part with recommendations outlined by the ACI-ASCE Committee 326[14] and with results of tests on a 10-inch-thick reinforced concrete slab (**L**/**d** = 7) which failed in shear as described in Appendix B.

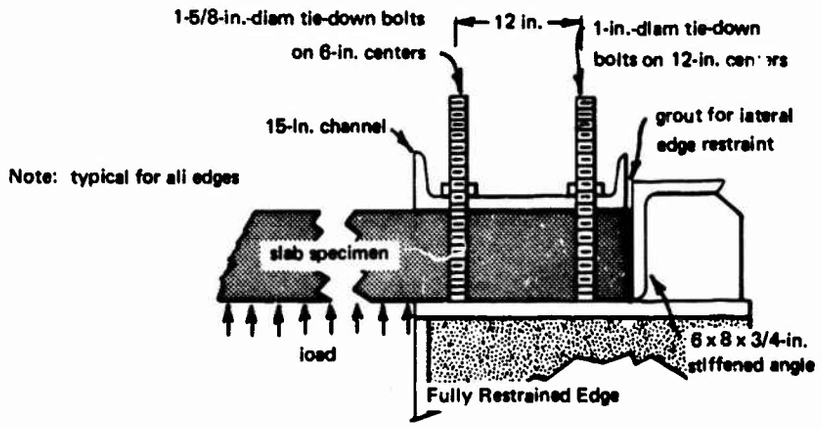

Figure 22. Type of edge restraint.

Supports. All edges were fully clamped and laterally restrained against outward movement as shown in Figure 22. Rotational restraint was provided by clamping the edges of the slab between the face of the slab loader and a frame formed from steel channels. The channels were 15[50 with 1-inch-thick stiffener plates welded to the web every 6 inches along the length of the channel. The steel frame was drawn tight against the slab by an inner ring of 1-5/8-inch-diameter threaded studs on 6-inch centers and by an outer ring of 1-inch-diameter studs on 12-inch centers. Hydrostone grout was placed between the steel frame and slab to assure a uniform bearing surface. Nuts were threaded onto the studs, and an air wrench was used to tighten them against the channels. The slab edges were restrained against outward movement by an expansive Embeco pre-mixed grout placed between the edges of the slab and an 8 x 6 x 1-inch angle welded to the loader around the perimeter of the slab. The angle was reinforced with 1/2-inch stiffeners on 6-inch centers.

Material Properties. The slabs were cast using a 3,500-psi concrete mix made from Victor Type II portland cement, crushed San Gabriel aggregate with a maximum size of 3/8 inch, and San Gabriel sand with a fineness modulus of 2.82. Mix proportions were 1.00:3.80:3.11 by weight, with a water-cement ratio ranging from 0.81 to 0.89 by weight. The cement factor was 4.9 sacks per cubic yard. The average concrete strength of each slab is summarized in Table 1. These values are based on tests of three standard 6 x 12 concrete control cylinders cast from the same mix used in the slab.

The longitudinal reinforcement in each slab was either No. 3 or 4 intermediate grade deformed bars. All bars of each size were from the same lot and satisfied the requirements of ASTM Specifications A15-56T and A305-56T. A typical stress-strain curve for each size bar is shown in Figure 23. As indicated, the No. 3 and 4 bars exhibited a linear stress-strain curve relationship up to a well-defined yield stress of 49,600 and 47,400 psi, respectively. The yield range was flat to a minimum strain of 2.4%.

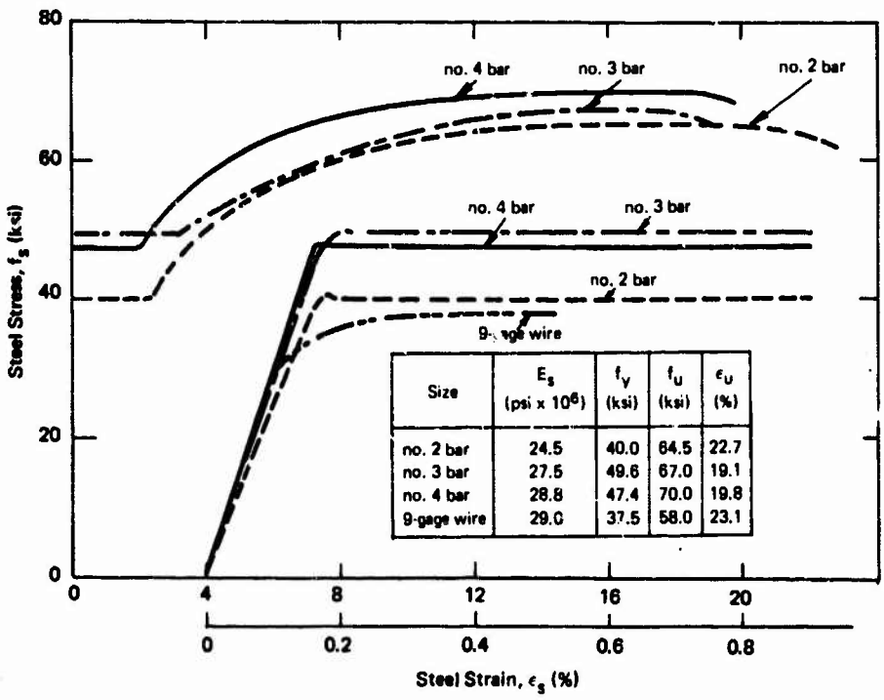

Size	E_s (psi x 10^6)	f_y (ksi)	f_u (ksi)	ϵ_u (%)
no. 2 bar	24.5	40.0	64.5	22.7
no. 3 bar	27.5	49.6	67.0	19.1
no. 4 bar	28.8	47.4	70.0	19.8
9-gage wire	29.0	37.5	58.0	23.1

Figure 23. Stress-strain curves for reinforcement.

Fabrication. The slabs were cast in a mold which matched the support surface of the slab loader and location of the tie-down studs. To form a template for the mold, a 10-inch-thick reinforced concrete slab was cast on the NCEL slab loader. Then the reinforced concrete mold was cast; wooden dowels simulated the vertical tie-down studs. To assure a smooth flat surface on the cast slabs, 1/2-inch steel plate was used on the mold surface which corresponds to the 6 x 6-foot loading surface of the slab specimen. All slab specimens were cast in the mold with what was to be the loaded face of the slab in contact with the bottom face of the mold.

The reinforcing bars were strain-gaged and the reinforcing cage assembled. The zigzag stirrups were tied with wire to the top and bottom longitudinal bars, and lifting hooks were wired to the stirrups at the quarter points of the span. The zigzag stirrups held the longitudinal bars firmly in position during the casting. Finally, the reinforcing cage was positioned in the mold by hydrostone cubes placed between the bars and the face of the mold.

To create holes in the slab for the tie-down studs, Shelby round seamless steel tubes with a length equal to the slab thickness were centered over the wooden dowels. The 20-gage metal tubes had inside diameters of 1.680 inches for the inner ring of tubes and 1.055 inches for the outer ring.

The concrete was mixed in a horizontal, nontilting, drum-type mixer of 16-cubic-foot capacity. Two batches of concrete were required to cast each 3- and 4.75-inch-thick slab; three batches were required for the 6-inch-thick slab. The concrete was vibrated internally with an electric probe-type vibrator.

The slabs and companion control cylinders were removed from their molds 4 days after casting and cured under wet burlap until about 6 days before testing. During the curing period, the burlap was watered once a day, 5 days a week; curing times are shown in Table 1.

Measurements

The type and location of measurements for each slab are shown in Figure 24. The applied load was measured at five points with 300-psi-capacity Dynisco pressure transducers (bonded strain gage type). A transducer was located at the quarter point of each diagonal of the slab. Located 1-1/2 inches from the face of the slab, the pressure-sensing diaphragm of the transducer was oriented perpendicular to the plane of the slab to measure the side-on overpressure.

Deflections were recorded at the center of the slab and sixth point of the span with Bourns Model 108 linear potentiometers. Potentiometer DC had a 10-inch deflection capacity; DE and DW had six-inch capacities (Figure 24).

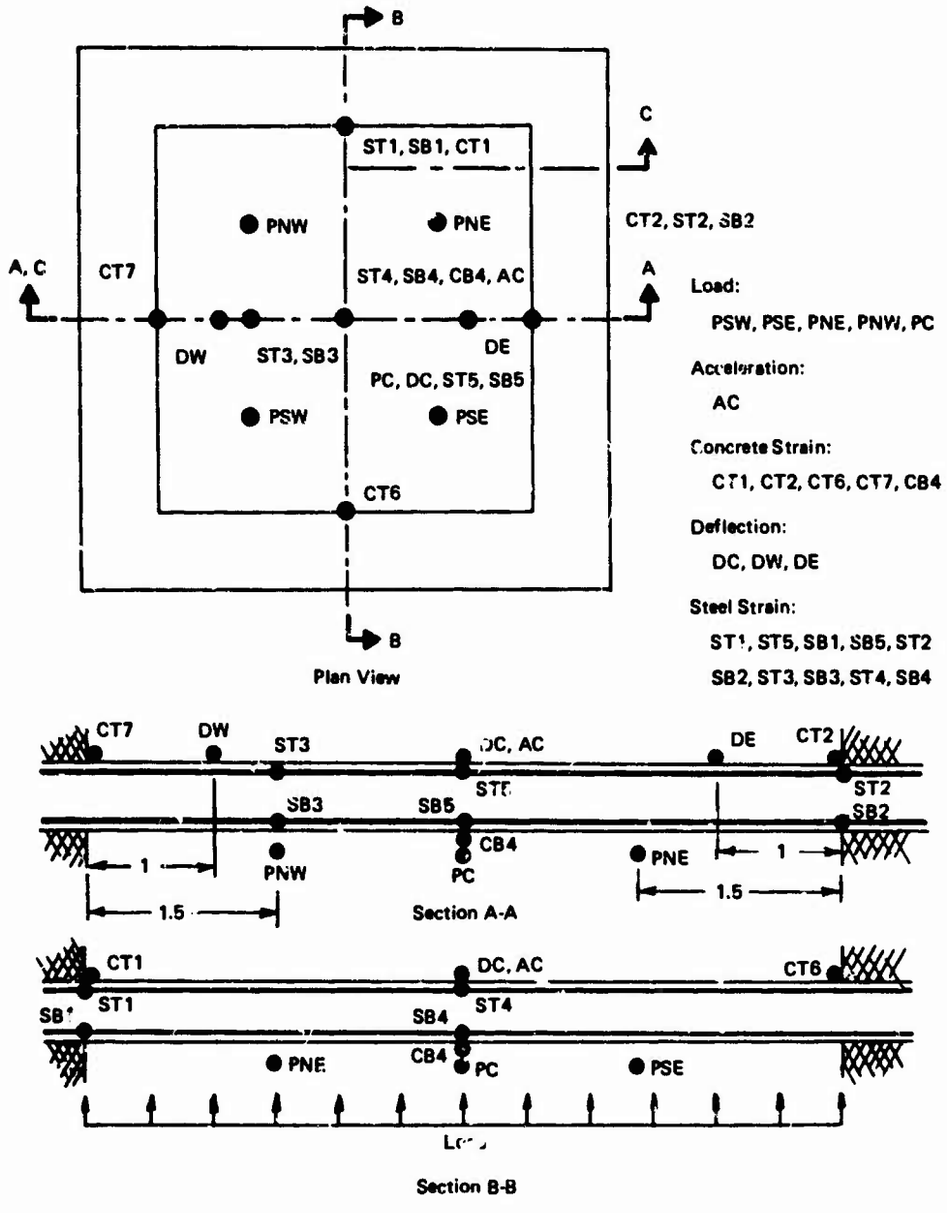

Figure 24. Details of instrumentation.

Acceleration of the center of the slab, AC (Figure 24), was recorded with a 300-g-capacity Statham accelerometer.

Steel strains were measured at the support line and center of the slab with Micro Measurement foil strain gages, type EA-06-500BH-120. Two gages were placed diametrically opposite each other on the bar and wired into opposite arms of a four-arm Wheatstone bridge circuit.

Concrete strains at the support line on the unloaded face of the slab were measured with Baldwin-Lima-Hamilton (BLH) wire strain gages, type A12. The concrete strain, CB4 (Figure 24), at the center of the slab on the loaded face was measured with a BLH wire strain gage, type A9-2.

Data Recording Equipment

All measurements were recorded on magnetic tape at a speed of 60 in./sec by a Honeywell Model LAR 7300 Laboratory Recorder. This is a seven-track, direct-record, multiple-speed tape recorder.

The data gathering system was a Model FMT 290 made by Vector Manufacturing Company. The system consists of seven racks (modules) of low-level voltage control oscillators with four channels per rack. Each rack contains four standard IRIG frequencies. The center frequencies are 70, 52.5, 40, and 30 kHz with a linear bandwidth of ±7.5% of the center frequency. The four frequencies were multiplexed onto one rack of the seven-track tape recorder.

Test Procedure

For the static tests, the uniform pressure on the slab was increased slowly and continuously until either the Franko water seal ruptured or the reinforcing steel commenced to fracture. To apply pressure to the slab, a positive displacement pump injected water into the cavity of the slab loader. During the loading cycle, a continuous trace of pressure versus center slab deflection was recorded by a Varian x - y plotter. This allowed a visual record of the stage of behavior as the test progressed. All other measurements were recorded at regular load increments on magnetic tape.

For the dynamic tests, the slabs were clamped to the slab loader, and each firing tube was loaded with the Primacord required to develop the desired peak overpressure. Steel plugs were threaded into the ends of each tube, and a blasting cap was inserted in the hole of each steel plug to make contact with the ends of the Primacord charge. The leads from each cap were wired in series to a master control circuit. Finally, a switch was closed to start an electromechanical sequence control timer which started the recording equipment, detonated the Primacord charge, and stopped the recording equipment. A continuous trace of measurements was recorded on magnetic tape.

After each test, damage was assessed, and the slab was photographed. It was then either removed from the loader or loaded again at a higher load level depending upon the damage.

RESULTS AND DISCUSSION

Data Reduction

The experimental data recorded on magnetic tape was reduced and plotted by the NCEL data reduction facility.[15] At the facility, the magnetic tape was played back by an Ampex FR-100 reproducer, through a Data Control Systems Discriminator to a Control Logic Incorporated Analog-to-Digital Converter, and finally into an IBM Data Processing System, IBM 1620-II. The computer output consisted of digitized data on punched cards and plots for each measurement at time intervals of 0.25 msec. Plots of most of the data are presented in Appendix C.

Static Resistance and Behavior

The resistance and deflection of the slabs under a uniformly distributed static load are given in Table 2 for the stages of behavior defined in Figure 25. The variations of resistance with the center deflection are shown in Appendix D (Figures D-1, D-2, and D-3). However, discrete data points are not shown in these figures; the curves were recorded as a continuous function during each cycle of loading. The point on each curve where the resistance decreases suddenly to zero does not necessarily correspond to total collapse of the slab. Instead, this point corresponds to rupture of one or more reinforcing bars and/or rupture of the Franko water seal caused by a combination of excessive slab deflections, large cracks, and disintegrated concrete.

Slabs 3S1 and 6S1 required more than one cycle of loading to failure. The first cycle of loading on 3S1 prematurely ruptured the Franko water seal at a center deflection of 4 inches. On the second cycle of loading, the resistance curve tended to follow the path of the resistance curve for the companion slab, 3S3, which received one loading cycle to failure. Slab 6S1 required nine cycles of loading (Figure D-3); each cycle terminated by a ruptured water seal. The envelope curve to the resistance diagrams (Figure D-3) is an estimate of the flexural resistance diagram for slab 6S1. The envelope curve is distorted by a local "dimple" failure in the slab; the ninth cycle of loading caused a center area (roughly 2s by 2s inches square) of the slab to dimple outward. This local dimpling effect produced larger deflections at midspan for a given resistance level than if this effect had not been present.

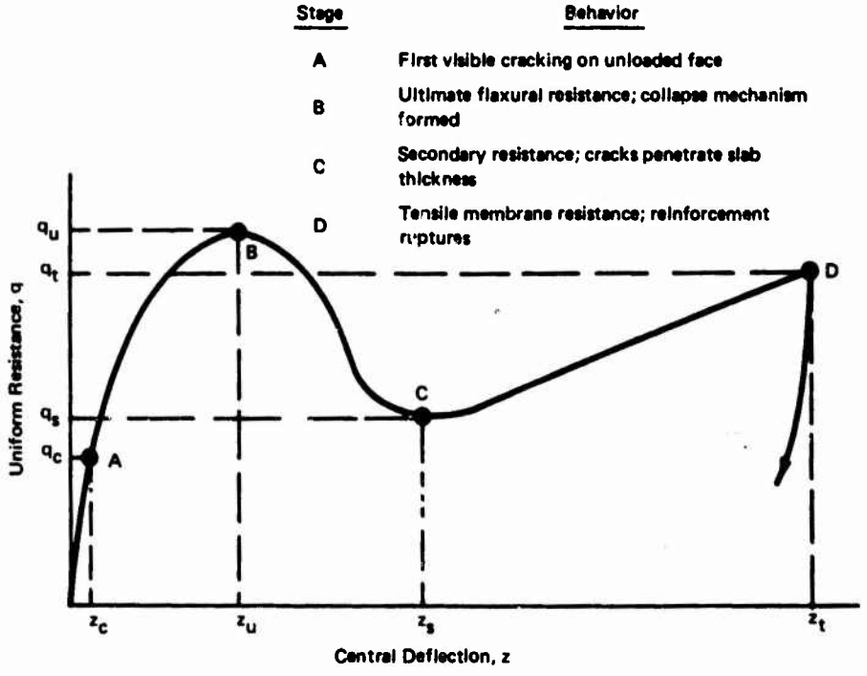

Figure 25. Stages of behavior defined for slab with longitudinal edge restraint.

The shape of the resistance-deflection curve is similar for all slabs. However, the reduction in resistance after developing the ultimate flexural resistance was least for the slab with the highest reinforcement ratio (6S1). This finding agrees with the trend shown in Figure 19 and test results reported by MIT.[6]

Elastic Stiffness. In the early stages of loading, restraint against outward movement of the edges induced compressive membrane forces in the plane of the slab. These forces delayed the onset of flexural cracking and increased the elastic stiffness of the slab.

For the case of a uniformly distributed load, **q**, the elastic stiffness, **k**, relative to the deflection at the center of the slab, **z**, is given by the equations in Table 3. For the slabs loaded statically, the stiffness computed from the equations listed in Table 3 is compared with the measured stiffness in Figure 26. The computed stiffness is based on $\mu = 0.2$ and the modulus of elasticity, E_c, recommended by the current ACI Building Code.[13] It is clear from Figure 26 that the line with slope k_{fc} gives the best approximation of the elastic behavior of the test slabs. The stiffness of the thickest slab, 6S1, was much less than the computed values. This disparity can be attributed to the shear deformations in the slab which are not considered in the theory.

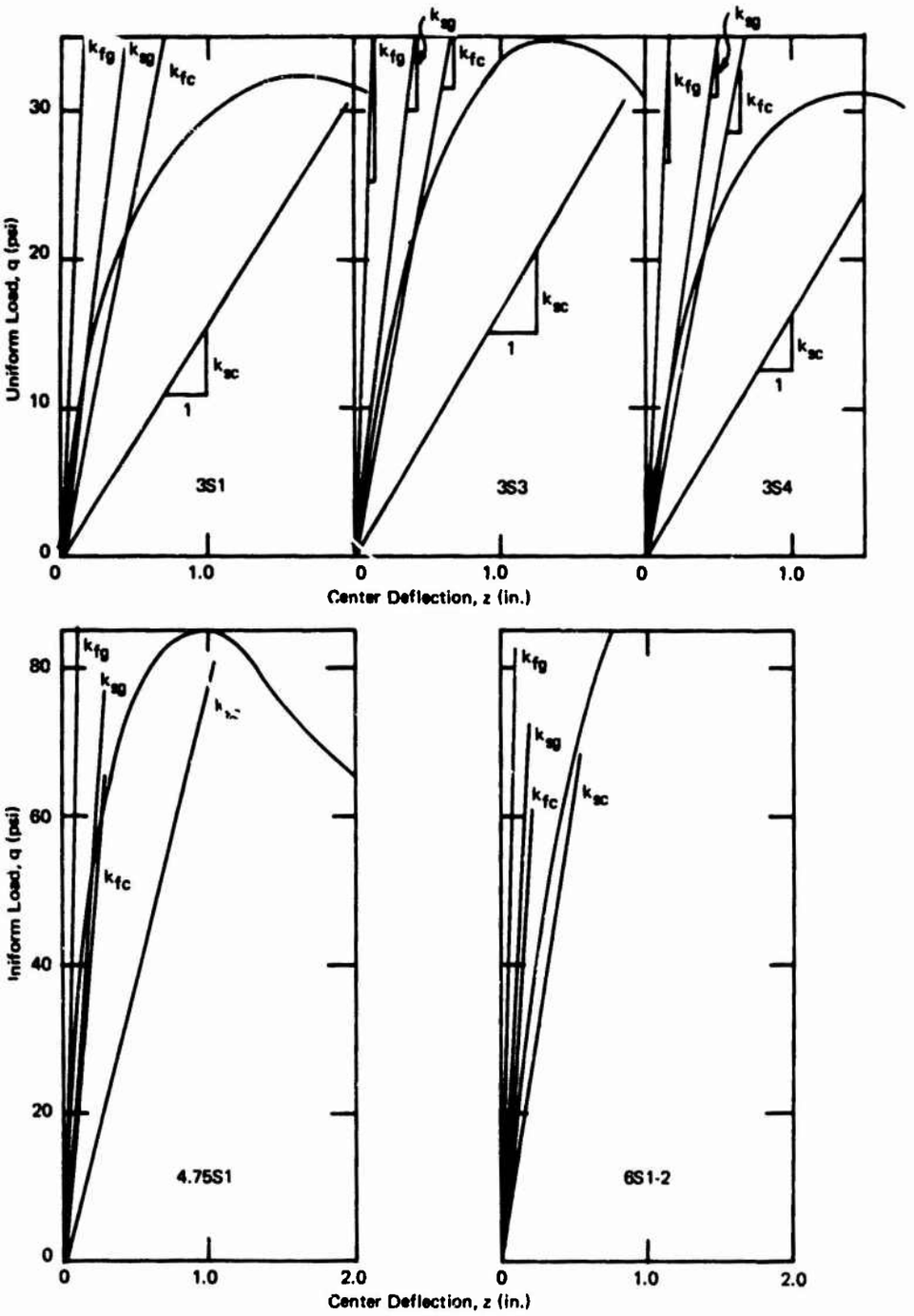

Figure 26. Comparison between measured and computed stiffness.

Table 2. Measured Static Resistance and Deflection At Various Stages of Behavior

(Stages of behavior defined in Figure 25.)

Slab No.	First Visible Cracking				Ultimate			Secondary				Tensile Membrane			
	Resistance		Deflection		Resistance	Deflection		Resistance		Deflection		Resistance		Deflection	
	q_c (psi)	q_c/q_u (%)	z_c (in.)	z_c/t	q_u (psi)	z_u (in.)	z_u/t	q_s (psi)	q_u/q_s	z_s (in.)	z_s/t	q_t (psi)	q_t/q_u	z_t (in.)	z_t/t
3S1	16	49	0.29	0.10	32.4	1.52	0.51	20.1	1.61	3.75	1.25	29.0	0.90	5.50	1.83
3S2	12	51	0.19	0.06	23.5	1.00	0.33	0.0	—	—	—	—	—	—	—
3S3	18	52	0.32	0.11	34.6	1.36	0.45	16.6	2.08	3.25	1.08	42.5	1.23	8.50	2.84
3S4	17	53	0.31	0.10	32.1	1.35	0.45	21.0	1.54	4.00	1.33	30.5	0.95	8.02	2.68
4.75S1	39	46	0.17	0.04	85	0.92	0.20	50.0	1.70	3.60	0.76	74.0	0.87	6.88	1.45
6S1	92	51	0.25	0.04	182	1.10*	0.18*	143.0	1.27	—	—	—	—	—	—

* Average value from seventh and ninth cycle of loading.

Table 3. Equations for Stiffness of Slabs Under Uniform Load

Type of Support	Type of Cross Section	
	Gross Nontransformed	Cracked Transformed
Simple	$k_{sg} = \frac{E_c}{(1-\mu^2)L^4}\left(\frac{I_g}{0.00406}\right)$	$k_{sc} = \frac{E_c}{(1-\mu^2)L^4}\left(\frac{I_c}{0.00406}\right)$
Fixed	$k_{fg} = \frac{E_c}{(1-\mu^2)L^4}\left(\frac{I_g}{0.00126}\right)$	$k_{fc} = \frac{E_c}{(1-\mu^2)L^4}\left(\frac{I_c}{0.00126}\right)$

Note: the constants 0.00406 and 0.00126 were taken from Tables 35 and 8 of Reference 16 and do not account for the effect of lateral edge restraint.

Concrete Cracking and Failure Mode. The onset of cracking in the loaded face of each slab could not be recorded, because the loaded face was covered by the Franko water seal. The amount of static resistance at which cracks became visible on the unloaded face is listed in Table 2. Note that first cracking appeared at a resistance ranging from 46 to 53% of the measured ultimate flexural resistance.

The growth of cracks in each slab followed the same general pattern. Hairline cracks first appeared near the center of the slab and extended outward a short distance in every direction toward the edges. Cracks forming parallel to the diagonals increased rapidly in length and number with increasing deflection. These cracks lengthened to within about 11 inches of the slab corners where most of the cracks fanned out and terminated short of the support line. When crushing of concrete initiated along the support lines, the number and width of cracks along the diagonals increased rapidly. Crushing generally started near the center of each support line and progressed toward and across each corner. This general pattern of cracking and disintegration of concrete continued until the collapse mechanism had formed sufficiently to develop the ultimate flexural resistance and cause a drop in resistance with further deflection.

As the slab resistance decreased to a secondary resistance level (Figure 25), slab deflections increased, causing tension cracks to spread into all quadrants of the slab. At this stage of behavior, tension cracks following the path of the reinforcing bars were widest, particularly near the center of the slab. Water began leaking through the slab to the unloaded face, indicating

that many of these cracks penetrated the entire depth of the slab. The initial stage of tensile membrane behavior was quite obvious. Concrete crushing was now severe along the support line, particularly near each corner of the slab.

Acting as a tensile membrane, the slab resistance increased gradually with further deflection until one or more reinforcing bars ruptured in tension—near the center of a support line—and/or the Franko water seal burst. At this point the loading was terminated. The extent of cracked and crushed concrete at this stage of behavior is shown by the photographs in Appendix E. Note the ruptured steel (Figures E-10 and E-13) and the relative displacement of the slab near the center of each support line (Figure E-6); these were caused by the slab taking the shape of a tensile membrane. The photographs show the least damage in slab 6S1, but the maximum deflection of this slab was only 0.75t inch; whereas, the maximum deflection was more than 1.5t inches for all other slabs.

The extent of cracking and crushed concrete at two different stages of tensile membrane behavior can be compared in the photographs of slabs 3S1 (Figure E-1) and 3S3 (Figure E-3). The photographs were taken after a maximum center deflection of 1.8t inches for slab 3S1 and 2.8t inches for 3S3.

Deflection Profile. Deflection profiles of slab 3S4 at several levels of resistance are shown in Figure D-5. Observe that the deflection profile consists of two nearly straight lines for center deflections near the ultimate flexural resistance of the slab (q_u = 32.5 psi). This observation supports a major assumption upon which the theory for the ultimate flexural resistance was formulated; namely, the quadrants of the collapse mechanism are a plane surface.

Ultimate Deflection. The theory showed that the resistance of a longitudinally restrained slab is deflection sensitive; the ultimate flexural resistance depends upon the center deflection required to develop the collapse mechanism. Therefore, the accuracy of any method for predicting the ultimate flexural resistance depends, in part, upon the accuracy of Equation 15 for predicting the ultimate deflection.

Ultimate deflections computed from Equation 15 are compared with measured values in Table 4. The comparison includes NCEL slabs and longitudinally restrained square slabs tested by MIT[6] and Wood.[4] Instead of solving Equation 15 directly by assuming $f_s = f'_s = f_y$, exact solutions were obtained by an iteration procedure involving f_s and f'_s with the aid of an IBM 1620 computer. The computed stresses in the steel are listed in Table 5.

It appears that the disparity between the measured and computed ultimate deflection (Table 4) increases as the ratios, N_{ue}/N_{be} and/or N_{ud}/N_{bd} (Table 5), approach and exceed the value 1.0. This is reasonable to expect since (1) Equation 15 does not apply for $N_u/N_b > 1$, and (2) the thrust-moment interaction diagram is most sensitive to the limiting strain capacity of the concrete for thrust levels near the balanced thrust (see Figure 4). This observation suggests that in design, the cross section should be proportioned so that the average thrust induced along a hinge line is less than about 80% of the balanced thrust. This requirement is also important to insure that sections along the hinge lines have (1) sufficient rotational capacity to fully develop the collapse mechanisms, and (2) adequate shear resistance to prevent a premature failure. In certain cases, the average shear stress based on the depth of "effective" concrete (c_e) can increase as the thrust approaches or exceeds the balanced thrust. For such cases, the shear stress can exceed the shear resistance of the section and cause a premature shear failure before the section has rotated sufficiently to develop the flexural collapse mechanism. For example, for MIT slabs 47 and 49 which failed in shear, the ratio N_u/N_b exceeded 1.0. At some ratio of center deflection to slab thickness the compressive membrane forces induced in the slab reach a limiting value, regardless of the span-thickness ratio. In other words, the ultimate deflection given by Equation 15 must be bounded by an upper limiting value. According to Equation 15, the upper bound for z_u/t is $1 + q_e d_e/tk_1 - q_e d_d/tk_1$ which corresponds to large values of L/t. However, the test data plotted in Figure 27 suggests that the limiting value of z_u/t is a value much less than 1.0. An empirical value for the limiting ultimate deflection based on the correlation shown in Figure 27 is

$$\frac{z_u}{t} < 0.42 \qquad (19)$$

Equation 19 implies that compressive membrane forces induced in a slab are maximum at $z_u/t \leq 0.42$. For identical sections along the edge and diagonal of the slab, Equation 19 controls for $L/t > 18$.

Ultimate Flexural Resistance. All slabs failed in a flexural mode under static pressures greater than the capacity computed on the basis of simple yield line theory (Equation 18). The measured resistance at various stages of behavior is compared with Equation 18 in Table 6. The ratio of measured ultimate flexural resistance to yield-line resistance (q_u/q_y) ranged from 1.34 to infinity (for the slab with no steel reinforcement). This ratio increased with decreasing steel percentages in accordance with the trend shown in Figure 19.

Table 4. Theoretical Versus Measured Deflection and Resistance At Ultimate Strength of Slab

Slab No.	Failure Mode at Ultimate	Steel Strength, f_y (ksi)	Concrete Strength, f'_c (psi)	Slab Thickness, t (in.)	Span-Thickness Ratio, L/t	Reinforcement*								Ultimate Defl	
						Edge				Diagonal				Measured, z_u/t	Theory, z_u/t
						p_e (%)	d_e (in.)	p'_e (%)	d'_e (in.)	p_d (%)	d_d (in.)	p'_d (%)	d'_d (in.)		
3S1	Flexural	49.6	3,550	3.00	24.0	0.815	2.25	0.815	0.75	0.815	2.25	0.815	0.75	0.51	0.420
3S2	Flexural	—	4,140	3.00	24.0	0.0	—	0.0	—	0.0	—	0.0	—	0.33	0.420
3S3	Flexural	49.6	4,120	3.00	24.0	0.815	2.25	0.815	0.75	0.815	2.25	0.815	0.75	0.46	0.420
3S4	Flexural	49.6	3,295	3.00	24.0	0.815	2.25	0.0	—	0.815	2.25	0.0	—	0.45	0.420
4.75S1	Flexural	47.4	3,165	4.75	15.2	0.889	3.75	0.889	1.00	0.889	3.75	0.889	1.00	0.20	0.249
6S1	Flexural	47.4	3,615	6.00	12.0	1.33	5.00	1.33	1.00	1.33	5.00	1.33	1.00	0.18‡	0.148
MIT 42§	Flexural	—	5,060	0.75	20	0.0	—	0.0	—	0.0	—	0.0	—	0.48	0.420
MIT 44§	Shear	—	4,320	0.75	20	0.0	—	0.0	—	0.0	—	0.0	—	0.36	0.420
MIT 46§	Flexural	60.0	5,490	0.75	20	0.0	—	1.0	0.19	1.00	0.56	0.0	—	0.43	0.420
MIT 47§	Shear	55.0	4,570	1.50	10	0.0	—	1.0	0.28	1.00	1.22	0.0	—	0.10	0.141
MIT 48§	Flexural	60.0	4,870	0.75	20	0.0	—	2.0	0.19	2.00	0.56	0.0	—	0.56	0.420
MIT 49§	Shear	55.0	4,620	1.50	10	0.0	—	2.0	0.28	2.00	1.22	0.0	—	0.11	0.192
FS 12**	Flexural	33.8	4,550††	2.25	30.2	0.0	—	0.26†	0.44	0.26	1.81	0.0	—	0.40	0.42
FS 13**	Flexural	33.8	3,700††	2.25	30.2	0.26	1.81	0.26	0.44	0.26	1.81	0.26	0.44	0.40	0.42

* Depths listed are mean values.

† Difference between measured and theoretical ultimate resistance attributed to compression steel near corners of slab (see Figure 21); this was neglected in calculations.

‡ Premature local "dimple" failure near center of slab.

§ Reference 6.

¶ Shear failure.

** Reference 4.

†† Based on $f'_c = 0.77\,u$, where u = reported cube strength; coefficient 0.77 recommended by Wood (Reference 4).

sus Measured Deflection and Resistance At Ultimate Strength of Slab

Reinforcement*								Ultimate Deflection			Ultimate Flexural Resistance		
Edge				Diagonal				Measured, z_u/t	Theory, z_u/t	Measured / Theory	Measured, q_u (psi)	Theory, q_u (psi)	Measured / Theory
p_e (%)	d_e (in.)	p_e' (%)	d_e' (in.)	p_d (%)	d_d (in.)	p_d' (%)	d_d' (in.)						
0.815	2.25	0.815	0.75	0.815	2.25	0.815	0.75	0.51	0.420	1.21	32.2	30.4	1.06
0.0	–	0.0	–	0.0	–	0.0	–	0.33	0.420	0.79	23.6	21.8	1.08
0.815	2.25	0.815	0.75	0.815	2.25	0.815	0.75	0.45	0.420	1.07	34.6	33.3	1.04
0.815	2.25	0.0	–	0.815	2.25	0.0	–	0.45	0.420	1.07	32.1	25.6	1.24†
0.889	3.75	0.889	1.00	0.889	3.75	0.889	1.00	0.20	0.249	0.81	85.0	88.7	0.96
1.33	5.00	1.33	1.00	1.33	5.00	1.33	1.00	0.18‡	0.148	1.21‡	182.0‡	214.7	0.85‡
0.0	–	0.0	–	0.0	–	0.0	–	0.48	0.420	1.14	35.6	36.4	0.98
0.0	–	0.0	–	0.0	–	0.0	–	0.36	0.420	¶	26.0	31.2	¶
0.0	–	1.0	0.19	1.00	0.56	0.0	–	0.43	0.420	1.02	59.5	47.8	1.24
0.0	–	1.0	0.28	1.00	1.22	0.0	–	0.10	0.141	¶	209.0	222.0	¶
0.0	–	2.0	0.19	2.00	0.56	0.0	–	0.56	0.420	1.33	55.0	47.2	1.16
0.0	–	2.0	0.28	2.00	1.22	0.0	–	0.11	0.192	¶	220.0	228.0	¶
0.0	–	0.26	0.44	0.26	1.81	0.0	–	0.40	0.42	0.96	15.4	15.5	0.99
0.26	1.81	0.26	0.44	0.26	1.81	0.26	0.44	0.40	0.42	0.96	13.2	13.7	0.97

ed to compression steel near corners of slab (see Figure 21); this was neglected in calculations.

recommended by Wood (Reference 4).

Table 5. Theoretical Thrust, Moments, and Steel Stresses At Ultimate Strength of Slab

Slab No.	Thrusts						Moments						Steel Stresses			
	Corner			Center			Edge			Diagonal			Edge		Diagonal	
	N_{ue}/t (ksi)	N_{be}/t (ksi)	N_{ue}/N_{be}	N_{ud}/t (ksi)	N_{bd}/t (ksi)	N_{ud}/N_{bd}	$\bar{M}_{ue}/t^2$ (ksi)	M_{ye}/t^2 (ksi)	$\bar{M}_{ue}/\bar{M}_{ye}$	$\bar{M}_{ud}/t^2$ (ksi)	M_{yd}/t^2 (ksi)	$\bar{M}_{ud}/M_{yd}$	f_{se} (ksi)	f'_{se} (ksi)	f_{sd} (ksi)	f'_{sd} (ksi)
3S1	1.20	1.250	0.96	0.95	1.250	0.76	0.474	0.230	2.06	0.474	0.230	2.06	49.6	48.8	49.6	48.8
3S2	1.38	1.625	0.85	1.09	1.625	0.67	0.374	0.0	∞	0.374	0.0	∞	–	–	–	–
3S3	1.38	1.425	0.97	1.09	1.425	0.76	0.522	0.240	2.17	0.522	0.240	2.17	49.6	48.8	49.6	48.8
3S4	0.82	0.850	0.97	0.68	0.850	0.68	0.376	0.210	1.79	0.376	0.210	1.79	49.6	–	49.6	–
4.75S1	1.08	1.200	0.90	0.95	1.200	0.75	0.487	0.245	1.99	0.487	0.245	1.99	47.4	47.4	47.4	47.4
6S1	1.22	1.425	0.85	1.13	1.425	0.79	0.689	0.390	1.76	0.689	0.390	1.76	47.4	47.4	47.4	47.4
MIT 42*	1.66	2.00	0.85	1.31	1.95	0.67	0.452	0.0	∞	0.452	0.0	∞	–	–	–	–
MIT 44*	1.43	1.70	0.86	1.13	1.67	0.68	0.389	0.0	∞	0.389	0.0	∞	–	–	–	–
MIT 46*	1.64	2.60	0.64	1.27	1.275	0.99	0.485	0.05	9.7	0.601	0.310	1.94	–	29.4	50.3	–
MIT 47*	1.45	2.25	0.65	1.34	1.20	1.12	0.479	0.05	9.6	0.545	0.335	1.63	–	48.1	44.2	–
MIT 48*	1.21	2.75	4.40	0.87	0.65	1.34	0.372	0.10	3.7	0.620	0.562	1.10	–	9.6	44.6	–
MIT 49*	1.26	2.70	4.67	1.11	0.75	1.48	0.429	0.10	4.3	0.636	0.615	1.04	–	26.4	39.6	–
FS 12**	1.51	1.80	0.84	1.12	1.65	0.68	0.425	0.012	35.4	0.436	0.055	7.9	–	33.8	33.8	–
FS 13**	1.22	1.40	0.87	0.97	1.40	0.69	0.372	0.065	5.7	0.372	0.065	5.7	33.8	33.8	33.8	33.8

* Reference 3.

** Reference 4.

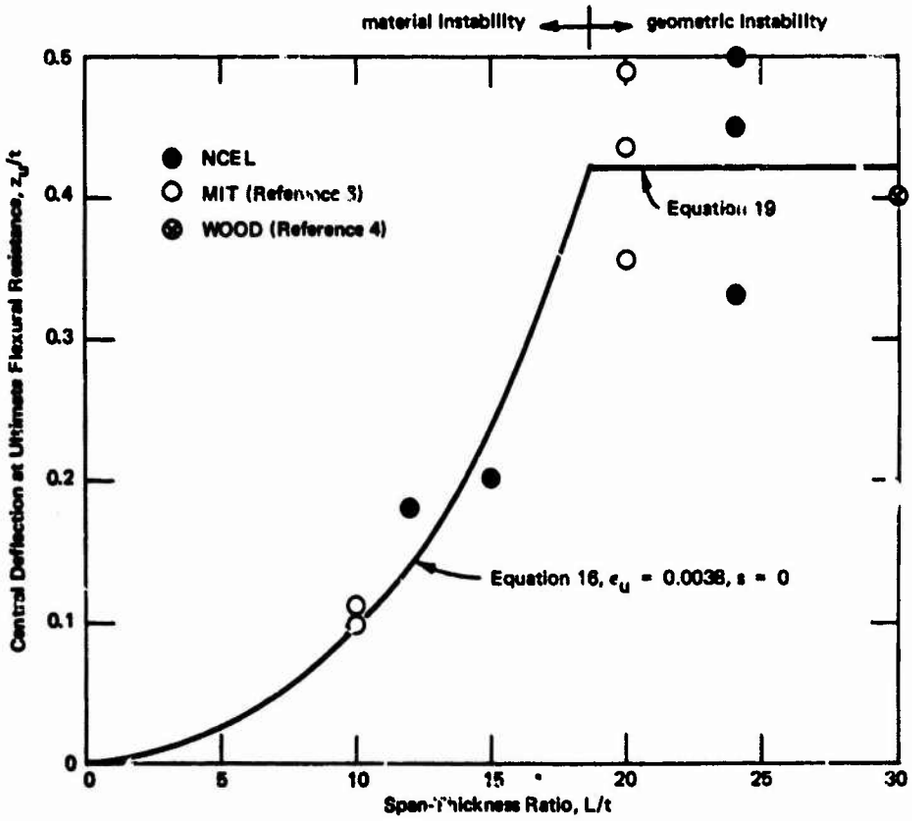

Figure 27. Central deflection at ultimate flexural resistance.

The ratio q_u/q_y shown in Table 6 is greater for slab 3S4 ($p'/p = 0$) than for slabs 3S1 and 3S3 ($p'/p = 1$). This finding confirms the trend shown in Figure 19 which indicates that for small tensile reinforcement ratios, the enhancement factor decreases as p'/p increases.

The effect of longitudinal edge restraint on ultimate flexural resistance is obvious from the behavior of slab 3S2 which had no reinforcement. To develop the same resistance, this slab without longitudinal edge restraint would require approximately 1.05% of steel (based on simple yield line theory). Note also that slab 3S2 had no shear reinforcement but was still capable of developing a flexural collapse mechanism (see Figure E-2).

Table 4 compares the measured ultimate flexural resistance with the resistance computed from Equation 17. The disparity is greatest for slab 3S4. This is attributed to the reinforcement, in the unloaded face of the slab (see Figure 21), which acted as compression steel near the corners and along the ends of each diagonal.

Interaction diagrams for cross sections of the slabs listed in Table 4 are shown in Figures 28 through 31. Each diagram is marked with the theoretical coordinates of the induced average thrust and corresponding

Table 6. Measured and Computed Secondary Resistance and Deflection

Slab No.	Yield Line Resistance,* q_y (psi)	Ratio Measured To Yield Line Resistance†			Deflection At Secondary Resistance, z_s‡			
		Cracking, q_c/q_y	Ultimate, q_u/q_y	Secondary, q_s/q_y	Measured, z_s (in.)	k = 20, $f_s = f_y$§ (in.)	k = 13.5¶	
							$f_s = f_u$ (in.)	$f_s = f_y$ (in.)
3S1	19.2	0.83	1.67	1.03	3.75	2.74	3.00	4.05
3S2	0.0	∞	∞	—	—	—	—	—
3S3	20.0	0.90	1.73	0.83	3.25	2.83	3.10	4.20
3S4	17.6	0.96	1.82	1.20	4.00	5.00	5.40	7.40
4.75S1	51.2	0.76	1.66	0.98	3.60	4.20	4.20	6.22
6S1	136.0	0.67	1.34	1.04**	5.10**	5.56	5.60	8.26

* From Equation 18, using values of M_{ye} and M_{yd} given in Table 5.

† q_c, q_u, q_s are measured values listed in Table 2.

‡ From Equation 21.

§ Empirical value based on best agreement between experiment and theory.

¶ Theoretical value for square slab (Reference 17).

** Based on extrapolation of resistance diagram (q_s = 142 psi, z = 5.10 in.).

moment resistance of sections along the edges and diagonals of the slab when the flexural collapse mechanism forms. According to the diagrams for the NCEL slabs (Figure 28), all slabs were under-reinforced ($N_u < N_b$). Yet the induced average thrust was great enough to enable sections along the edges and diagonals to develop nearly the optimum moment resistance of the section, M_B. By comparison, Figure 29 shows that all reinforced MIT slabs were over-reinforced (MIT slabs 42 and 44 did not have any steel reinforcement); the induced thrust was greater than the balanced thrust. This implies that the MIT slabs had limited rotational capacity along the hinge lines and formed a brittle "collapse mechanism." The mode of failure (Table 4) and shape of the resistance diagrams for MIT slabs 47 and 49 (Figure 11 of Reference 6) confirm the behavior indicated by Figure 29. Thus, the cross section of a longitudinally restrained slab should be designed so that the induced average thrust at ultimate is less than N_b. This will prevent the formation of a brittle collapse mechanism which can precipitate a premature shear failure from disintegration of concrete, particularly in slabs having a low span-thickness ratio where shear stresses are high.

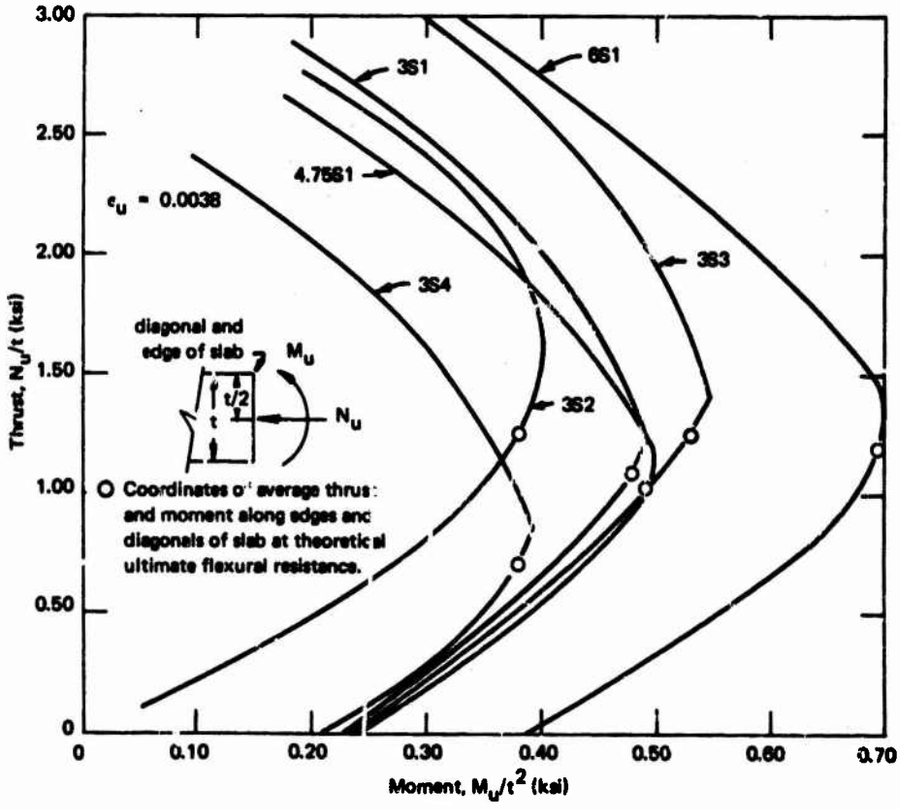

Figure 28. Moment-thrust interaction curves for NCEL slabs.

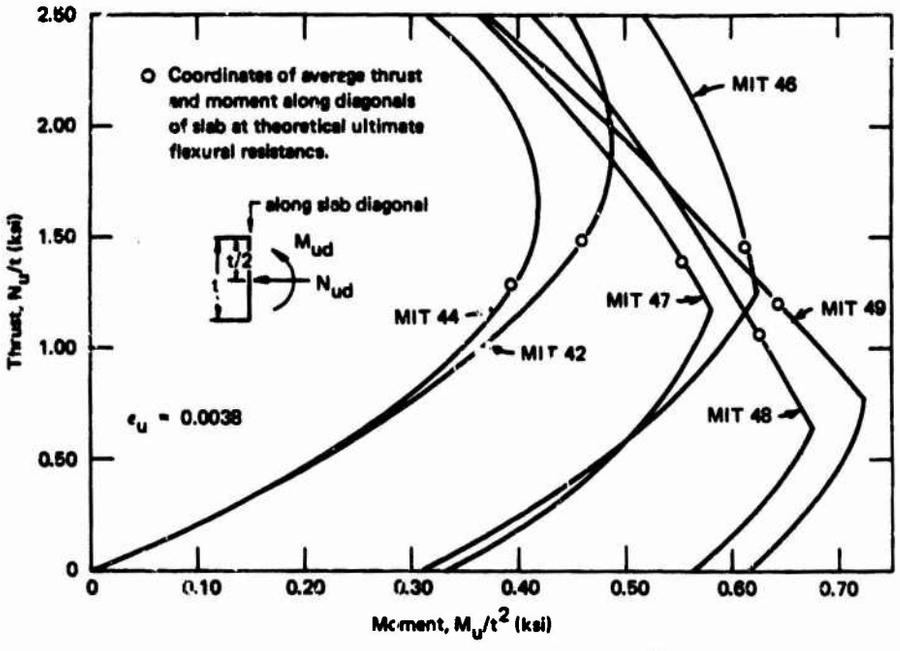

Figure 29. Moment-thrust interaction curves for MIT[6] slabs (diagonal).

Secondary Resistance and Deflection. After the collapse mechanism formed, the slab resistance decreased. Further deflection of the slab and/or disintegration of concrete along hinge lines decreased the compressive membrane forces which, in turn, reduced the moment resistance of sections along hinge lines. This reduction in moment resistance lowered the slab resistance to a secondary resistance level (point C in Figure 25).

The secondary resistance level, q_s, very nearly corresponded with the simple yield line resistance, q_y, as shown in Table 6. This equivalence is reasonable since the minimum resistance should correspond to a change of membrane forces from compression to tension in the central region of the slab.

Since $q_r/q_y \approx 1$, then $q_u/q_s \approx q_u/q_y$. Therefore, the curves plotted in Figure 19 show the effect of span-thickness ratio and reinforcement ratio on the reduction in slab resistance after the collapse mechanism forms.

The test results support the trend shown by the curves in Figure 19. For example, the ratio q_u/q_s (Table 2) was smallest for slab 6S1 which had the most steel ($p = 1.33\%$) and largest for slab 3S2 which had the least steel ($p = 0\%$).

The effect of slab properties and level of induced thrust on the drop in resistance is illustrated in Figure 32. Three cases are considered in the figure: (1) $N_u < N_b$ and $p < p_b$; (2) $N_u < N_b$ and $p \cong p_b$; and (3) $N_u > N_b$ and $p < p_b$.

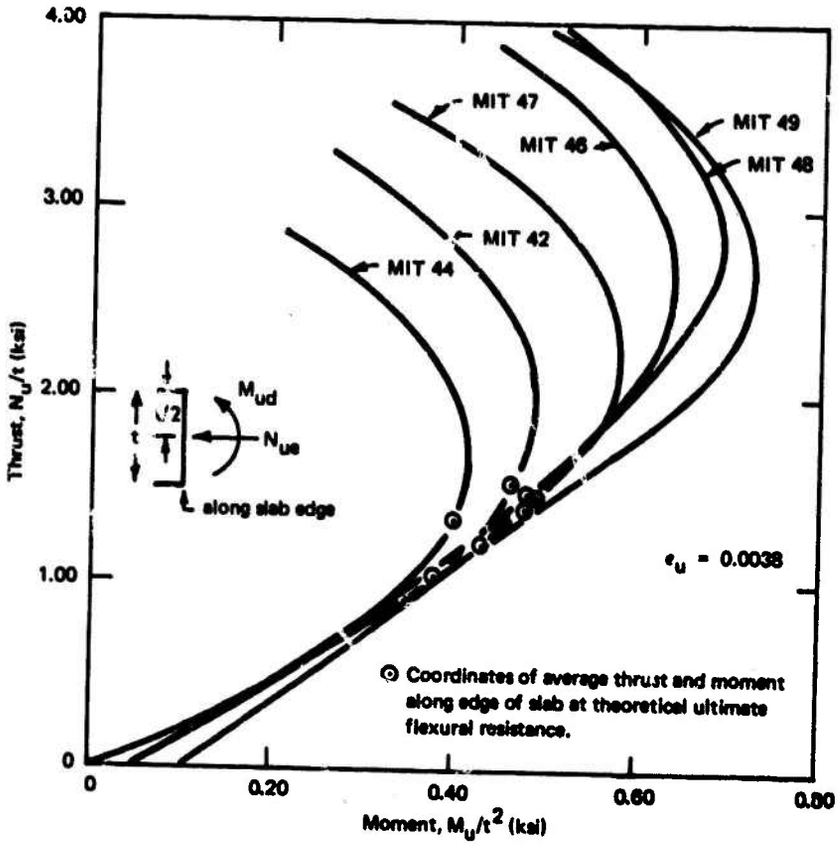

Figure 30. Moment-thrust interaction curves for MIT[6] slabs (edge).

Consider case 1 in Figure 32. An increasing static load on a slab causes the thrust and moments along hinge lines to follow path A-B shown on the interaction diagram. At point B, the ultimate flexural resistance is developed; the collapse mechanism forms and concrete begins to crush along the hinge lines. Further deflection of the slab causes the induced thrust and moment resistance to decrease along path B-C. At point C, the thrust is zero and $q = q_y$. More deflection produces negative thrust and positive moments which together cause the resistance to begin increasing again. Case 2 is similar to case 1 except the reinforcing index, pf_y/f'_c, is such that M_B is only slightly greater than M_y. Therefore, the drop in resistance for case 2 is much less than for case 1, as illustrated by the resistance diagram in Figure 32.

For case 3, $N_u > N_B$. Therefore, the induced thrust and moment resistance along hinge lines correspond to point B'' when the collapse mechanism forms. Because the slab resistance drops after reaching B'', the thrust and moment must decrease from B'' along some path B''-C''. The moment resistance along hinge lines at point C'' is shown to be less than M_y because the degree of crushing at point B'' can reduce the depth of

effective concrete along hinge lines. Thus, the moment resistance at point C'' would be less than M_y, causing q_s to be less than q_y as shown in the resistance diagram.

Park[17] developed expressions for the resistance of uniformly loaded slabs acting as a tensile membrane. The theory assumes that the reinforcement acts as a plastic membrane and the concrete is ineffective. For the case of a square slab, Park's expression for the resistance in terms of the center deflection is

$$q = k(p + p')\frac{d f_s}{L^2} z \qquad (20)$$

For $q = q_s = q_y$, $z = z_s$ and from Equation 20, an expression for the center deflection corresponding to the secondary resistance level is

$$z_s = \frac{(L/d)^2 d q_y}{k(p + n') f_s} \qquad (21)$$

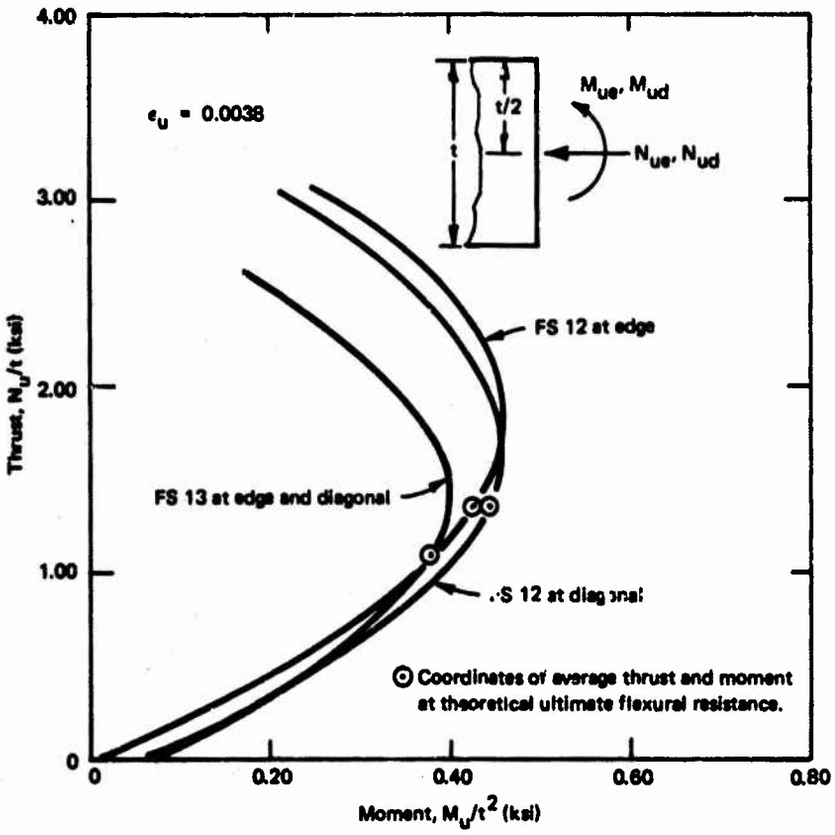

Figure 31. Moment-thrust interaction curves for Wood's[4] slabs.

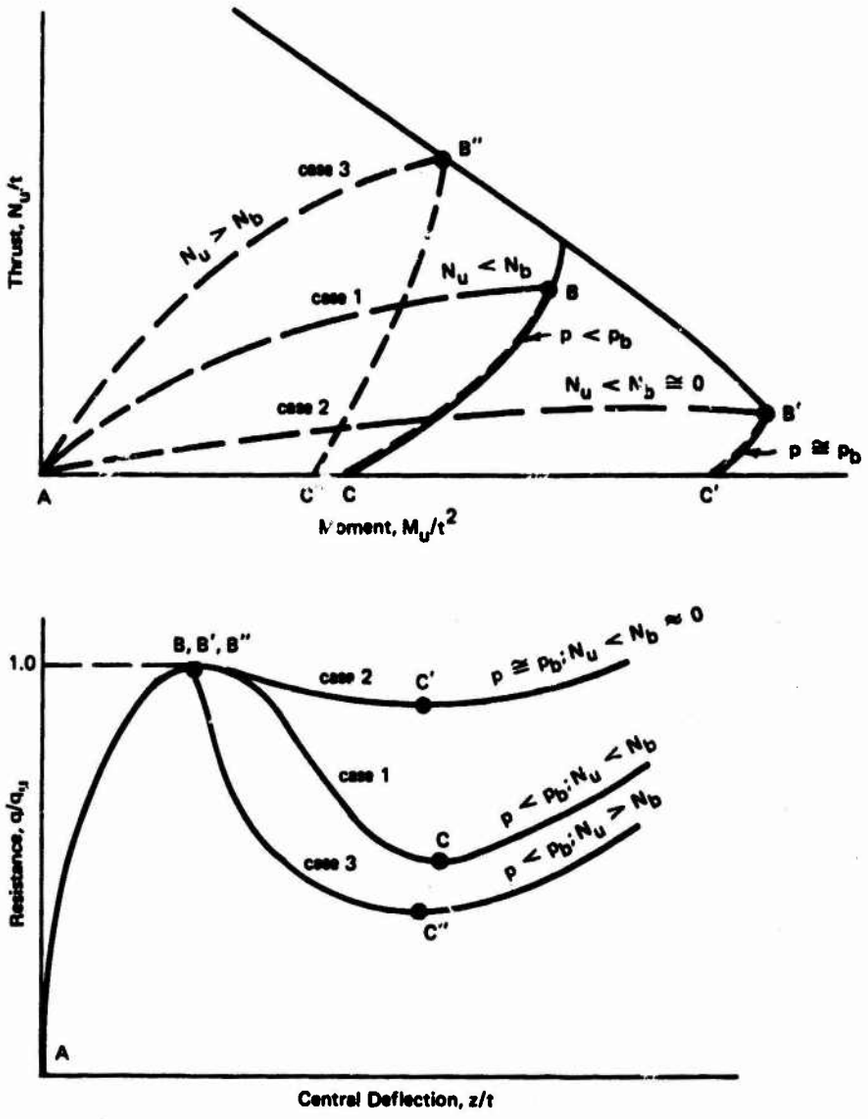

Figure 32. Effect of thrust and reinforcement ratio on secondary resistance level.

The secondary resistance deflection, z_s, computed from Equation 21, is compared with measured values in Table 6. For a square slab, k = 13.5, based on pure tensile membrane action.[17] However, it is evident from the pattern of cracking in the slabs (Appendix E) and from test results reported by Park[17] that pure membrane action does not occur, particularly in deep slabs and at slab deflections near the secondary resistance level. In fact, based on the deflection profiles shown in Figure D-5, the slab surface is more nearly a mechanism of plane quadrants instead of a pure tensile membrane at $z = z_s$.

Therefore, the distribution of thrust is closer to that shown in Figure 17. This means compressive forces can still exist near the corners when tensile forces act in the central region. These compressive forces near the corners can significantly enhance the slab resistance as illustrated by Wood's "perspex" model of a slab mechanism (see Reference 4, Plate VIII). The error in Equation 21 from assuming the slab is a pure membrane, particularly in deep slabs, was adjusted by the factor k (Equation 21). Table 6 shows that $k = 20$ yielded the best correlation with measured values of z_s. Another major source of error in Equation 21 stems from the assumed steel stress, f_s. The steel stress may be closer to f_u when $z = z_s$, but it seems more logical to assume, in Equation 21, that $f_s = f_y$, based on the agreement between the measured value of q_s and q_y (Table 6).

Tensile Membrane Resistance and Collapse. Near C on the resistance diagram (Figure 25), the membrane forces in the central region of the slab began to change from compression to tension. Beyond C, the tensile membrane region grew outward toward the supports which began to resist inward movement at the edges. Cracks began to penetrate the entire depth of the concrete, and yielding of reinforcement spread throughout this region. The top and bottom reinforcement acted as a tensile membrane, causing the slab resistance to increase with deflection until the reinforcement began to rupture. The resistance and deflection at collapse are listed in Table 2.

The extent of tensile membrane action in the 3- and 4-3/4-inch-thick slabs is obvious from the amount of cracking (see Appendix E). Tensile membrane action was minor in slab 6S1; the extent of cracking at the end of testing (Figure E-7) was slightly more than when the ultimate flexural resistance was developed. However, in terms of either span length or thickness, slab 6S1 was deflected much less than the other slabs.

Park[17] found that a safe, maximum value for the central deflection after tensile membrane action is:

$$z_t = 0.1\,L \qquad (22)$$

For the test slabs, Equation 22 yields $z_t = 7.2$ inches. This is a reasonable value based on those listed in Table 2.

The tensile membrane resistance of a square slab in terms of the center deflection is given by Equation 20. This equation gives a conservative estimate of the resistance carried by tensile membrane action for $f_s = f_u$.

Dynamic Behavior

Three slabs were subjected to dynamic loads. Slab 3D1 required three cycles of loading to failure. The third loading caused a local failure; concrete missile fragments were blasted loose from the reinforcing mesh. Slabs 4.75D1 and 4.75D2 were subjected to seven and five cycles of loading, respectively. Both slabs received very little damage prior to the last cycle of loading (see Figure E-9). However, the last cycle of loading totally destroyed the slabs (see Figures E-10 through E-12). For example, slab 4.75D1 resisted a peak dynamic load equal to 87 psi (shot 6) without even minor cracking, but it was totally destroyed under a slightly higher load (98 psi).

The peak loads, deflections, accelerations, and strains are listed in Table 7. Appendix C presents plots of the applied load (Figure C-1); center deflection (Figures C-2 through C-5); acceleration (Figure C-6); and strains (Figures C-7 through C-12).

The air leakage deflection was detected by a sudden decrease in the measured pressure level (see Figure C-1). The air leakage deflection for slabs 3D1, 4.75D1, and 4.75D2 ranged from 0.71t to 0.81t. Comparing these deflections with the static resistance diagrams in Appendix D, it can be seen that air leakage originated at center deflections corresponding to the valley in the resistance diagram.

The variations of dynamic resistance with center deflection are shown in Figures D-6 through D-8 (Appendix D). The dynamic resistance, computed at time increments of 0.25 msec, is equal to the difference between the measured load and the product of the equivalent mass (K_{LM} m) times the measured acceleration. Resistance functions are shown for values of K_{LM} equal to 0.51 and 0.65.

The plots indicate that the variation in resistance is similar under static and dynamic loading. It should be noted that the ultimate flexural resistance is developed at about the same deflection under static and dynamic load. After the ultimate resistance is developed, resistance decreases with increasing deflections. Based on the difference between the computed dynamic resistance and measured static resistance, the dynamic increase factor (DIF) is 1.3 to 1.6.

Method of Dynamic Analysis

Predicting the dynamic response of a longitudinally restrained slab requires a method suitable for a structural element which exhibits a nonlinear resistance diagram. The energy balance method[18] is ideal for the analysis of such an element provided the element can be represented by a single-degree-of-freedom system, and the loading is either an impulse or a step pulse.

The test slabs were represented by a single-degree-of-freedom system. This approximation involved the assumption that, for a given center deflection, the deflected shape of the slab is the same under static and dynamic loading. Neglecting strain rate effects, this assumption implies that for a given center deflection, the internal strain energy in the slab is the same under static and dynamic loading. Therefore, the resistance diagram for the equivalent spring-mass system was taken to be the static resistance diagram but adjusted to account for strain rate effects on the strength of the steel and concrete. Applied to this equivalent system, the energy balance method yielded valuable conclusions regarding the dynamic response of longitudinally restrained slabs.

Energy Balance Method. The energy balance method is based upon the principle that, at the time of maximum deflection and zero velocity, the work done by the applied load must equal the strain energy in the slab. The method involves the graphical presentation of the strain energy in the slab and the external work done by the applied load as a function of the center deflection of the slab. Such an energy diagram is shown in Figure 33.

Curve A, in Figure 33, represents the strain energy absorbed by the slab for any center deflection, **z**. The ordinate to the curve for any deflection is the area under the dynamic resistance diagram up to that deflection. A unique feature of the energy curve is the dimple in the curve caused by the "hump" in the resistance diagram. If instead, the same slab were longitudinally unrestrained, the flexural resistance diagram would have no hump, and the corresponding energy curve would be concave downward for all deflections. There is no dimple in the energy curve for a longitudinally unrestrained slab. The significance of this dimple in the curve becomes evident shortly.

The work done by a step pulse is linearly proportional to the center deflection of the slab. Therefore, the external work done by such a load is represented by a straight line which passes through the origin and has a slope equal to the constant dynamic pressure, p_o. The dashed lines in the energy diagram of Figure 33 represent the external work for three different pressure levels.

At the point of intersection of curve A and an external work line, the kinetic energy of the slab vanishes; the strain energy stored in the slab equals the external work done by the applied load, p_o. Therefore, the deflection, **z**, corresponding to this point of intersection defines the maximum dynamic deflection of the slab under the applied load, p_o. To define this maximum dynamic deflection, z_m, produced by a given peak dynamic load, p_o, it is necessary to know the dynamic resistance function, q_d.

Table 7. Dynamic Test Results: Peak Load, Deflection, Acceleration, Strain, and Strain Ra

Slab No.	Load, p_o (psi)	Deflection		Accel, a_m (g)	Peak Strain and Average Strain Rate, ϵ_m (%) and $\dot{\epsilon}$ (in./in									
		z_m (in.)	t_m (msec)		ST1	ST2	ST3	ST4	ST5	SR1	SB2	SB3	SB4	SB
3D1-1	3.5	0.05	5.2	43	-0.02/0.07	NT	NT	NT	NT	NT	NT	NT	NT	NT
3D1-2	10.5	0.09	7.1	71	-0.03/0.06	-0.03/0.06	0.01/0.0	0.12/0.35	0.09/0.25	0.08/0.18	0.07/0.18	-0.01/0	-0.02/0.04	-0.01/
3D1-3	39.0**	10+	>100	112	-0.06/0.14	-0.06/0.14	0.05/0.01	NT	Y/0.25	Y/0.36	Y/0.64	-0.05/0.01	NT	-0.04/ 0.06/
4.75D1-1	10.5	0.03	4.0	31	-0.02/0.07	-0.02/0.10	0.01/0.03	0.02/0.05	0.02	0.01/0.06	0.01/0.06	-0.01/0.03	-0.01/0.03	-0.01/
4.75D1-2	18.0	0.05	4.2	95	-0.06/0.20	-0.03/0.11	0.01/0.05	0.03/0.14	0.03/0.12	0.03/0.12	0.03/0.13	-0.01/0.05	-0.03/0.11	-0.02/
4.75D1-3	50.0	0.37	7.0	190	-0.15/0.33	-0.06/0.12	0.03/0.05	0.17/0.49	0.16/0.49	0.18/0.50	0.19/0.51	-0.04/0.11	-0.05/0.12	-0.12/
4.75D1-4	62.0	0.46	7.5	210	-0.18/0.40	NT	NT	0.23/0.72	0.38/1.01	0.60/0.96	Y/0.90	-0.05/0.10	-0.07/0.15	-0.14/
4.75D1-5	77.0	0.60	7.0	215	-0.26/0.47	-0.09/0.18	0.09/0.25	0.44/1.12	Y/2.20	Y/2.24	–	-0.06/0.18	-0.10/0.19	-0.19/
4.75D1-6	87.0	0.76	9.4	260	NT	-0.30/0.64	0.12/0.34	Y/1.02	–	–	–	-0.05/0.14	-0.10/0.20	Y/0.5
4.75D1-7	98.0	12+	>30	265	NT	-0.35/0.78 0.38/4.0	Y/0.20	–	–	–	–	-0.05/0.14 0.38/0.72	-0.05/0.24 >0.40/0.47	–
4.75D2-1	11.0	0.04	4.2	39	-0.02/0.0	-0.03/0.09	NT	NT	0.05/0.20	0.03/0.15	NT	NT	-0.04/0.22	-0.03/
4.75D2-2	91.0	0.77	7.1	320	-0.11/0.30	-0.05/0.10	0.05/0.30	0.43/1.10	0.60/1.12	Y/1.90	NT	-0.12/0.02	-0.60/0.81	-0.24/
4.75D2-3	55.0	0.50	6.0	230	-0.10/0.20	-0.07/0.20	0.06/0.06	0.38/0.96	0.46/1.00	–	NT	-0.06/0.12	-0.15/0.32	-0.34/
4.75D2-4	91.0	0.96	7.7	325	-0.23/0.28	-0.20/0.28	0.11/0.11	0.53/2.10	Y/2.30	–	NT	-0.12/0.20	Y/1.30	-0.60/
4.75D2-5	110.0	9.2+	> 25	388	Y/2.1	Y/1.40	NT	Y/1.11	–	–	NT	–	–	–

* NT = no trace; Y = strain exceeded capacity of gage.

** Long rise time (see Figure B-1).

ic Test Results: Peak Load, Deflection, Acceleration, Strain, and Strain Rates

Peak Strain and Average Strain Rate, e_m (%) and $\dot{e}$ (in./in./sec)*											
ST4	ST5	SB1	SB2	SB3	SB4	SB5	CT1	CT2	CT6	CT7	CB4
NT	NT	NT	NT	NT	NT	NT	NT	NT	NT	NT	NT
0.12/0.35	0.09/0.25	0.08/0.18	0.07/0.18	-0.01/0	-0.02/0.04	-0.01/0.02	-0.04/0.05	-0.04/0.04	-0.05/0.05	-0.03/0.05	NT
NT	Y/0.25	Y/0.36	Y/0.64	-0.05/0.01	NT	-0.04/0.01 0.06/0.01	-0.16/0.25	-0.19/0.26	-0.15/0.24	-0.15/0.24	0.45/0.30
0.02/0.05	0.02	0.01/0.06	0.01/0.06	-0.01/0.03	-0.01/0.03	-0.01/0.02	-0.03/0.13	-0.03/0.11	-0.03/0.10	-0.04/0.12	-0.04/0.16
0.03/0.14	0.03/0.12	0.03/0.12	0.03/0.13	-0.01/0.05	-0.03/0.11	-0.02/0.11	-0.07/0.29	-0.04/0.26	-0.05/0.28	-0.05/0.26	-0.05/0.27
0.17/0.49	0.16/0.49	0.18/0.50	0.19/0.51	-0.04/0.11	-0.05/0.12	-0.12/0.32	-0.19/0.44	-0.14/0.44	-0.19/0.43	-0.20/0.58	-0.22/0.58
0.23/0.72	0.38/1.01	0.60/0.96	Y/0.90	-0.05/0.10	-0.07/0.15	-0.14/0.35	-0.22/0.63	-0.20/0.64	-0.23/0.64	-0.30/0.70	-0.32/0.74
0.44/1.12	Y/2.20	Y/2.24	–	-0.06/0.18	-0.10/0.19	-0.19/0.49	-0.40/0.96	-0.28/0.72	-0.28/0.98	-0.38/1.13	-0.51/1.14
Y/1.02	–	–	–	-0.05/0.14	-0.10/0.20	Y/0.50	-0.50/1.92	-0.32/0.75	NT	-0.38/1.48	-0.42/1.56
–	–	–	–	-0.05/0.14 0.38/0.72	-0.05/0.24 >0.40/0.47	–	NT	-0.43/1.64	NT	-0.30/1.08	-0.40/1.40
NT	0.05/0.20	0.03/0.15	NT	NT	-0.04/0.22	-0.03/0.20	-0.02/0.10	-0.03/0.14	-0.03/0.14	-0.03/0.14	-0.04/0.16
0.43/1.10	0.80/1.12	Y/1.90	NT	-0.12/0.02	-0.60/0.81	-0.24/0.48	-0.25/0.60	-0.30/0.80	-0.23/0.60	-0.33/0.80	-0.40/0.80
0.38/0.96	0.46/1.00	–	NT	-0.06/0.12	-0.15/0.32	-0.34/0.76	-0.15/0.60	-0.15/0.60	-0.13/0.60	-0.14/0.87	-0.31/0.90
0.53/2.10	Y/2.30	–	NT	-0.12/0.20	Y/1.30	-0.60/0.83	-0.24/0.70	-0.18/0.70	-0.25/0.68	-0.30/0.88	-0.58/1.16
Y/1.11	–	–	NT	–	–	–	–	–	–	–	–

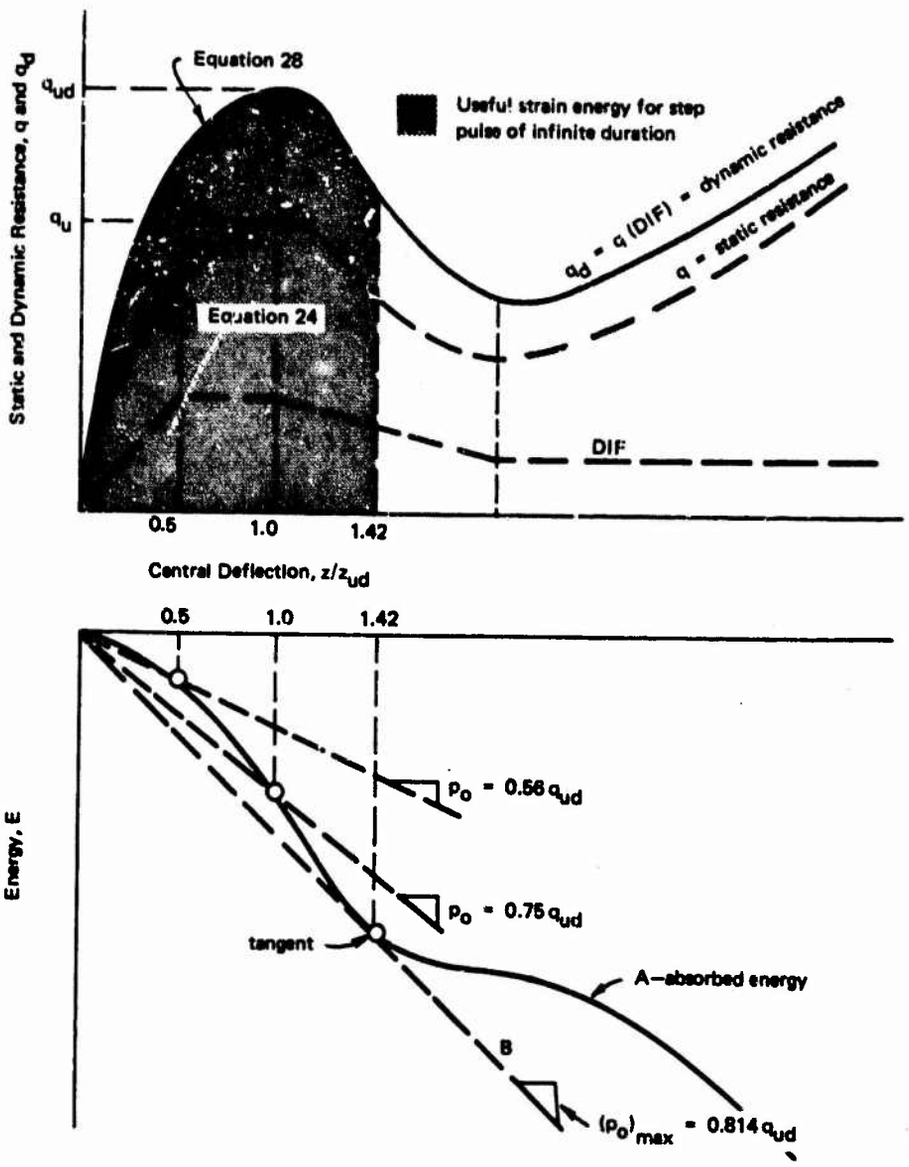

Figure 33. Energy diagram for longitudinally restrained slab.

Dynamic Resistance Function. In considering the static flexural resistance diagram shown in Figure 33, the coordinates of the point corresponding to ultimate flexural resistance (z_u, q_u) are defined by Equations 15 and 17, respectively. Assuming a vertical tangent at (0, 0) and horizontal tangent at (z_u, q_u), the resistance function, q, is of the form

$$\frac{[q]^n}{q_u{}^n} + \frac{(z_u - z)^n}{z_u{}^n} = 1 \qquad n = \text{constant} \qquad (23)$$

Solutions for Equation 23 for a wide range of values for n were compared with the measured resistance functions (Appendix D). The value n = 1.8 gave the best fit; substituting n = 1.8 in Equation 23 and rearranging terms,

$$q = q_u \left[1 - \left(1 - \frac{z}{z_u}\right)^{1.8}\right]^{1/1.8} \qquad z < z_s \qquad (24)$$

Equation 24 is compared with the measured resistance functions in Figure 34.

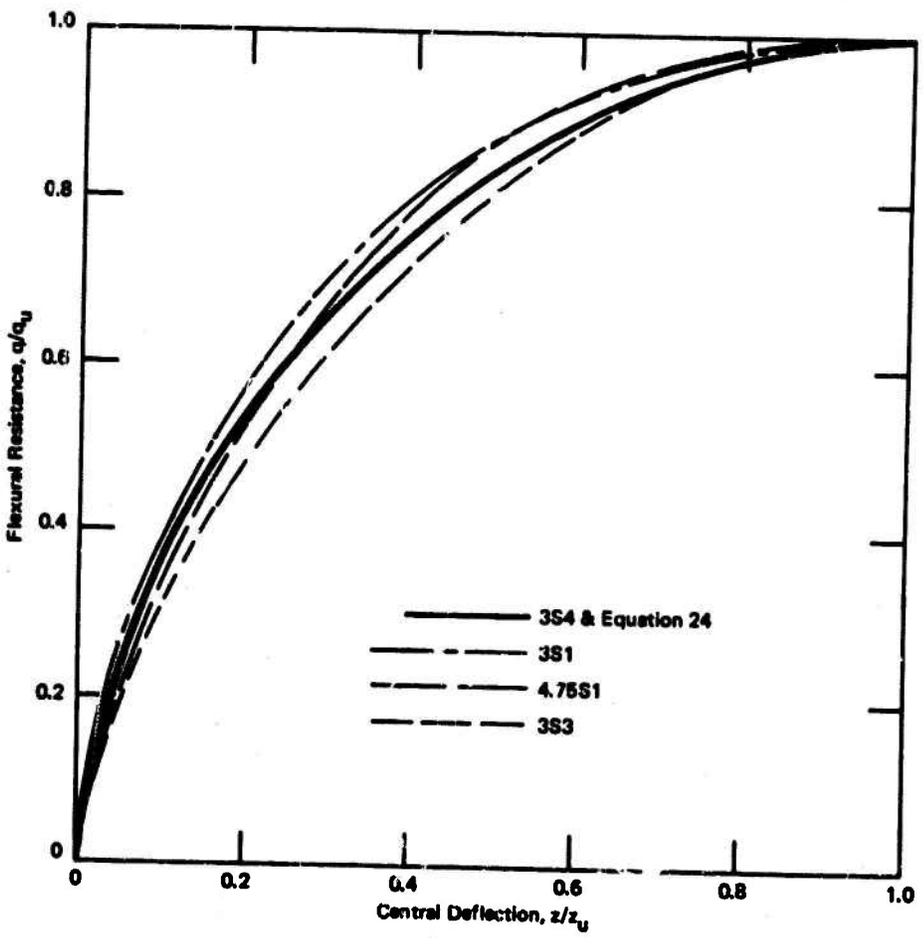

Figure 34. Measured static resistance diagrams compared with Equation 24.

Under rapid rates of straining that occur in a blast-loaded slab, the steel and concrete develop higher strengths than they do when the slab is loaded statically.[19,20] This increase in material strength is described by the dynamic increase factor, DIF, which varies with strain rate. For a given strain rate, the dynamic increase factors for steel and for concrete are different but are the same order of magnitude. Therefore, it is generally assumed that for a given cross section,

$$DIF = \frac{f'_{cd}}{f'_c} = \frac{f_{yd}}{f_y} \tag{25}$$

Figure 35 shows the effect of increases in the strength of the steel and concrete in a slab on the resistance and deflection at ultimate flexural failure. The circled points in Figure 35 are ratios of q_{ud}/q_u and z_{ud}/z_u, calculated from Equations 17 and 15, respectively, for several values of DIF. Note that DIF applied to the strength of steel and concrete in Equation 17 yields the same result as

$$q_{ud} = (DIF)\, q_u \tag{26}$$

Figure 35 also shows that the increase in strength of steel and concrete does not affect the ultimate deflection. This is apparent from inspection of Equation 15 in which the value for DIF cancels in the expression for q_e and q_d. Thus,

$$z_{ud} = z_u \tag{27}$$

Therefore, the dynamic resistance function can be described as

$$q_d = q_{ud}\left[1 - \left(1 - \frac{z}{z_{ud}}\right)^{1.8}\right]^{1/1.8} \tag{28}$$

Dynamic Response. Figure 36 considers the simple spring-mass system with the resistance function, q, under a dynamic load, p(t). At the point on the energy diagram where the external work done by the applied load equals the internal strain energy (Figure 33),

$$\int_0^{z_m} p(t)\, dz = \int_0^{z_m} q_d\, dz \tag{29}$$

where z_m = maximum dynamic deflection.

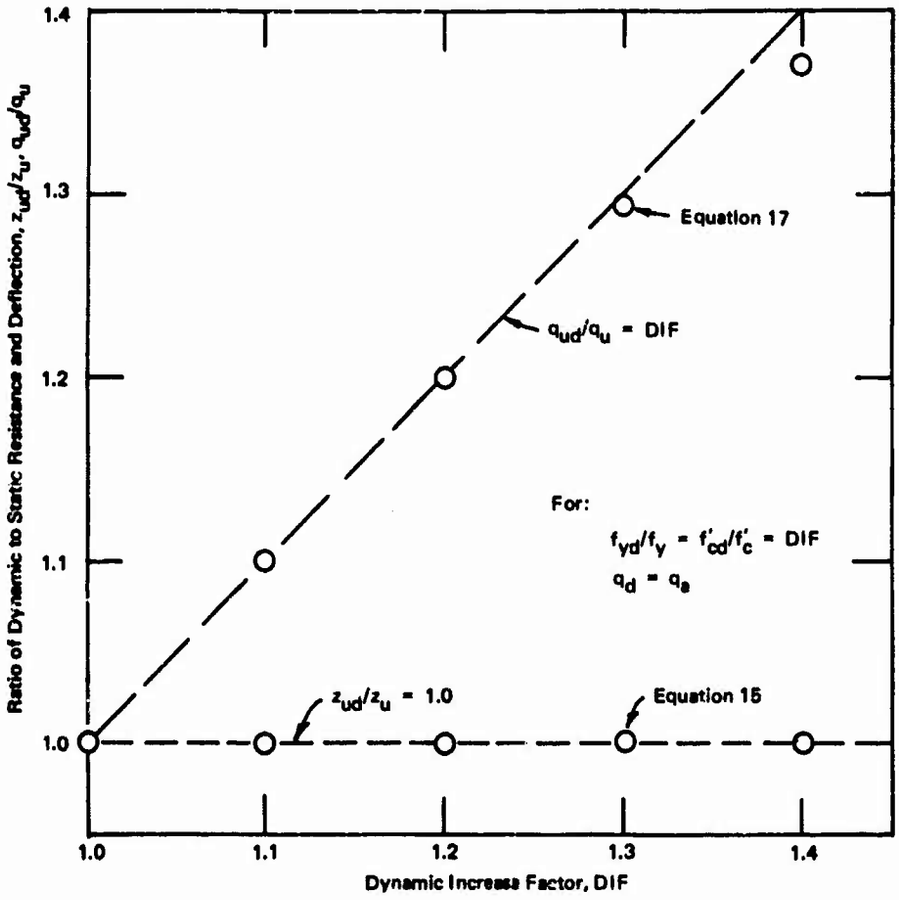

Figure 35. Effect of increase in strength of steel and concrete on dynamic resistance and deflection at ultimate.

For a step pulse and a resistance function described by Equation 28 (curve A in Figure 36), Equation 29 becomes

$$p_o z_m = q_{ud} \int_0^{z_m} \left[1 - \left(1 - \frac{z}{z_{ud}} \right)^{1.8} \right]^{1/1.8} dz \qquad (30a)$$

Therefore,

$$\frac{p_o}{q_{ud}} = \frac{1}{z_m} \int_0^{z_m} \left[1 - \left(1 - \frac{z}{z_{ud}} \right)^{1.8} \right]^{1/1.8} dz \qquad (30b)$$

Equation 30b is plotted in Figure 36.

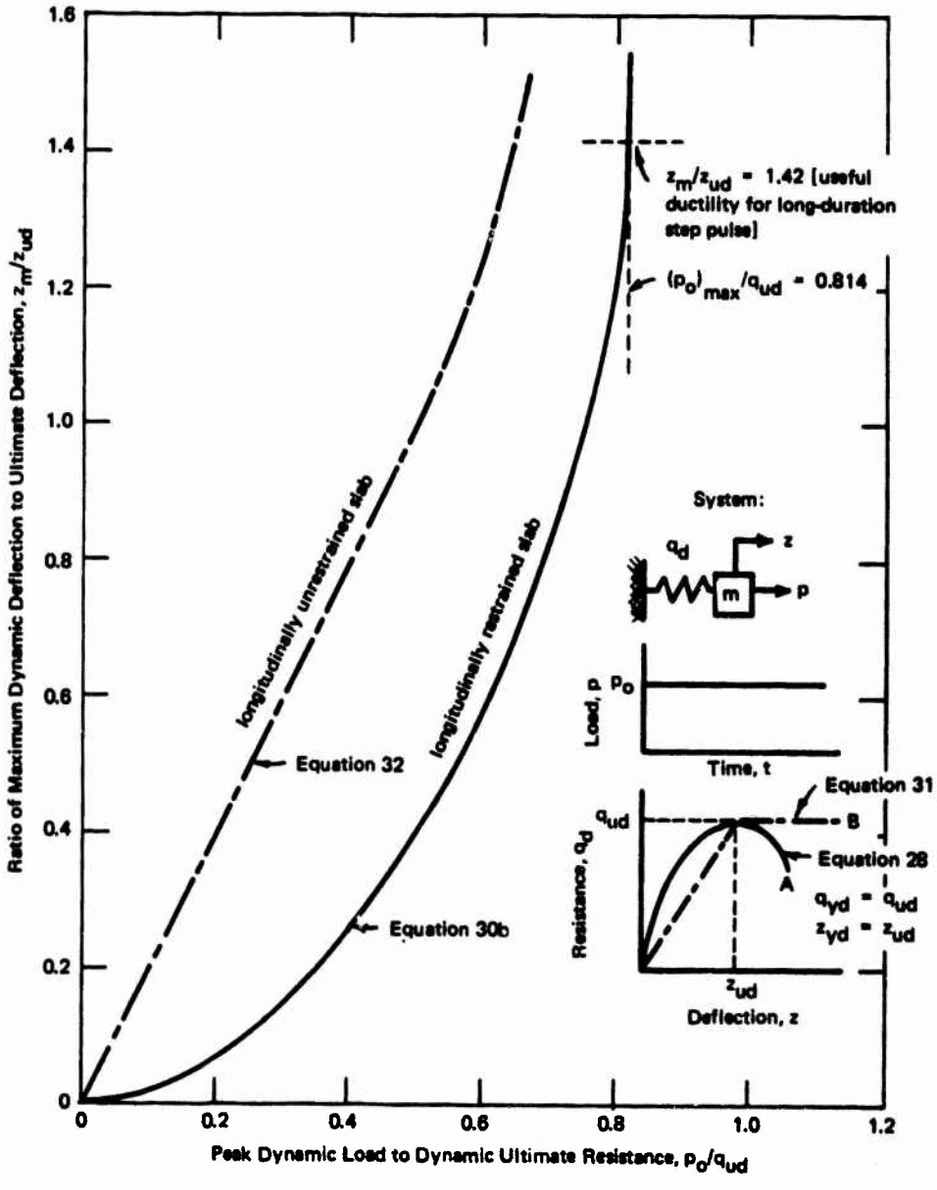

Figure 36. Maximum response of restrained slab to step pulse.

If the slab is longitudinally unrestrained, the resistance function can be described by two straight lines (curve B in Figure 36). The function has an initial stiffness, q_{yd}/z_{yd}, and a "yield" deflection, z_{yd}, when the collapse mechanism forms. Thereafter, the slab deflects plastically with a resistance q_{yd} or

$$q_d = \left(\frac{q_{yd}}{z_{yd}}\right) z \qquad z \leq z_{yd}$$

$$q_d = q_{yd} \qquad z \geq z_{yd} \tag{31}$$

For a step pulse and a resistance function described by Equation 31 (curve B in Figure 36), Equation 29 becomes

$$\frac{p_o}{q_{yd}} = \frac{1}{2}\left(\frac{z_m}{z_{yd}}\right) \qquad z_m \leq z_{yd}$$

$$\frac{p_o}{q_{yd}} = 1 - \frac{0.5}{(z_m/z_{yd})} \qquad z_m \geq z_{yd} \tag{32}$$

Equation 32 is plotted in Figure 36. The resistance function is normalized by letting $q_{yd} = q_{ud}$ and $z_{yd} = z_{ud}$.

The maximum dynamic deflections computed from the response chart in Figure 36 are compared with measured values in Table 8. The ultimate flexural resistance and deflection used in conjunction with Figure 36 were computed from Equations 17, 26, 16, and 27. The DIF was assigned the value 1.40 for all slabs. Note that the disparity between theory and experiment is greatest for the lowest load levels (3D1-1, 4.75D1-1, and 4.75D2-1). This difference is attributed to the assumption that DIF = 1.40 for elastic response, which is in error. However, the questionable accuracy of these small measured peak deflections based on the resolution of the transducers did not justify a more refined analysis.

Effect of Longitudinal Restraint on Maximum Deflection. Another consideration is that of two slabs, identical except for the degree of longitudinal edge restraint. One slab is fully restrained against longitudinal movement at the edges, the other is longitudinally unrestrained. The idealized resistance function for each slab is given in Figure 37. If each slab is subjected to the same peak dynamic load, p_o, the maximum deflection will be least for the longitudinally restrained slab (see Figure 37). Note that the reduction in maximum deflection can be as large as 90% and depends upon the enhancement factor, q_{ud}/q_{yd}. For

the normal range of steel percentages used in slabs ($0.25\% < p < 1.0\%$), the enhancement factor ranges from 1.4 to 3.5 (see Figure 19). According to Figure 37, for this range in enhancement factor, the maximum dynamic deflection of the restrained slab will be 2/5 to 1/10th the peak value of the unrestrained slab. In other words, by neglecting the presence of longitudinal restraint, the maximum dynamic deflection under the design load can be 2/5 to 1/10th the peak value, based on simple yield line theory and an elasto-plastic resistance function.

Load Capacity and Useful Strain Energy. For a step pulse, the dynamic load capacity, $(p_o)_{max}$, is the slope of a straight line which passes through the origin of the energy diagram and is tangent to the strain energy curve (line B in Figure 33). For any long-duration step pulse with a peak load greater than $(p_o)_{max}$, line B never intersects curve A; the external work always exceeds the internal strain energy so the slab never reaches static equilibrium. For the practical range of steel percentages, the stiffness of the slab in the tensile membrane region is not great enough to cause the absorbed energy curve to intersect the tangent line at some deflection greater than the deflection corresponding to the tangent point.

For a longitudinally restrained square slab having a resistance function described by Equation 28, and applying the principle described above, the dynamic load capacity of the slab for a step pulse is

$$(p_o)_{max} = 0.814\, q_{ud} \qquad (33)$$

From Equation 26,

$$(p_o)_{max} = 0.814\,(DIF)\, q_u \qquad (34)$$

The dynamic load capacity computed from Equation 34 is compared with measured values in Table 9. The static ultimate flexural resistance, q_u, was computed from Equation 17 for the slab properties listed in Table 1. The dynamic increase factor, DIF, is an average value (1.40) based on the measured strain rates in the steel and concrete. This value is further supported by the general increase indicated by the dynamic resistance diagrams shown in Appendix D.

For DIF = 1.40, Equation 34 yields

$$(p_o)_{max} = 0.814\,(1.40)\, q_u = 1.14\, q_u \qquad (35)$$

Thus, for a step pulse of infinite duration, a longitudinally restrained slab will collapse under a peak dynamic load which is approximately 14% greater than the static ultimate flexural resistance.

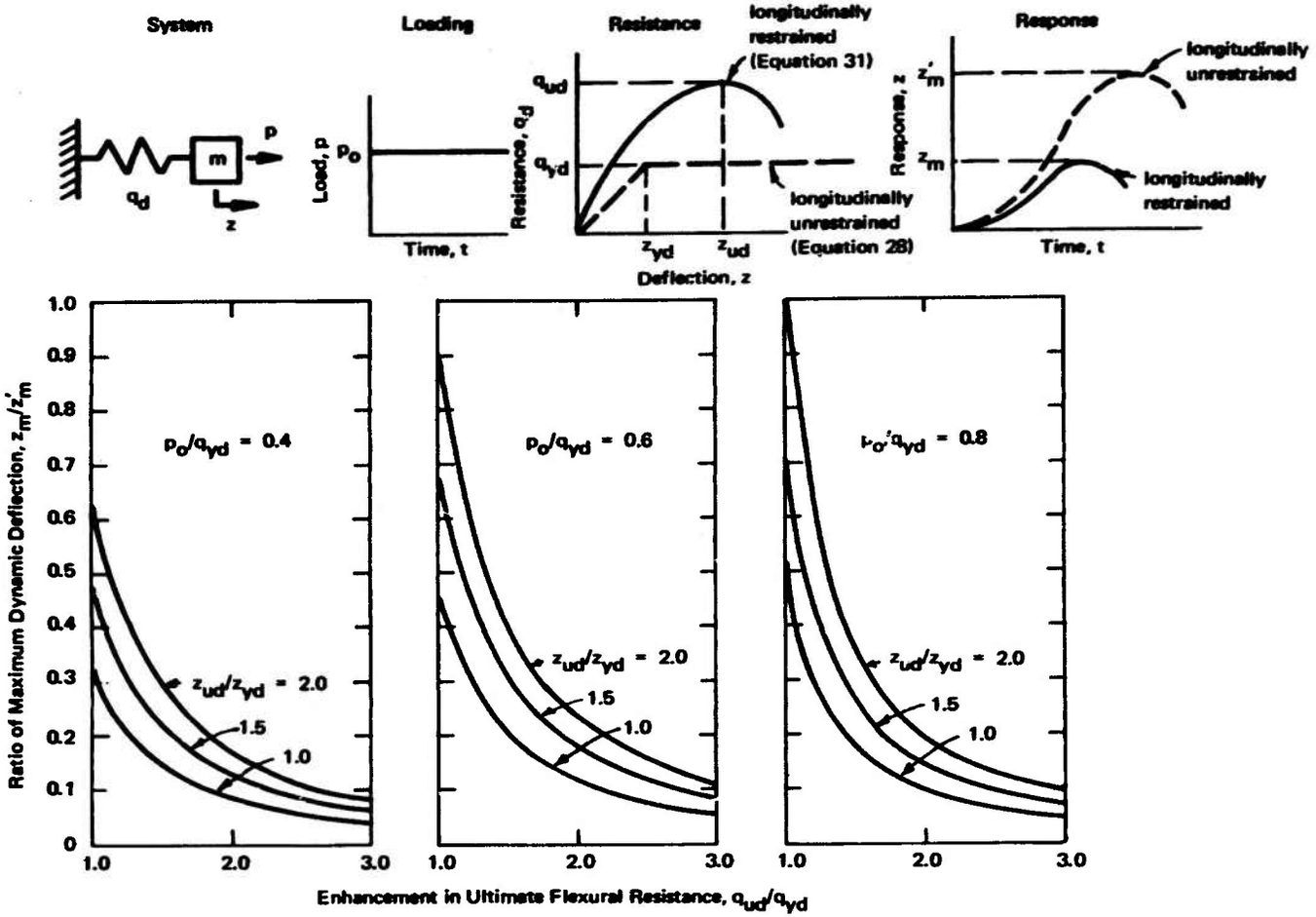

Figure 37. Effect of longitudinal edge restraint on maximum dynamic deflection.

Table 8. Measured and Computed Maximum Dynamic Deflection

Slab No.	Measured Peak Load, p_o (psi)	Theoretical Ultimate				Maximum Dynamic Deflection			
		Resistance		Deflection, z_{ud} (in.)	Load Ratio, p_o/q_{ud}	Theory		Measured z_M (in.)	Measured / Theory
		q_u (psi)	q_{ud} (psi)			z_M/z_{ud}	z_M (in.)		
		Column 1*	Column 2†	Column 3‡	Column 4§	Column 5¶	Column 6**		
3D1-1	3.5	31.8	44.5	1.26	0.08	0.02	0.03	0.05	1.66
3D1-2	10.5				0.23	0.09	0.11	0.09	0.82
4.75D1-1	10.5	90.9	127.0	1.18	0.08	0.02	0.02	0.03	1.50
4.75D1-2	18.0				0.14	0.04	0.05	0.05	1.00
4.75D1-3	50.0				0.39	0.25	0.30	0.37	1.23
4.75D1-4	62.0				0.49	0.37	0.44	0.46	1.04
4.75D1-5	77.0				0.60	0.57	0.67	0.60	0.90
4.75D1-6	87.0				0.68	0.77	0.91	0.76	0.84
4.75D2-1	11.0	95.0	133.0	1.18	0.09	0.02	0.03	0.04	1.33
4.75D2-2	91.0				0.68	0.77	0.91	0.77	0.85
4.75D2-3	55.0				0.41	0.27	0.32	0.50	1.56
4.75D2-4	91.0				0.68	0.77	0.91	0.96	1.05

* From Equation 17.
† From Equation 26 with DIF = 1.40.
‡ From Equations 16 and 27.
§ Measured peak load divided by Column 2.
¶ From Figure 36.
** Column 5 x Column 3.

Table 9. Measured and Computed Dynamic Load Capacity

Slab No.	Dynamic Resistance			Dynamic Load Capacity, $(p_o)_{max}$ (psi)		
	q_u (psi)*	DIF†	q_{ud} (psi)‡	Theory§	Measured¶	Measured / Theory
3D1	31.8	1.40	44.5	36.8	< 39	< 1.08
4.75D1	90.9	1.40	127.0	103.0	< 98	< 0.95
4.75D2	95.0	1.40	133.0	108.0	< 110	< 1.02

* From Equation 17.

† Average value based on measured strain rates in steel and concrete.

‡ From Equation 26.

§ From Equation 33.

¶ From Table 7.

What is the effect of longitudinal edge restraint on the dynamic load capacity of a slab? First consider an unrestrained slab with a resistance function described by Equation 31. Assume that the permissible maximum deflection is four times the effective yield-point deflection (ductility factor = 4). For this case, the peak dynamic load capacity is[18] $(p_o)_{max} = 0.88\, q_{dy}$ or $(p_o)_{max} = 1.10\, q_y$, with DIF = 1.25. Comparing the above expression with Equation 35,

$$\frac{(p_o)_{max} \text{ of slab with longitudinal restraint}}{(p_o)_{max} \text{ of slab without longitudinal restraint}} = \frac{1.14}{1.10}\left(\frac{q_u}{q_y}\right) \cong \frac{q_u}{q_y} \qquad (36)$$

Therefore, for a step pulse, the dynamic load capacity increases approximately in direct proportion to the enhancement factor, q_u/q_y. The material and geometric properties of the slab which affect this factor were discussed in a previous section.

The point where line B is tangent to curve A in Figure 33 defines the maximum allowable deflection and maximum useful strain energy which can be absorbed by the slab under a step pulse. Note that the useful strain energy capacity is approximately 25% of the total energy capacity of the slab. Also, the maximum allowable deflection is 1.4 times the dynamic ultimate deflection based on the resistance function defined by Equation 28 or

$$\left(\frac{z_m}{z_{ud}}\right)_{allowable} < 1.4 \quad \text{for } T/T_n > 10 \qquad (37)$$

Equation 37 limits the acceptable failure criteria for a longitudinally restrained slab under a step pulse of infinite duration. For example, even if either leakage of air overpressure through the slab ($z_m/z_s \approx 1$) or rupture of reinforcement ($z_m/z_t \approx 1$) are acceptable modes of failure, the maximum deflection must be limited to $z_m/z_{ud} = 1.4$. Otherwise, any long-duration load which produces deflection greater than $1.4\,z_{ud}$ will totally collapse the slab.

Period of Vibration. By equating the strain energy and kinetic energy of the slab to that of an equivalent spring-mass system, the period of vibration can be approximated as

$$T_n = 2\pi \sqrt{K_{LM}\left(\frac{m}{k_{fc}}\right)} \qquad (38)$$

where K_{LM} = load-mass factor = 0.63 (Reference 8).

m = $\gamma\, t/g$ = mass of slab per unit of surface area, psi-sec^2/in.

k_{fc} = stiffness of a "fixed" slab relative to the deflection at midspan based on a "cracked" transformed section, psi/in.

The expression for the slab stiffness, k_{fc}, is given in Table 3. This value was shown to correlate best with the measured stiffness shown in Figure 26.

The period of vibration computed from Equation 38 is compared with measured values in Table 10. The difference between measured and computed values increases with the level of loading, which is natural to expect. However, the measured and computed values are the same order of magnitude for the range of loadings.

Concrete Missile Fragments

Under certain conditions, concrete fragments are torn free from a slab under blast loading. These fragments act as missiles which could jeopardize the functional integrity of the slab. For such cases, ejection of concrete missile fragments is a failure criterion for design.

Three sources of concrete missile fragments are illustrated in Figure 38. Fragments can be caused by stress wave propagation through the slab, dynamic deflections in the tensile membrane region of behavior, and loads greater than the dynamic load capacity of the slab.

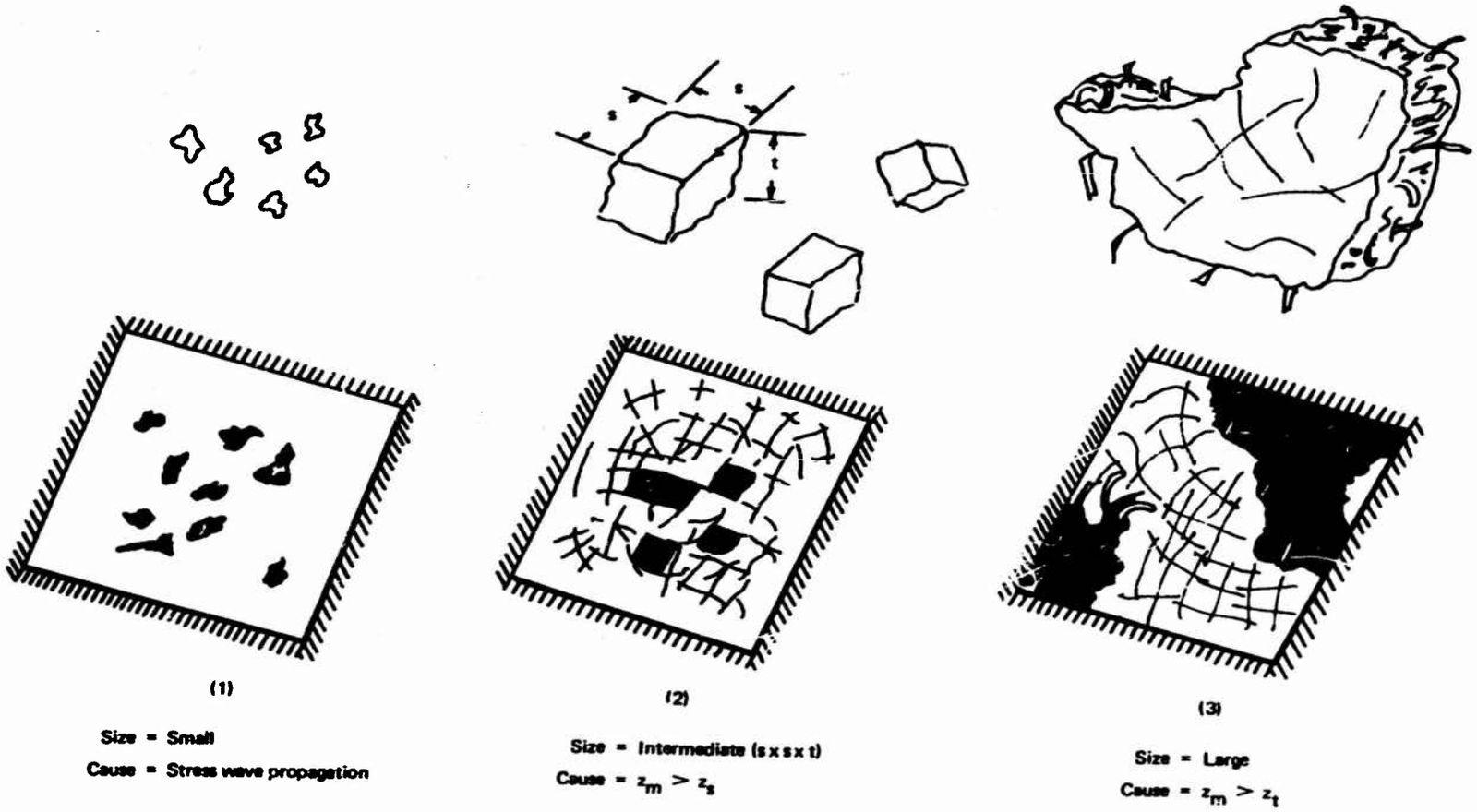

Figure 38. Three causes of concrete missile fragments.

Table 10. Measured and Computed Period of Vibration

Slab No.	Period of Vibration, T_n (msec)			
	Computed*	Measured		Measured/Computed
		Tested Value†	Average‡	
3D1	17.4	10.0, 12.5, 14.2	12.3	0.58-0.82 (0.71)
4.75D1	10.1	6.9, 7.0, 9.6, 10.0, 10.5, 10.5	9.1	0.69-1.04 (0.90)
4.75D2	10.0	6.9, 10.1, 11.5, 11.9	10.1	0.69-1.19 (1.01)

* From Equation 38.

† Values listed in order of increasing maximum dynamic deflections.

‡ Average values taken from acceleration-time and strain-time curves.

A blast wave striking the face of a slab will cause a stress wave to travel through the depth of the slab and reflect from the opposite face. The reflected wave will result in tensile stresses. Takahashi and Allgood[21] have shown that under certain conditions these stresses are sufficient to spall concrete from the unloaded face of the slab. The critical load duration, T_{cr}, corresponding to a peak load, p_o, that will initiate spalling of concrete at a distance h from the unloaded face of the slab is[21]

$$T_{cr} = \frac{2 p_o h}{c f_t'} \tag{39}$$

where c = velocity of shock wave

f_t' = tensile strength of concrete

It was concluded from Equation 39 that spalling could be a problem for high overpressures (several thousand psi) and very short load durations (less than about one msec). This explains why concrete did not spall from the unloaded face of the NCEL slabs (see Figure E-9); all slabs were subjected to long-duration loads of less than 100 psi.

Concrete missile fragments resulted from dynamic loads which deflected the slab into the tensile membrane mode of behavior. As the tensile membrane region spread outward from the center of the slab, the main reinforcement yielded, causing concrete blocks the size of the reinforcing mesh (s x s x t) to break loose from the slab. This type of missile fragment was apparent in slab 3D1-3 (Figure E-8). This source of missile fragments can be avoided by using either smaller-size bars closely spaced or lacing bars between the main reinforcement. The effectiveness of lacing bars was demonstrated by the behavior of slabs 4.75D1 and 4.75D2 (see Figures E-10 through E-12). These slabs underwent large tensile membrane deflections, but the lacing bars (see slab details in Figure 21) prevented this type of missile fragment. However, the lacing bars did not prevent severe spalling of concrete to the level of the reinforcement as shown in Figures E-11 and E-12.

Large missile fragments (Figure 38) resulted when deflections exceeded that corresponding to the capacity of the slab as a tensile membrane ($z_m > z_t$). Whole sections of the slab were torn loose from its support line where reinforcement yielded, necked down, and ruptured in tension (see Figure E-10). It would appear that the failure modes of either slab 3D1-3 (Figure E-8) or slab 4.75D1-7 (Figure E-10) are typical for slabs under long-duration loads greater than the value given by Equation 35. If the pressure on the slab is not relieved by blocks of concrete being freed from the reinforcing mesh, the pressure will deflect the slab until whole portions of the slab are eventually torn loose. Thus, closely spaced longitudinal bars and lacing bars can prevent intermediate-size missile fragments but will precipitate a much more violent and destructive mode of failure under long-duration loads.

FINDINGS AND CONCLUSIONS

The following findings and conclusions apply only to a uniformly loaded, square slab with edges fully restrained against rotation and partially restrained against translation. Unless otherwise noted, reference to dynamic load implies a step pulse.

1. The ultimate flexural resistance is increased by full or partial restraint against outward movement of the edges. The enhancement factor, q_u/q_y, can be several hundred percent. The exact magnitude depends primarily upon the cross-sectional properties of the slab, crushing strain of the concrete, span-thickness ratio, and degree of longitudinal restraint.

a. Steel Ratio. The enhancement factor increases with a decrease in the tensile steel ratio, p; the factor is infinite for $p = 0$ and approaches unity as p approaches the balanced steel ratio, p_b. In general, the effect of

compression steel depends on the ratio p'/p. For p greater than some critical value (0.6 to 0.8%), the enhancement factor increases with p'/p. For p less than the critical steel ratio, the factor decreases with p'/p (see Figure 19).

b. **Crushing Strain of Concrete.** The enhancement factor increases with the crushing strain of the concrete. Disintegration of the concrete limits the maximum in-plane thrust and moment resistance of the slab cross section and, therefore, the ultimate flexural resistance of the slab. An average crushing strain of 0.0038 in./in. gave the best correlation between theory and tests, although higher and lower strains were recorded in the tests.

c. **Span-Thickness Ratio.** For span-thickness ratios less than 18, material instability (concrete crushing) limits the enhancement factor which decreases with increasing span-thickness ratios. For span-thickness ratios greater than 18, geometric instability (similar to the snap-through deflection of a linkage) limits the enhancement factor which is independent of L/t (see Figure 19).

d. **Degree of Longitudinal Restraint.** The enhancement factor decreases with increasing amounts of longitudinal edge movement. The effect of edge movement on enhancement factor increases with span-thickness ratio; for a given span, the thicker the slab the more edge movement which can be tolerated without significantly reducing the ultimate flexural resistance (see Figure 18).

2. The flexural ultimate deflection *directly* depends upon the properties of the cross section, crushing strain of concrete, span-thickness ratio, and degree of longitudinal edge restraint (see Equation 15). For span-thickness ratios less than 18, this critical deflection is controlled by material instability; the latter is very sensitive to the parameters just cited (see Figures 15, 16, and 27). For span-thickness ratios greater than 18, the critical deflection is controlled by geometric instability which occurs at a center deflection equal to 0.42 t. This value is based on test data (see Figure 27).

3. The induced compressive thrust is a maximum when the midspan deflection reaches the critical deflection. Based on a collapse mechanism consisting of four plane quadrants, the thrust (theoretical) is maximum at the corners and minimum at midspan. At the corners, the maximum thrust is 80 to 100% of the balanced thrust, N_b, for $30{,}000 < f_y < 50{,}000$ psi and $p - p' < 2.5\%$. The balanced thrust is the thrust on the cross section, which would produce simultaneous yielding of tension steel and crushing of concrete at the extreme fiber. At midspan, the maximum thrust is 60 to 100% of the balanced thrust for $30{,}000 < f_y < 60{,}000$ psi, $p - p' < 1.5\%$; and $10 < L/t < 20$ (see Figures 12 and 13).

4. Cracking was first visible in the unloaded face of the slab at a static resistance ranging from 67 to 96% of the flexural resistance based on simple yield-line theory (Table 6).

5. The strength and behavior of longitudinally restrained slabs are deflection-sensitive. Initial slab deflections induce increasing compressive forces in the plane of the slab. These forces significantly enhance the stiffness, cracking resistance, and ultimate flexural resistance of the slab. However, strength and behavior rapidly deteriorate beyond a critical deflection. Cracking increases and the resistance decreases to a level very near that indicated by simple yield-line theory. Thereafter, resistance increases with deflection as the in-plane forces change from compression to tension near the central region of the slab. This deterioration in strength and behavior should not prohibit the initial strength and behavior from being utilized to resist a one-time dynamic load. Neither should it prohibit the entire strain energy capacity of the slab from being utilized to resist short-duration loads.

6. Air pressure leaked through the slab at center deflections slightly less than the secondary deflection, z_s, which corresponds to the valley in the static resistance function. The value of z_s can be approximated from Equation 21.

7. Any increase in static ultimate flexural resistance from longitudinal edge restraint provides an equivalent increase in the dynamic load capacity of the slab. For example, a slab with an enhancement factor of 2.5 can safely resist a peak dynamic load which is 2.5 times greater than the dynamic load capacity of the same slab with no longitudinal restraint. If this additional load carrying capacity is available, it can be utilized in the design of slabs to resist a one-time dynamic load. Utilizing the effects of longitudinal restraint could prove very economical in blast resistant design, particularly for large ratios of peak dynamic load to static working load.

8. The flexural resistance function can be calculated from the expressions summarized in Figure 39.

9. The response chart in Figure 36 will predict with reasonable accuracy the peak dynamic load required to produce a given dynamic deflection at the center of a longitudinally restrained slab.

10. A longitudinally restrained slab will collapse under a peak dynamic load greater than approximately 81% of the *dynamic* ultimate flexural resistance. If the dynamic increase factor (DIF) is 1.40, the required peak dynamic load to cause failure is 14% greater than the *static* ultimate flexural resistance.

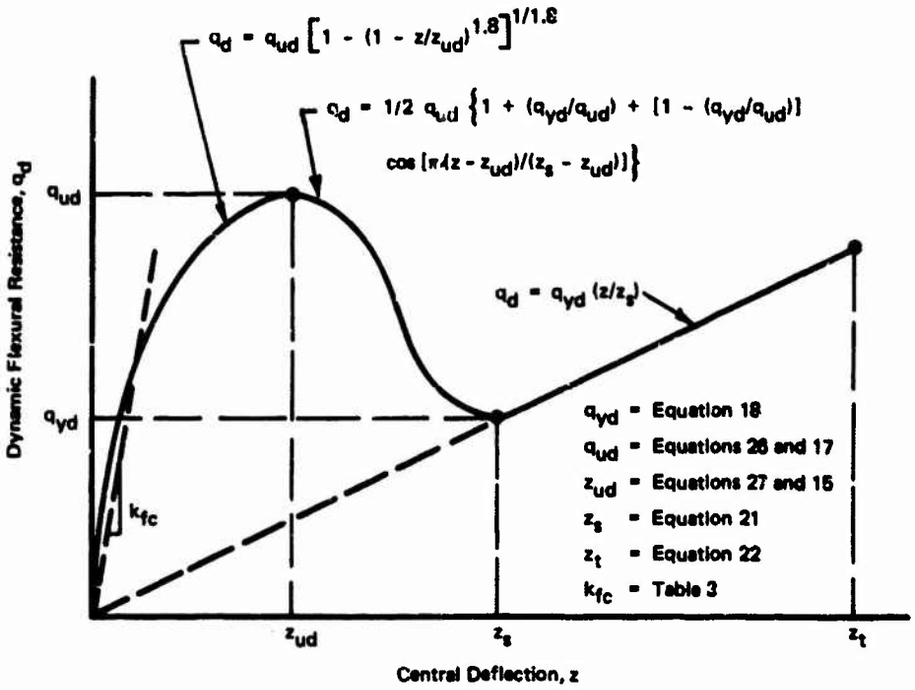

Figure 39. Resistance diagram for design.

11. The increase in flexural resistance of a longitudinally restrained slab under dynamic load is equivalent to the increase in strength of the steel and concrete from strain rate effects. The increase in strength for all slabs averaged 40% based on the measured strain rates and the dynamic resistance functions computed from measured loads and acceleration.

12. A long-duration dynamic load which produces deflections greater than 1.4 times the critical deflection, z_u, will totally collapse a longitudinally restrained slab.

13. Three potential sources of concrete missile fragments are:

(a) Stress wave propagation through the slab

(b) Dynamic deflections in the tensile membrane region of behavior

(c) Loads greater than the dynamic load capacity of the slab (Figure 38)

Theory indicates that fragments from source (a) could be a problem for high overpressures (several thousand psi) and very short load durations (less than about 1 msec). Fragments from source (b) are concrete blocks the size of the reinforcing mesh (s x s x t). This source is avoided by using either small

bars closely spaced or lacing bars between the main reinforcement. Fragments from source (c) can be very large sections of the slab which are torn loose from its support line when the reinforcement ruptures in tension.

14. The maximum dynamic deflection of a slab with full longitudinal restraint is 0.1 to 0.4 the peak value of an identical slab with no longitudinal restraint (Figure 37). If the designer neglects the presence of longitudinal restraint, the peak deflection can be 10 to 40% of the peak value he computes based on simple yield-line theory and an elasto-plastic resistance function.

15. The entire strain energy capacity of the slab can be utilized to resist very-short-duration loads provided precautions are taken to prevent local failure (concrete missile fragments).

DESIGN RECOMMENDATIONS

The following recommendations are based on theoretical and experimental results presented in this report. Recommendations are restricted to a uniformly loaded, square slab with edges fully restrained against rotation and partially restrained against translation.

Limiting Deflection

The maximum deflection under the design blast loading must be less than some specified limiting deflection. Generally, this deflection corresponds to a failure criterion associated with some stage of behavior such as inelastic response, concrete missile fragments, air leakage, or imminent collapse. Choice of failure criterion depends upon the function of the structure, surrounding media, and location of the slab in the structure. For example, the failure criterion may be air leakage for a roof slab above ground but may be imminent collapse if the slab is buried. Air leakage probably will not be the failure criterion if the load duration is less than about 0.7 times the period of vibration; the load will be off the slab before the cracks penetrate the thickness of the slab. Limiting deflections for various failure criteria are recommended in Table 11.

The duration of the load is very important if the failure criterion is imminent collapse. The portion of the resistance function corresponding to $z < 1.4\, z_{ud}$ is critical for long-duration loads. The total energy-absorbing capacity corresponding to rupture of reinforcement is critical for *efficiently* resisting loads which last a short time relative to the period of vibration.

Resistance Function

The dynamic resistance function must be defined to predict the response of the slab under the design blast loading. The function depends upon the cross-sectional properties, geometry, and edge restraint of the slab. Equations for computing the resistance function of the slab throughout its entire range of behavior are summarized in Figure 39.

Table 11. Limiting Deflection for Various Failure Criteria of Longitudinally Restrained Slabs

Failure Criterion	Limiting Deflection
Inelastic Response	$0.6\, z_{ud}$*
Air Leakage	z_s†
Concrete Missile Fragments	
With lacing bars	z_t‡
Without lacing bars	z_s†
Collapse	
$q_u/q_y > 1$, short-duration load	z_t‡
$q_u/q_y > 1$, long-duration load	$1.4\, z_{ud}$*
$q_u/q_y \approx 1$, long- or short-duration load	z_t‡

* z_{ud} is value given by Equations 15 and 27.

† z_s is value given by Equation 21.

‡ z_t is value given by Equation 22.

The ultimate flexural resistance can be determined from the following steps:

1. Construct the moment-thrust failure interaction diagram for typical sections along the edge and diagonal of the slab. Assume the stress-strain relationship for the concrete is that recommended by Hognestad[12] (Figure 3). Compute the moment at mid-thickness of the cross section (Figure 1).

2. Inspect the shape of the failure interaction diagram for optimum design. To gain maximum effect from longitudinal edge restraint, the balanced thrust should be at least 30 percent of the ultimate axial thrust capacity ($M_u = 0$). If not, decrease the area of steel and/or increase the slab thickness until this rule of thumb is satisfied.

3. Compute the critical deflection at midspan required to develop the crushing strain of the concrete along the hinge lines of the collapse mechanism (Equation 15, but value not to exceed Equation 19).

4. Compute the average thrust induced in the plane of the slab at ultimate flexural capacity. Compute the thrust at the corners $N_u(0)$ and midspan $N_u(L/2)$ from Equation 13. The average thrust is

$$\frac{1}{2}\left[N_u(0) + N_u(L/2)\right]$$

5. Enter the failure interaction diagrams with the average thrust from step 4 to find the average moment resistance of sections along the diagonal and edge ($\bar{M}_{ud}$ and $\bar{M}_{ue}$). If the average thrust is greater than the balanced thrust, revise the cross section, and begin with step 1.

6. Compute the static ultimate flexural resistance (Equation 17).

7. Compute the dynamic ultimate flexural resistance (Equation 26).

Period of Vibration

The period of vibration of the slab will vary with the level of response. However, the effective period of vibration (when the slab responds in a mode corresponding most nearly to its shape as it approaches failure) is

$$T_n = 2\pi \sqrt{K_{LM} \frac{m}{k_{fc}}} \qquad (38)$$

where $m = \gamma t/g$ = mass of slab per unit of surface area, psi-sec^2/in.

$k_{fc} = 792\, E_c I_c/(1 - \mu^2)L^4$ = stiffness of clamped slab relative to midspan deflection based on a cracked transformed section, psi/in.

$K_{LM} = 0.65$ = load-mass factor.[8]

Dynamic Response

For a long-duration load ($T/T_n > 6$), compute the ratio of peak dynamic load to dynamic ultimate resistance. Enter the dynamic response chart in Figure 36 with this ratio and read the maximum dynamic deflection. For a short-duration load ($T/T_n < 6$), use either numerical methods[8] or a gyrogram[9] to compute the maximum dynamic deflection under the applied load. For impulse loads ($T/T_n < 0.5$), use the energy method. Construct the strain energy curve for the slab (Figure 33), calculate the initial kinetic energy (square of the impulse divided by twice the mass), and find the deflection corresponding to a level of strain energy equal to the initial kinetic energy. This deflection is the maximum dynamic deflection of the slab under the impulse load.[8]

ACKNOWLEDGMENTS

B. R. Swihart, Professor of Civil Engineering at the University of Nebraska, assisted in the design of the NCEL slab loader and the test program. Dr. Salah Nosseir provided guidance during the later stages of testing, assisted in the reduction and analysis of data, and reviewed this report. T. J. Landrum and L. B. Foster supervised construction of the slab loader. F. H. Billingsley developed the "Franko" water seal for testing slabs under hydraulic pressure. Special acknowledgment is due W. Wilcoxson for computer program "Super" which was valuable in the reduction, analysis, and graphical presentation of the data.

Appendix A

NCEL SLAB LOADER

DESCRIPTION

The slab loader is a reinforced concrete, open-top box, 10 feet square by 4 feet deep, with a steel-lined chamber 6 feet square by 1 foot 6 inches deep. The slab specimen is placed on the top of the loader, fastened to the loader with anchor bolts located on its perimeter, and loaded by generating pressure inside the enclosed chamber of the loader.

The major elements of the slab loader are the chamber, firing tubes, baffle plates, and vent pipes (Figure A-1). The chamber is divided into four equal-size compartments. Each compartment houses a perforated steel firing tube which extends the length of the chamber. The chamber is divided by three equally spaced baffle plates, transverse to the firing tube axis, to control longitudinal shock reverberations. Between the plane of the firing tubes and the slab specimen, a grid system of baffle plates directs the dynamic pressures. Two vent pipes in opposite walls of the chamber control the pressure decay in the chamber.

The slab loader can provide various support conditions and accommodate slabs of different aspect ratios. The edges of the slab can be either clamped or simply supported as shown in Figure A-2. The edges can be restrained against lateral displacement by grouting between the edge of the slab and the stiffened angles welded on the top periphery of the slab loader. Slabs with an aspect ratio of 3:4 can be tested by closing one compartment of the chamber.

PRINCIPLE OF OPERATION

Static Loads

Static loads are applied to the slab by pumping water under pressure into the chamber (Figure A-3). First, the firing tubes are removed, and a steel plate is bolted to the chamber wall over each port hole to provide a positive water seal. The chamber is then filled with water to the level of the steel bearing plate which supports the slab. Finally, a Franko water seal is installed, and the chamber is sealed by clamping the slab specimen to the face of the slab loader. More water is then pumped into the chamber with a positive displacement pump to load the slab specimen to the desired hydrostatic pressure level.

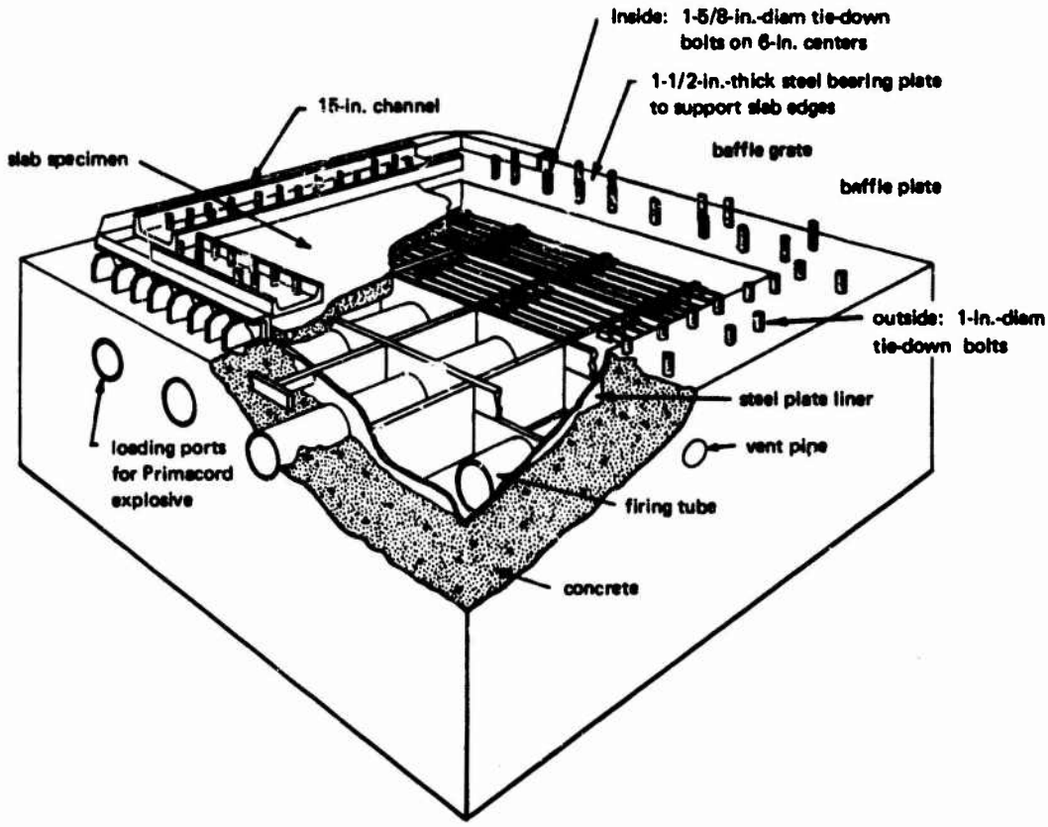

Figure A-1. NCEL slab loader, showing features for dynamic loads.

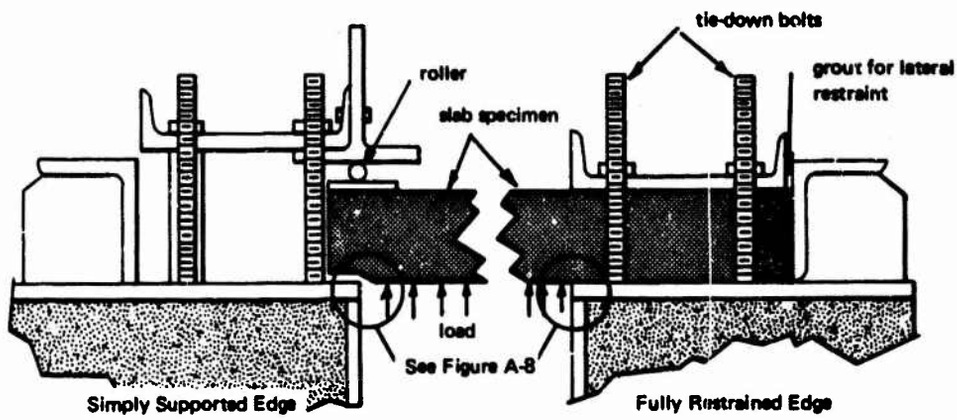

Figure A-2. Typical edge-support details.

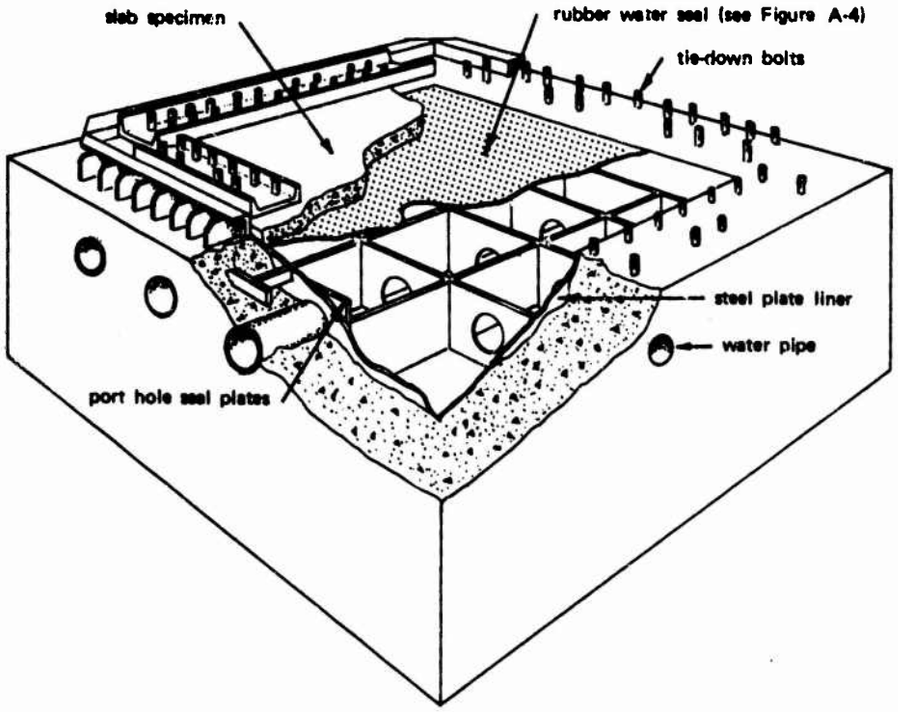

Figure A-3. NCEL slab loader, showing features for static loads.

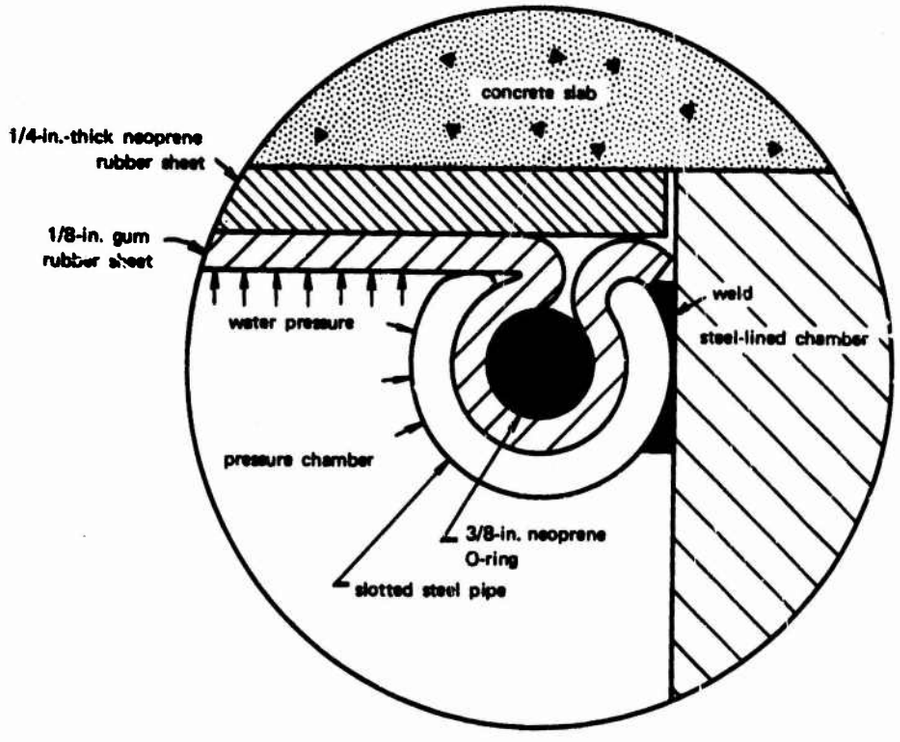

Figure A-4. Franko water seal for static loads.

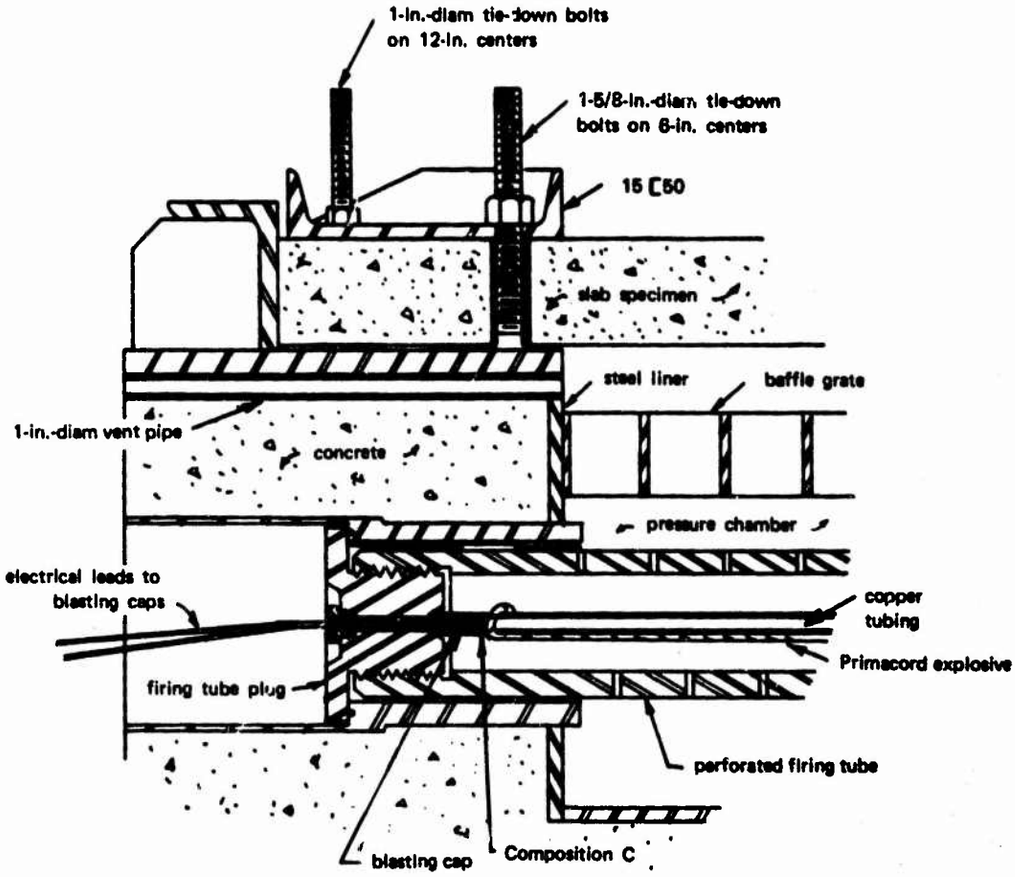

Figure A-5. Cross section of slab loader.

The Franko water seal (Figure A-4) consists of a slotted pipe welded to the top face of the chamber walls, a 3/8-inch-diameter rubber O-ring, and a 1/8-inch-thick gum rubber sheet, 6 feet 4 inches square. The edges of the gum rubber sheet are tucked into the slotted pipe and held in place by the O-ring. The O-ring is coated with a liquid soap; its length is stretched to reduce its diameter, and it is pushed into the slotted pipe. After installation, the tension on the O-ring is relieved to increase its diameter and provide a positive water seal. A 1/4-inch-thick neoprene sheet is placed over the gum rubber sheet to protect it from cracks which develop in the loaded face of the concrete slab specimen.

Dynamic Loads

Dynamic pressures are generated by detonating an explosive charge in each of the four firing tubes (Figures A-5 and A-6). The explosion raises the gas pressures in the firing tubes to between 5,000 and 10,000 psi. The gases discharge through the many small orifices in each tube (4-inch inside diameter, 1-inch wall thickness) to pressurize each compartment, thus loading the face of the slab specimen. Peak pressure is dependent upon the weight of the explosive charge as shown in Figure A-7. The rise time of load (approximately three quarters of a millisecond) is controlled by the vent area of the firing tubes, volume of the chamber (50 cubic feet), and the heat of the decomposed gases. The vent area consists of 71 rings of holes uniformly spaced along the length of each tube. Each ring consists of 15 holes (1/4-inch diameter) equally spaced on the circumference of the tube. The decay of the pressure is achieved by the cooling of the gases as heat is lost to the compartment walls, and by two 1-inch-diameter pipes which vent the gas pressure from the chambers to the atmosphere. Typical pressure-time relationships measured in the slab loader are shown in Figure A-8.

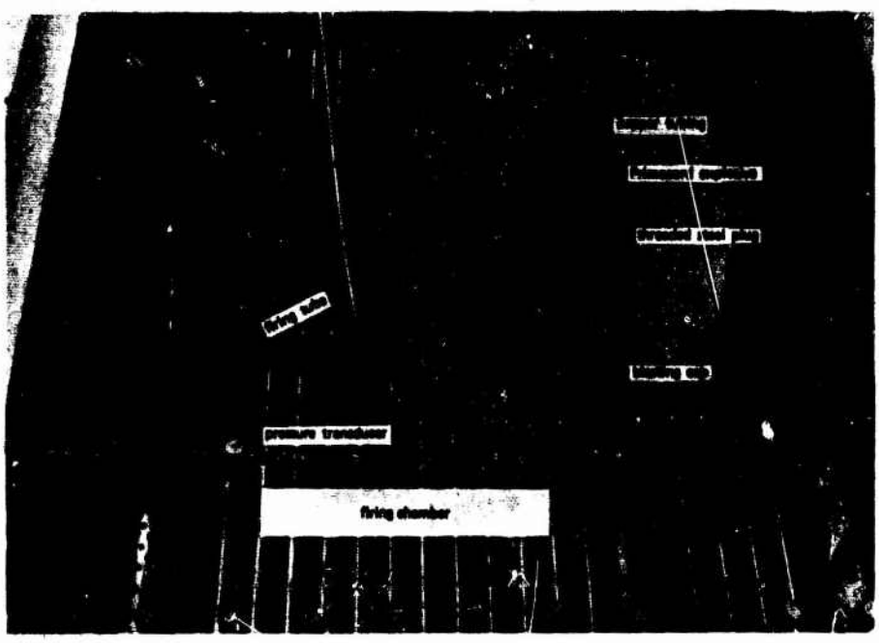

Figure A-6. Firing chamber.

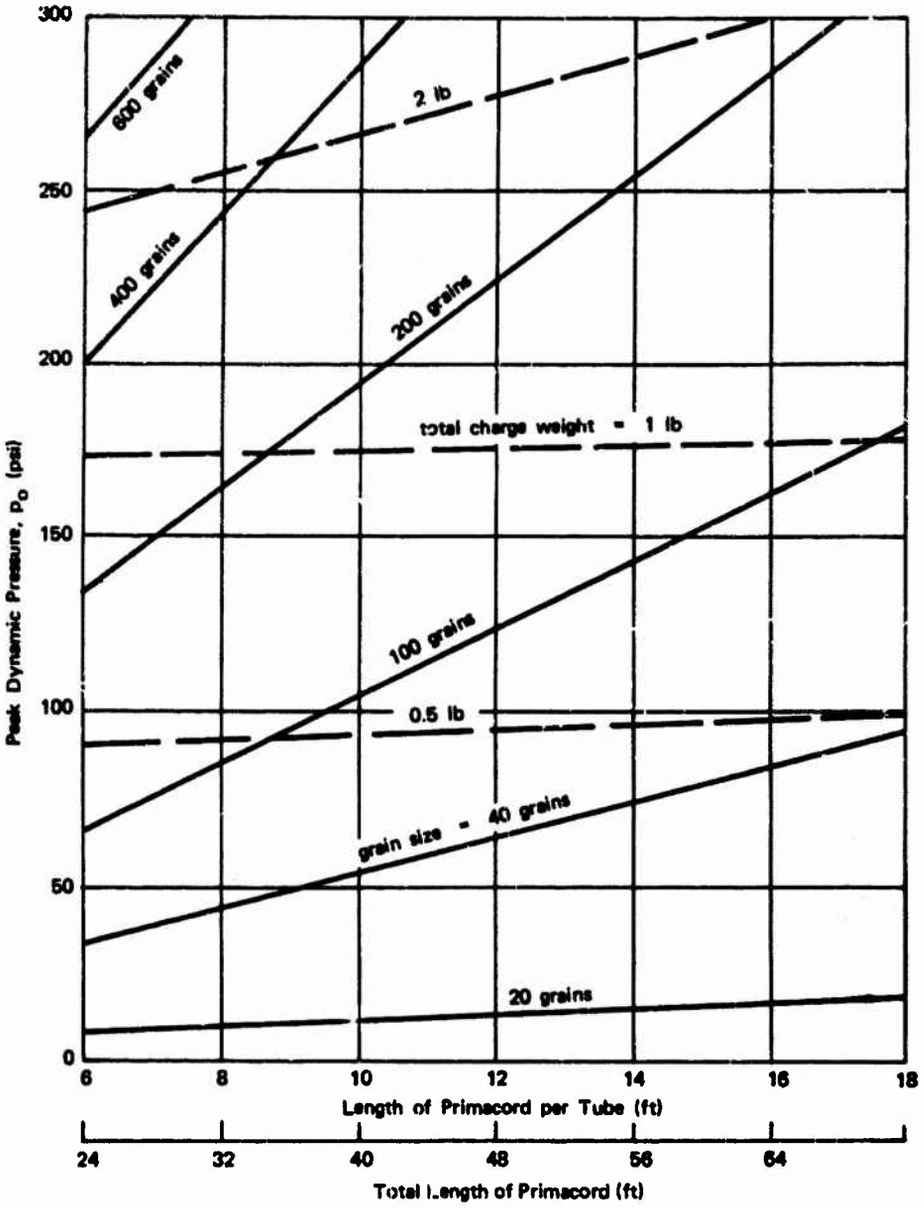

Figure A-7. Explosive charge chart.

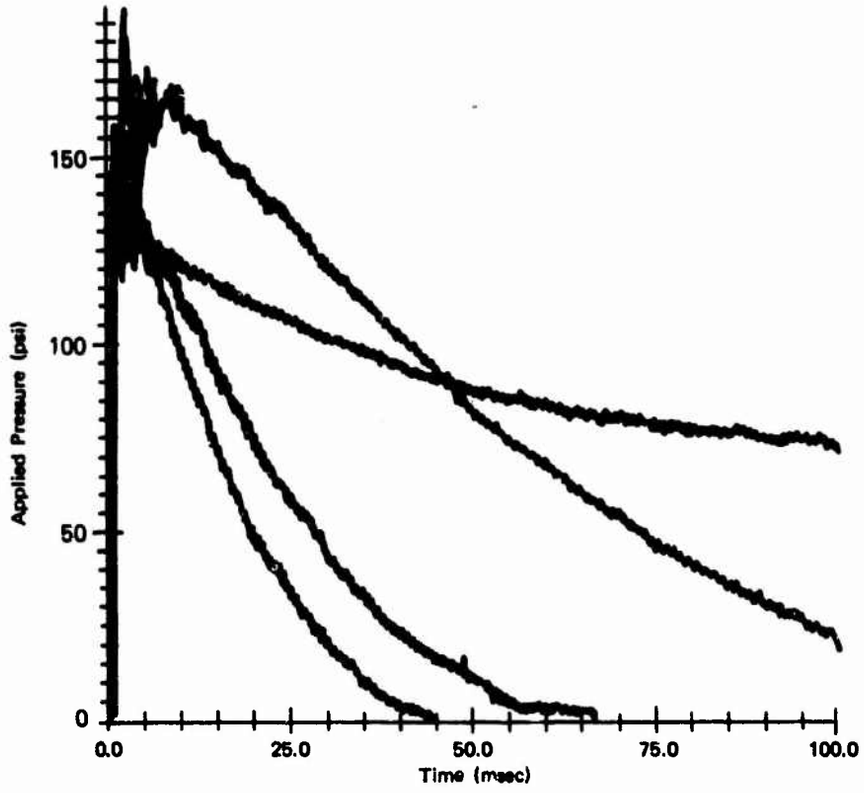

Figure A-8. Typical pressure-time curves for slab loader.

The explosive charge in each firing tube is composed of stripped PETN Primacord, nitrocellulose film, and Composition C explosive. The amount of Primacord required to produce a given pressure level is selected from the chart in Figure A-7. A combination of grain size and length of Primacord is chosen such that the charge extends the full length of each compartment. A length of nitrocellulose film (32 grains per foot), corresponding to 2/3 of the Primacord by weight, provides an 11.5 percent nitrogen content. The Primacord and nitrocellulose film are taped to a 6-foot length of copper tubing supported coaxially within the perforated firing tube by nitrocellulose disks. One booster pellet of Composition C (20 grains) is placed at each end of the charge in contact with the Primacord. A No. 8 engineering blasting cap is then placed in each end of each of the four firing tubes, in contact with the Composition C pellets. The eight blasting caps are wired in a series circuit and detonated by a 60-volt battery which delivers approximately 5 amperes to each cap.

Appendix B

SHEAR FAILURE OF 10-INCH-THICK SLAB

INTRODUCTION

Two 10-inch-thick reinforced concrete slabs were fabricated to serve as a closure for proof testing the NCEL slab loader to its design capacity of 300 psi. The results of these tests are reported here to provide basic data on the strength and behavior of thick reinforced concrete slabs under uniformly distributed loads.

DESCRIPTION OF SLABS

Both slabs were square with an overall length of 8 feet 4 inches and a clear span of 6 feet. Slab 10S1 was 10 inches thick (L/t = 7.20); slab 10.5S1 was 10.5 inches thick (L/t = 6.85).

Both slabs were clamped but longitudinally unrestrained at the edges. The edges were restrained against rotation by clamping them between the face of the slab loader and a steel frame formed from 15-inch channels. The channels were drawn tight against the slab by an inner ring of 1-5/8-inch-diameter studs spaced on 6-inch centers and an outer ring of 1-inch-diameter studs spaced on 12-inch centers. The degree of fixity provided by this clamping system is questionable for such a thick slab. Although the rotational restraint at the edges was not measured, the degree of fixity was much less than 100 percent. The edges were not grouted to prevent in-plane movements at the edges. However, some amount of lateral restraint certainly resulted from friction between the face of the slab and the steel bearing surface at the supports.

The slabs were reinforced with an orthogonal set of uniformly spaced bars in each face of the slab. Total amounts of reinforcement in each face were 1.30 percent for slab 10S1 and 1.72 percent for slab 10.5S1. The bars were continuous through the length of the slab and extended into the supports where the bars were securely hooked around longitudinal bars running parallel to the edge of the slab. A view of the reinforcing cage is shown in Figure B-1. The slab geometry and arrangement of reinforcement are described in Table B-1.

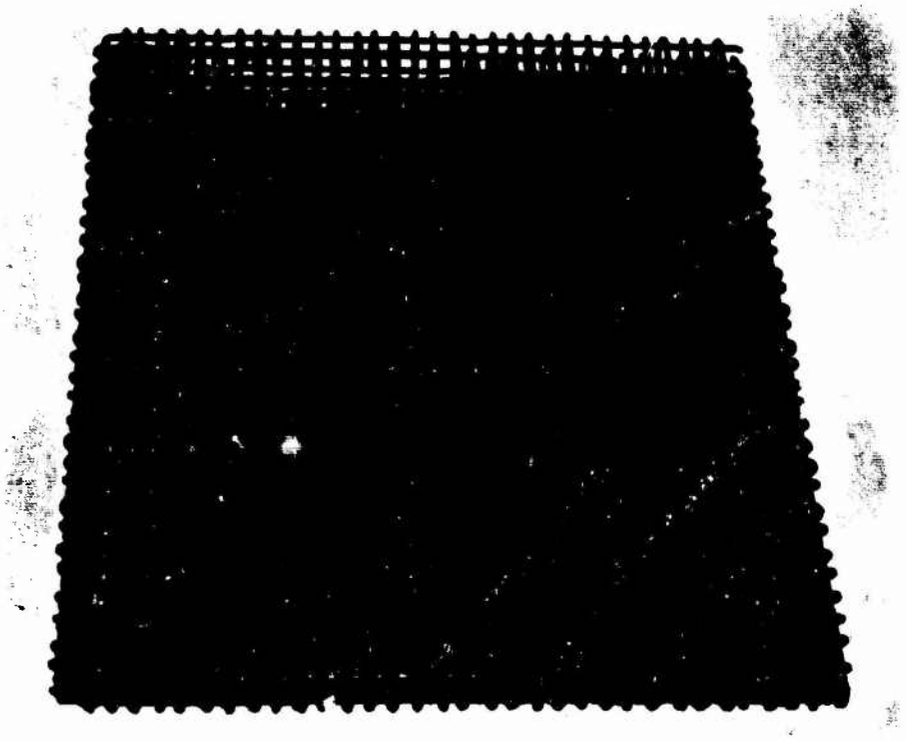

Figure B-1. Reinforcing cage for slab 10.5S1.

RESULTS AND DISCUSSION

The slab with no web reinforcement (10S1) failed prematurely in shear under a static uniform load of 210 psi. The slab with 2.4 percent web reinforcement (10.5S1) safely resisted several cycles of static and dynamic loadings ranging as high as 325 psi. Test results are summarized in Table B-1 and Figure B-2.

The shear failure of slab 10S1 knocked loose a truncated pyramid of concrete (see Figure B-3). The base of the pyramid, corresponding to the unloaded face of the slab, was very nearly a plane surface with dimensions equal to the clear span of the slab. The sides of the pyramid (failure surface) sloped inward toward the center of the slab at about a 45-degree angle. Failure of slab 10S1 was sudden and caused extensive disintegration of the concrete near the support line. The pulverized concrete extended almost to the loaded face of the slab (Figure B-3). The failure plane was well-defined by crevices half the depth of the slab.

The average ultimate shear stresses corresponding to six possible critical sections are listed in Table B-2. The ultimate shear stresses are high but are consistent with values reported for thick circular slabs.[7]

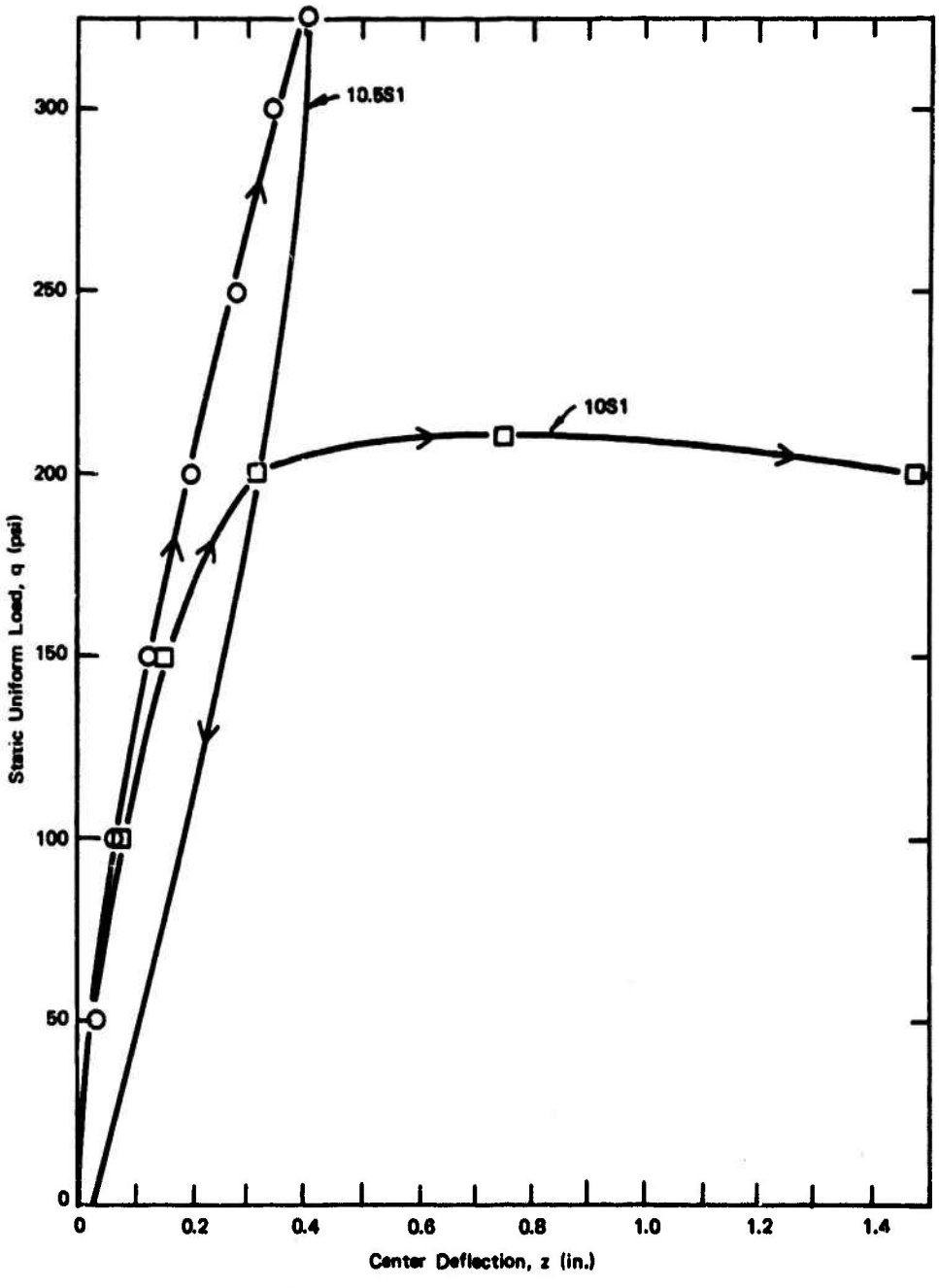

Figure B-2. Static resistance diagrams for slabs.

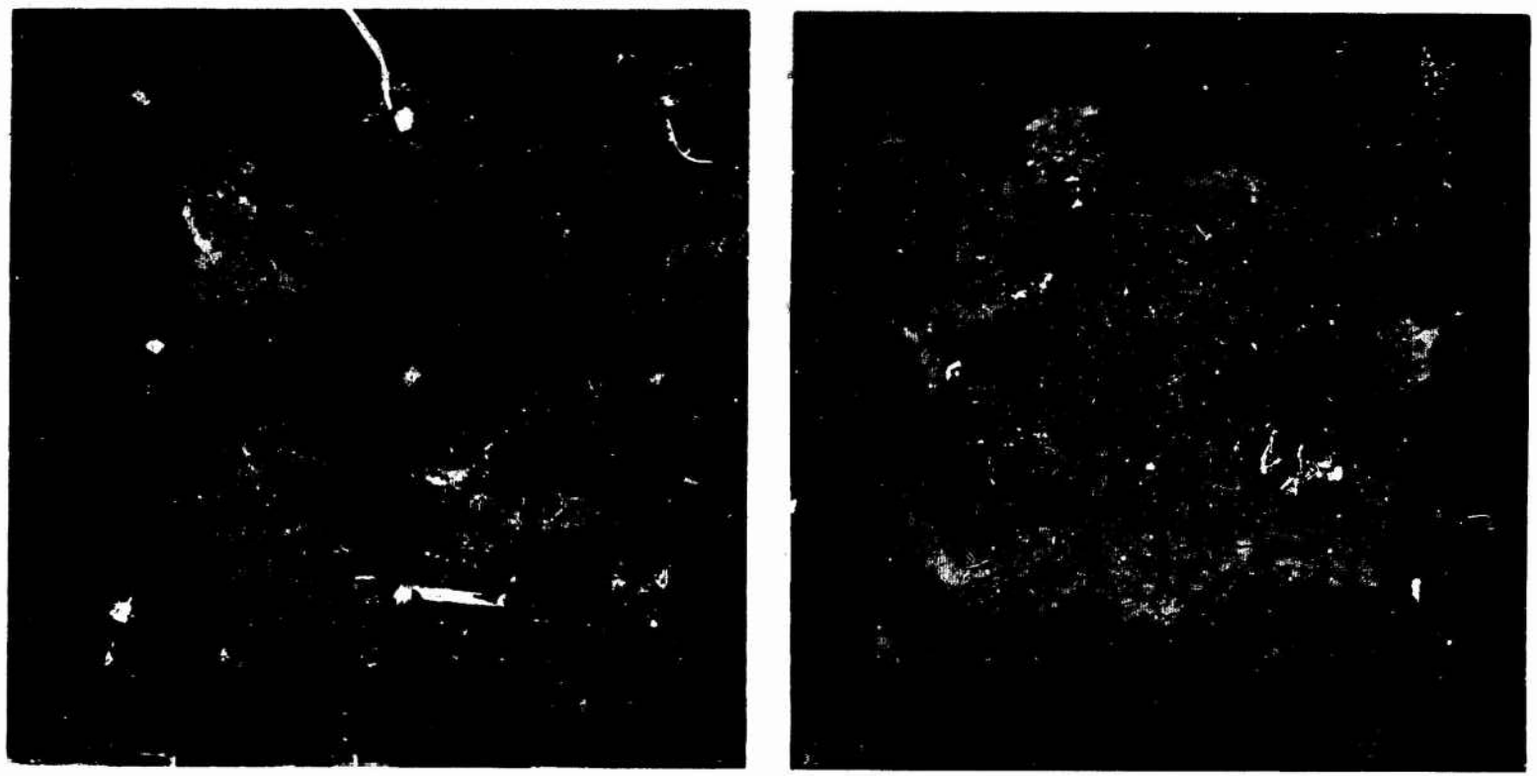

Loaded Face

Unloaded Face

Figure B-3. Slab 10S1 after test.

Table B-1. Slab Details

Slab No.	Concrete Strength, f'_c (psi)	Dimensions			Span Ratio		Longitudinal Reinforcement					Shear Reinforcement			
		Span, L (in.)	Thickness, t (in.)	Depth, d (in.)	L/t	L/d	Size No.	Spacing, s (in.)	Area p (%)	Area p' (%)	Strength, f_y (ksi)	Size No.	Area, r (%)	Spacing, s (in.)	Strength, f_y (ksi)
10S1	4,480	72	10.0	8.0	7.20	9.00	5	3	1.30	1.30	51.0	–	0.0	–	–
10.5S1	3,400	72	10.5	8.5	6.85	8.48	6	3	1.72	1.72	48.0	2	2.4	1.5	35.2

Table B-2. Average Ultimate Shear Stress

Slab No.	Concrete Strength, f'_c (psi)	Peak Load, q (psi)	Failure Mode	Average Shear Stress, $v_u/\sqrt{f'_c}$ *						Shear Steel, $rf_y/\sqrt{f'_c}$
				Section t in Thickness			Section d in Thickness			
				x = 0	x = t/2	x = t	x = 0	x = d/2	x = d	
10S1	4,480	210	shear	5.65	4.87	4.08	7.06	6.28	5.5	0.0
10.5S1	3,400	325	†	9.55	8.15	6.76	11.8	10.4	9.01	14.5

* Based upon either circular or square failure block:

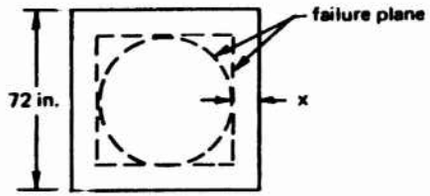

† No failure under three cycles of static loading to 325 psi and two cycles of dynamic loading to 305 psi.

Appendix C

EXPERIMENTAL DATA

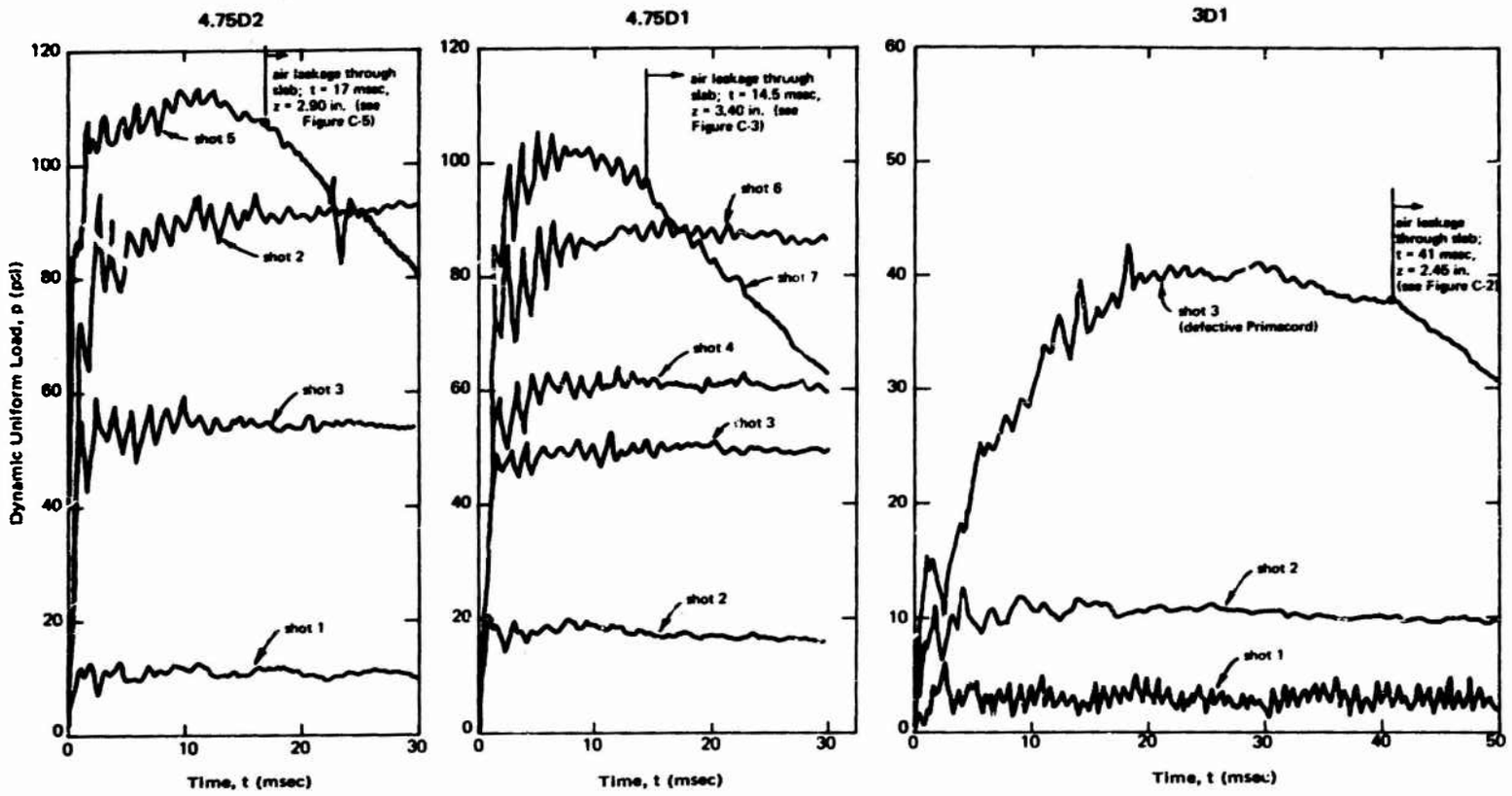

Figure C-1. Pressure-time curves for test slabs.

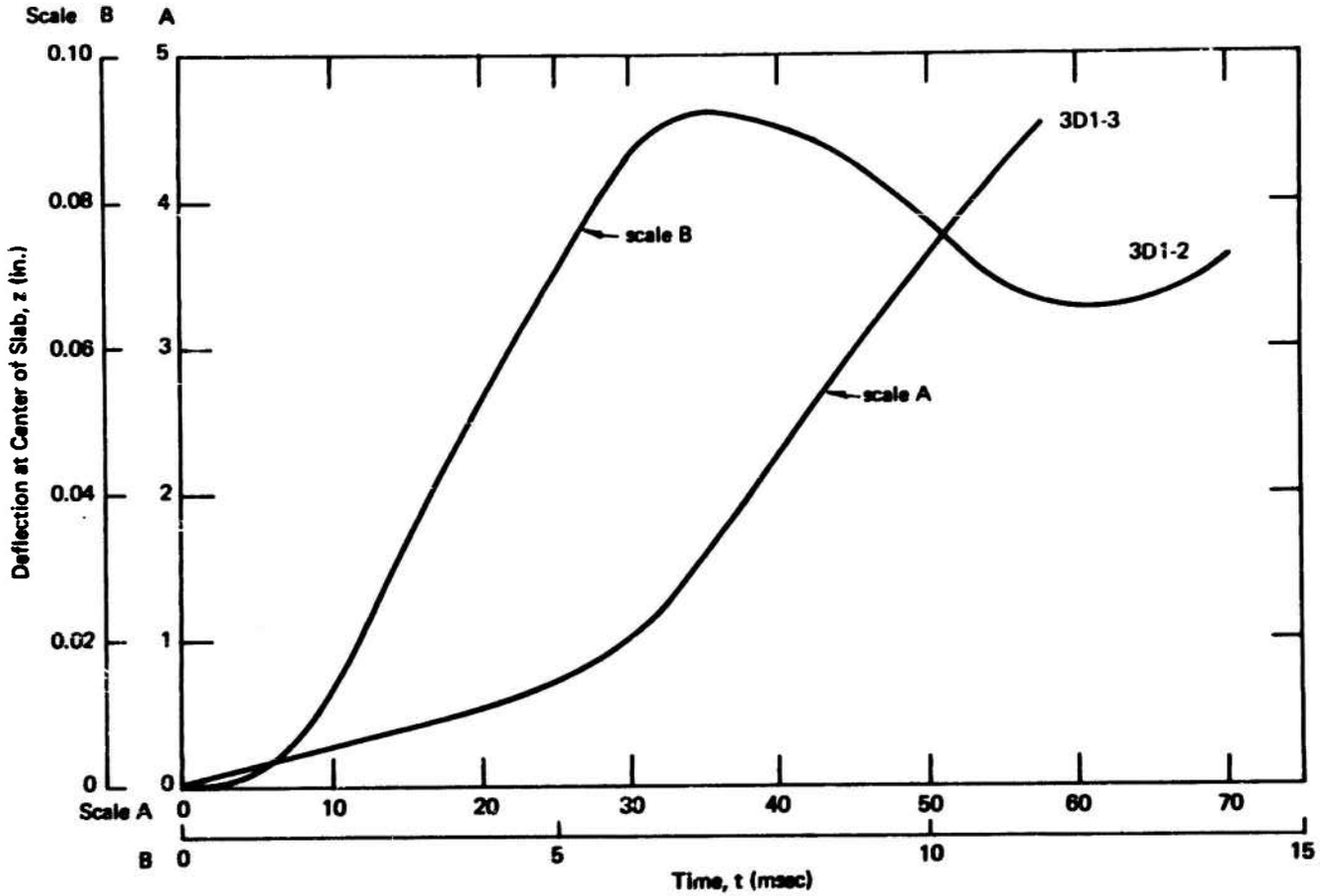

Figure C-2. Deflection-time curves for slab 3D1.

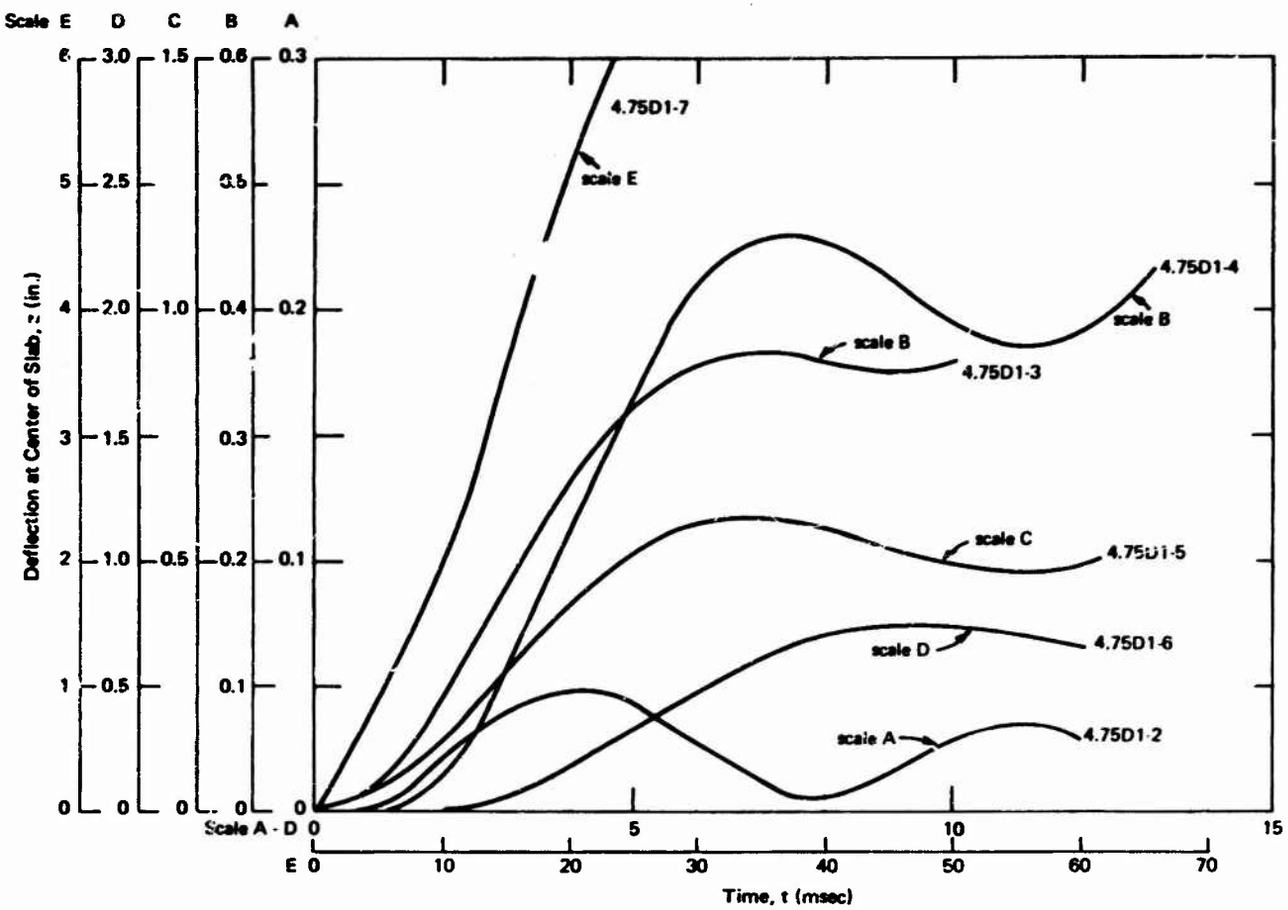

Figure C-3. Deflection-time curves for slab 4.75D1.

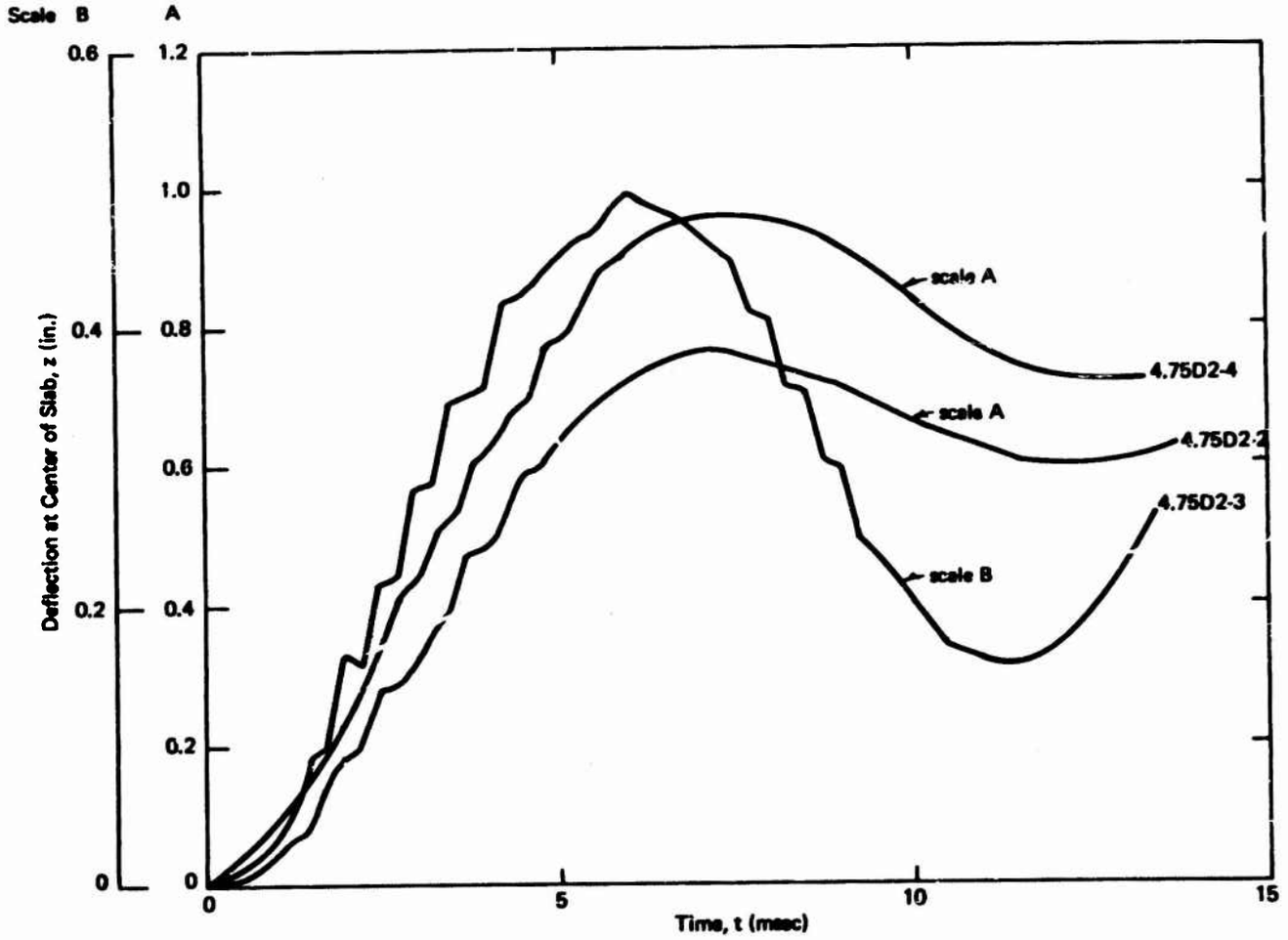

Figure C-4. Deflection-time curves for slab 4.75D2.

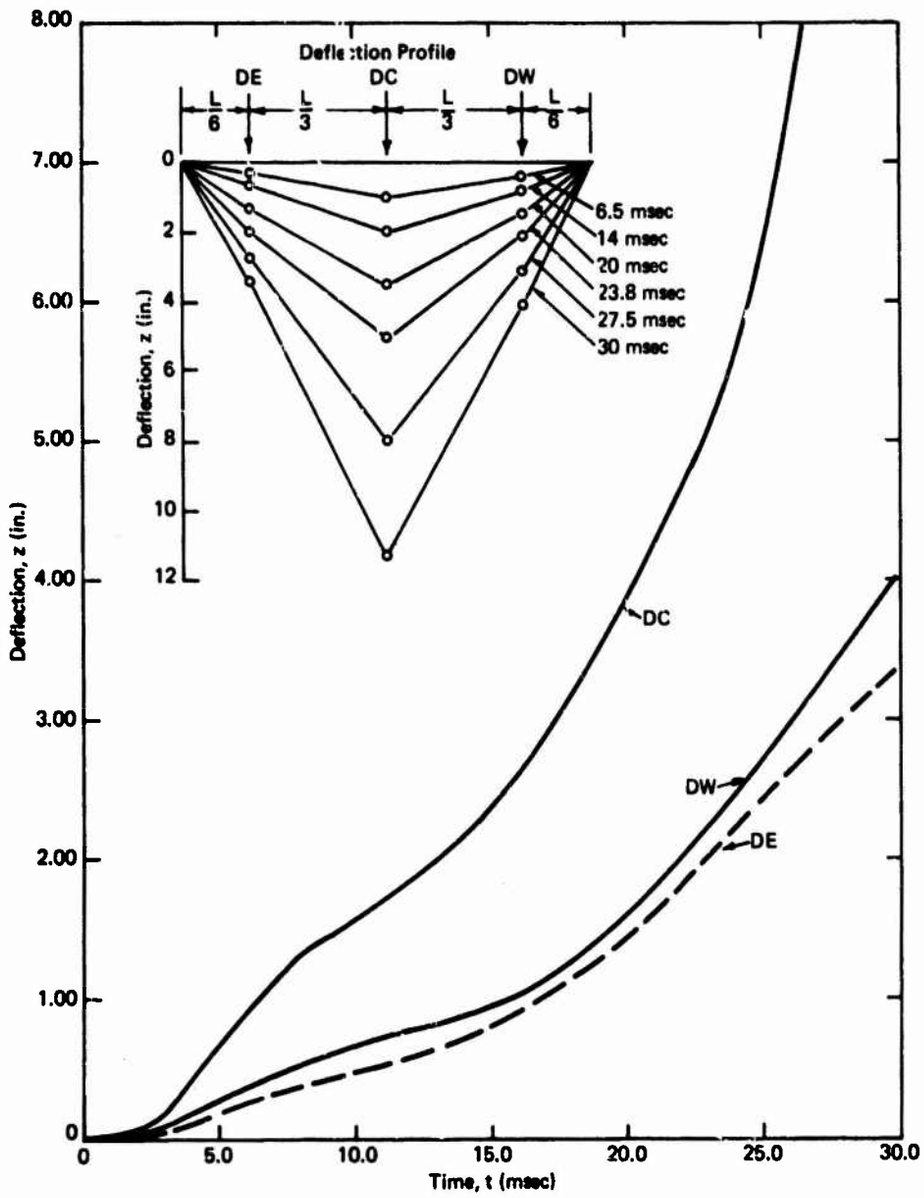

Figure C-5. Deflection-time curves for slab 4.75D2-5.

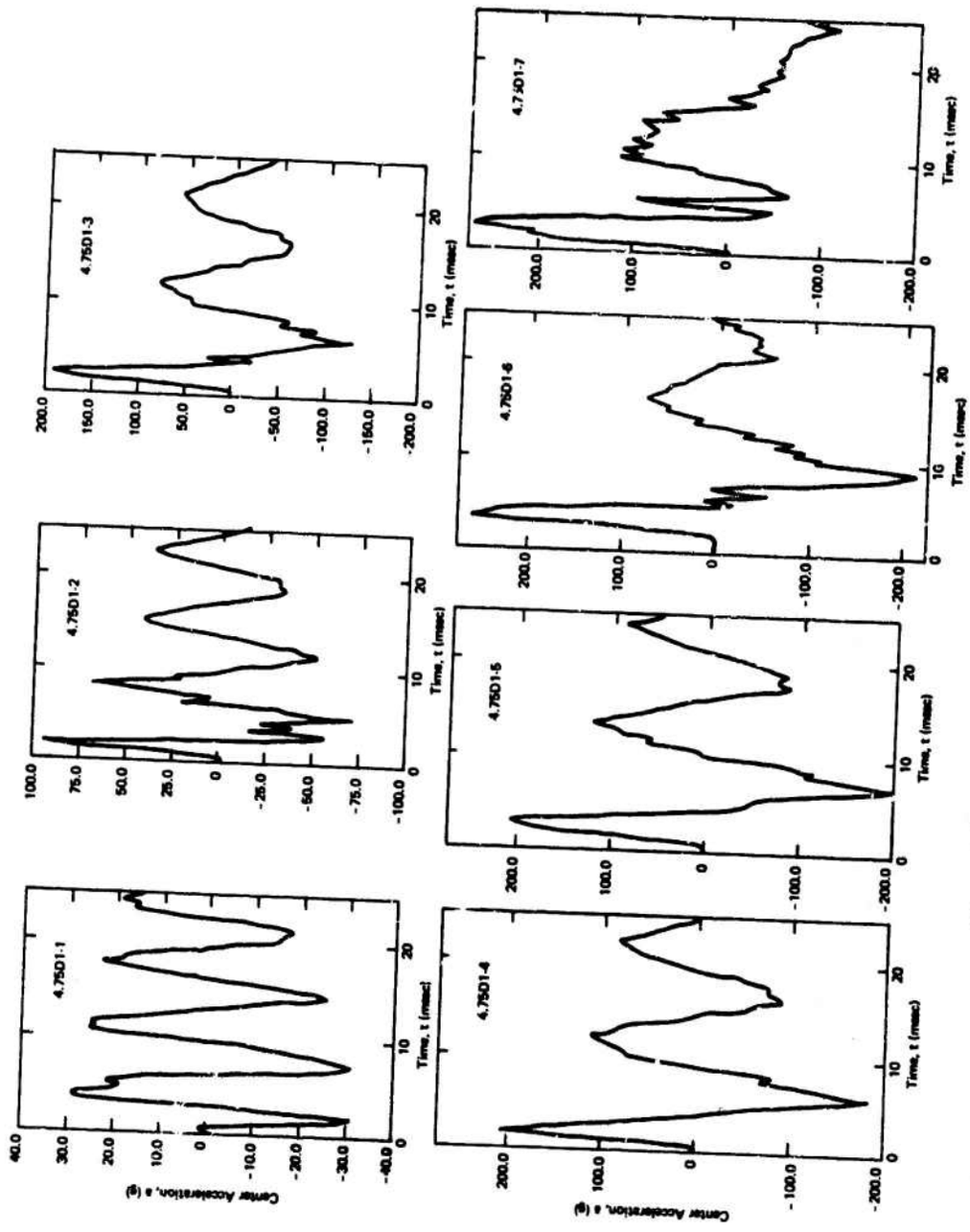

Figure C-6. Acceleration-time curves for slab 4.75D1.

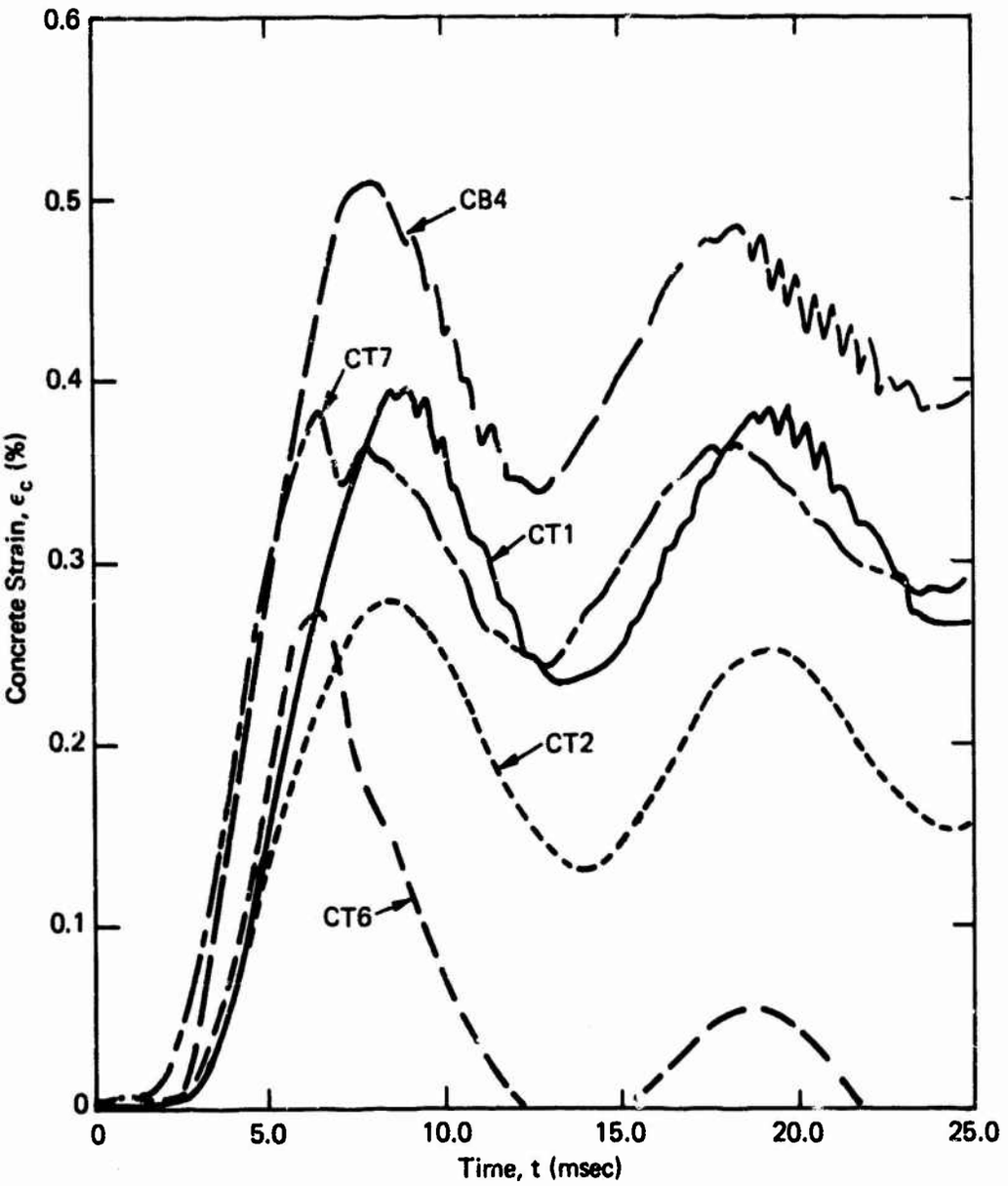

Figure C-7. Concrete strain-time curves for slab 4.75D1-5.

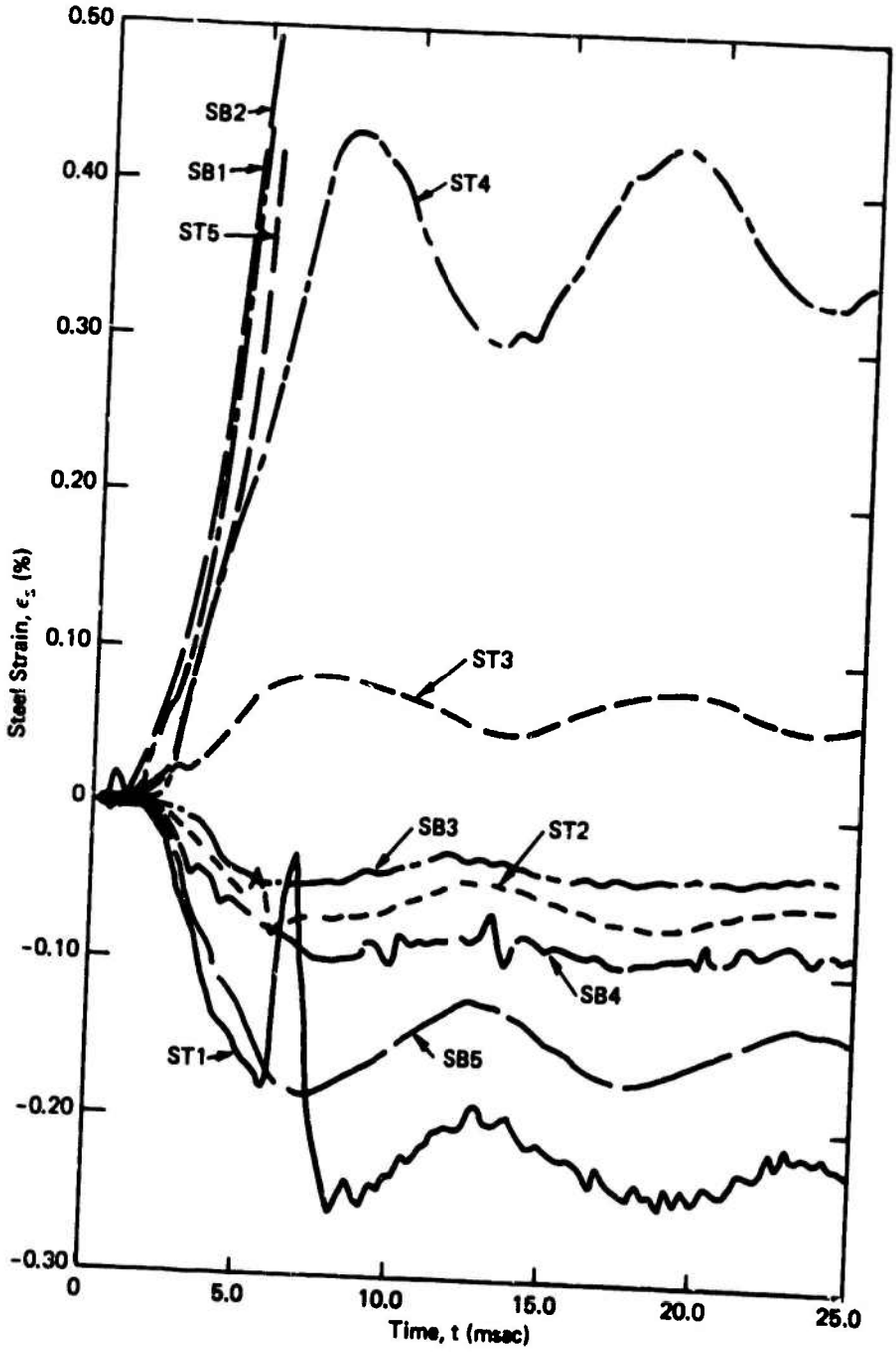

Figure C-8. Steel strain-time curves for slab 4.75D1-5.

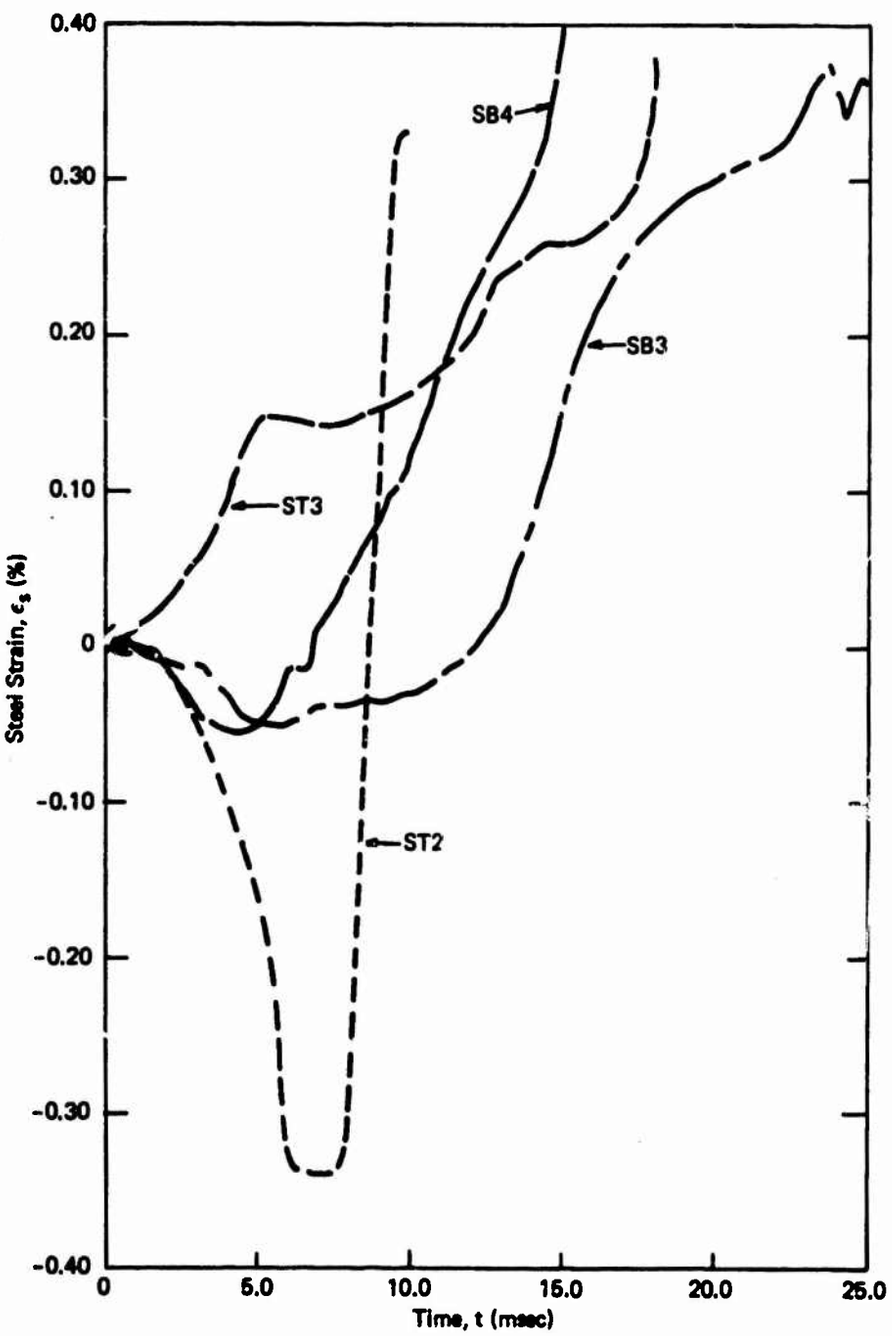

Figure C-9. Steel strain-time curves for slab 4.75D1-7.

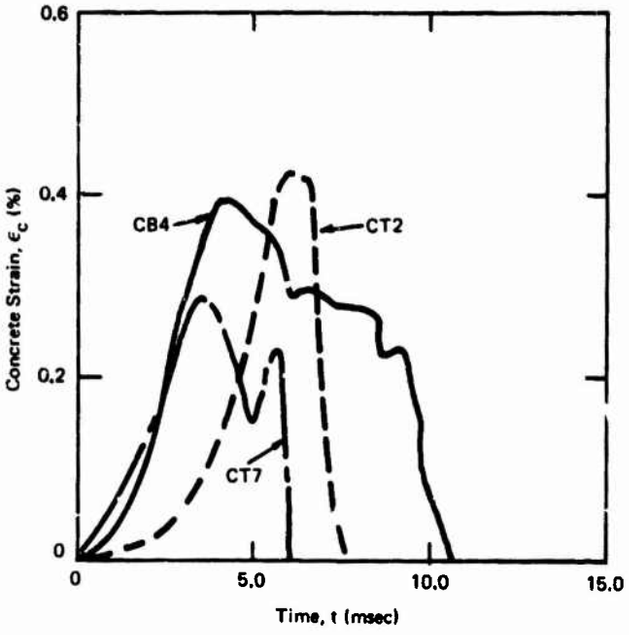

Figure C-10. Concrete strain-time curves for slab 4.75D1-7.

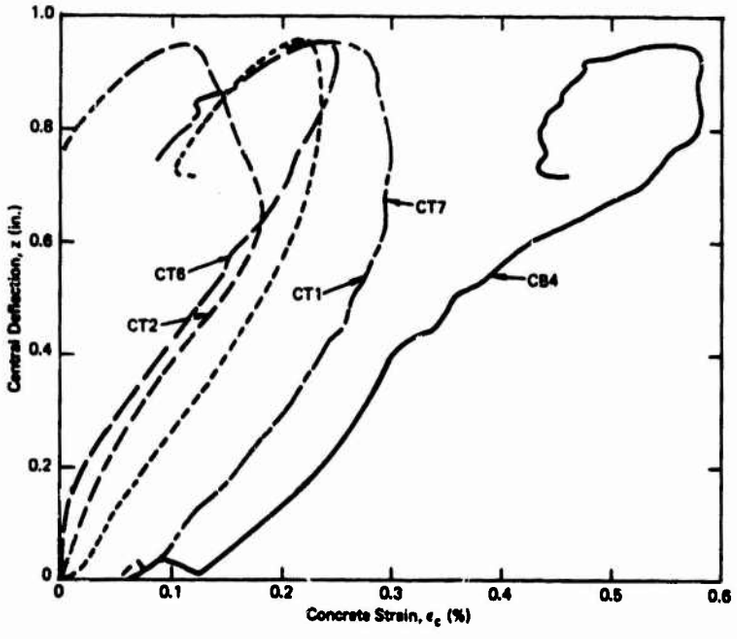

Figure C-11. Strain-deflection curves for slab 4.75D2-4.

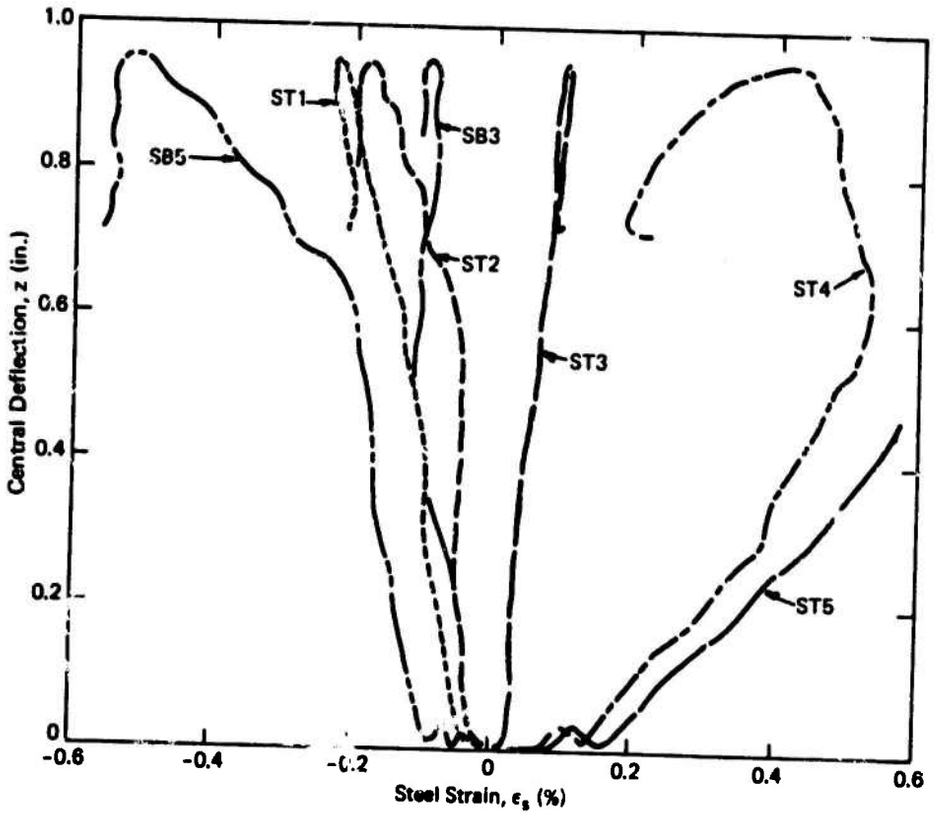

Figure C-12. Strain-deflection curves for slab 4.75D2-4.

Appendix D

STATIC- AND DYNAMIC-RESISTANCE DIAGRAMS

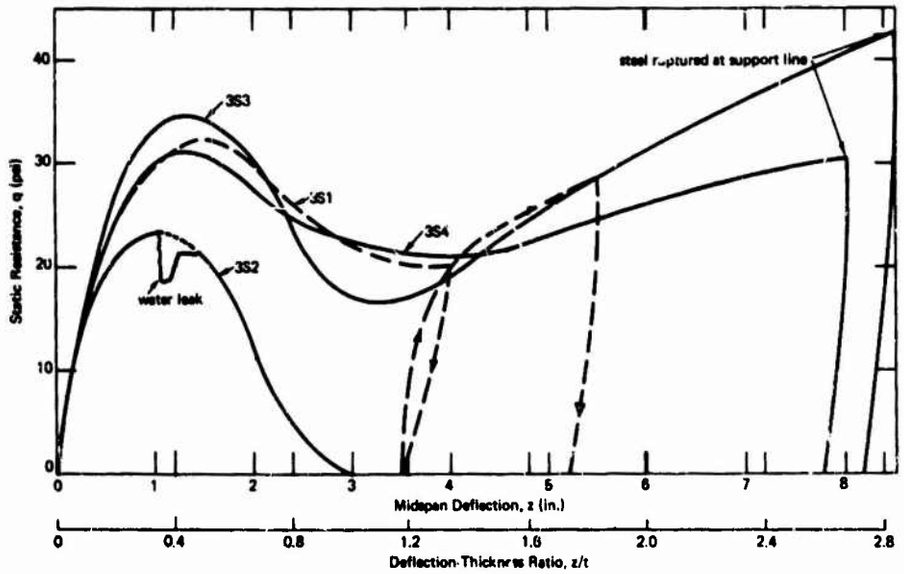

Figure D-1. Static resistance diagrams for 3-inch slabs.

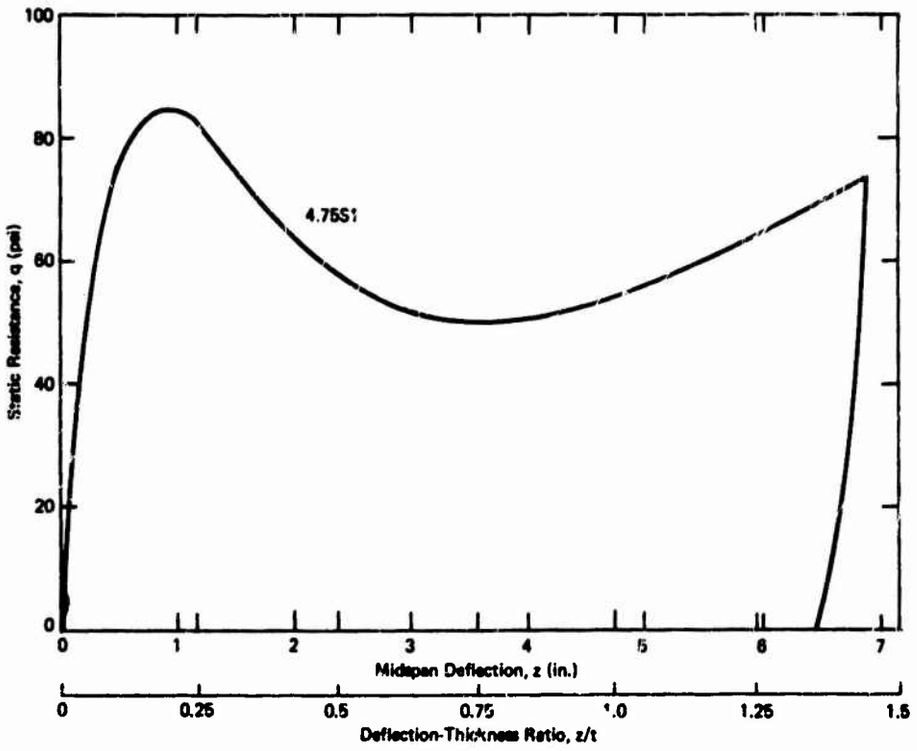

Figure D-2. Static resistance diagram for 4.75-inch slab.

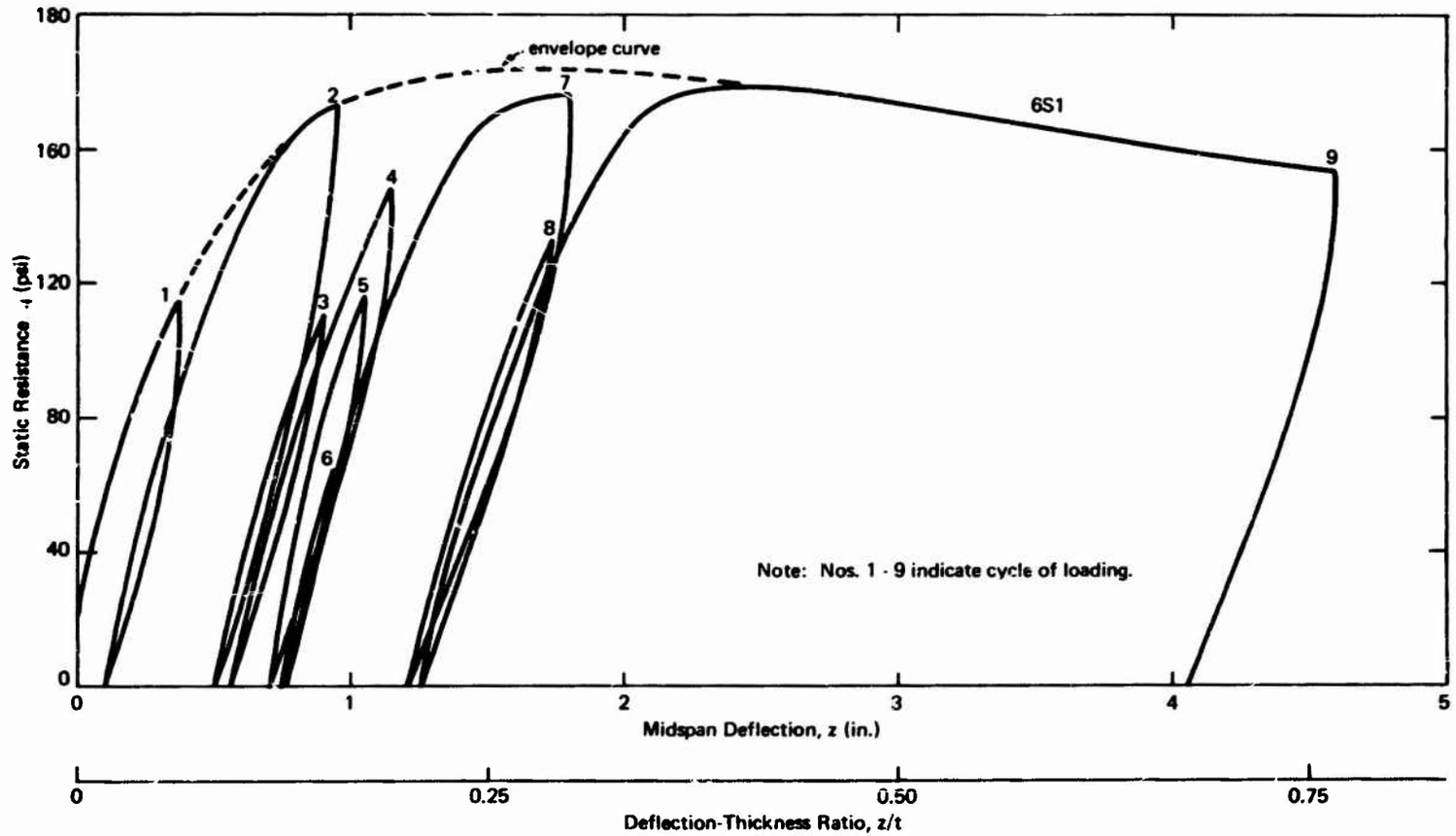

Figure D-3. Static resistance diagrams for 6-inch slab.

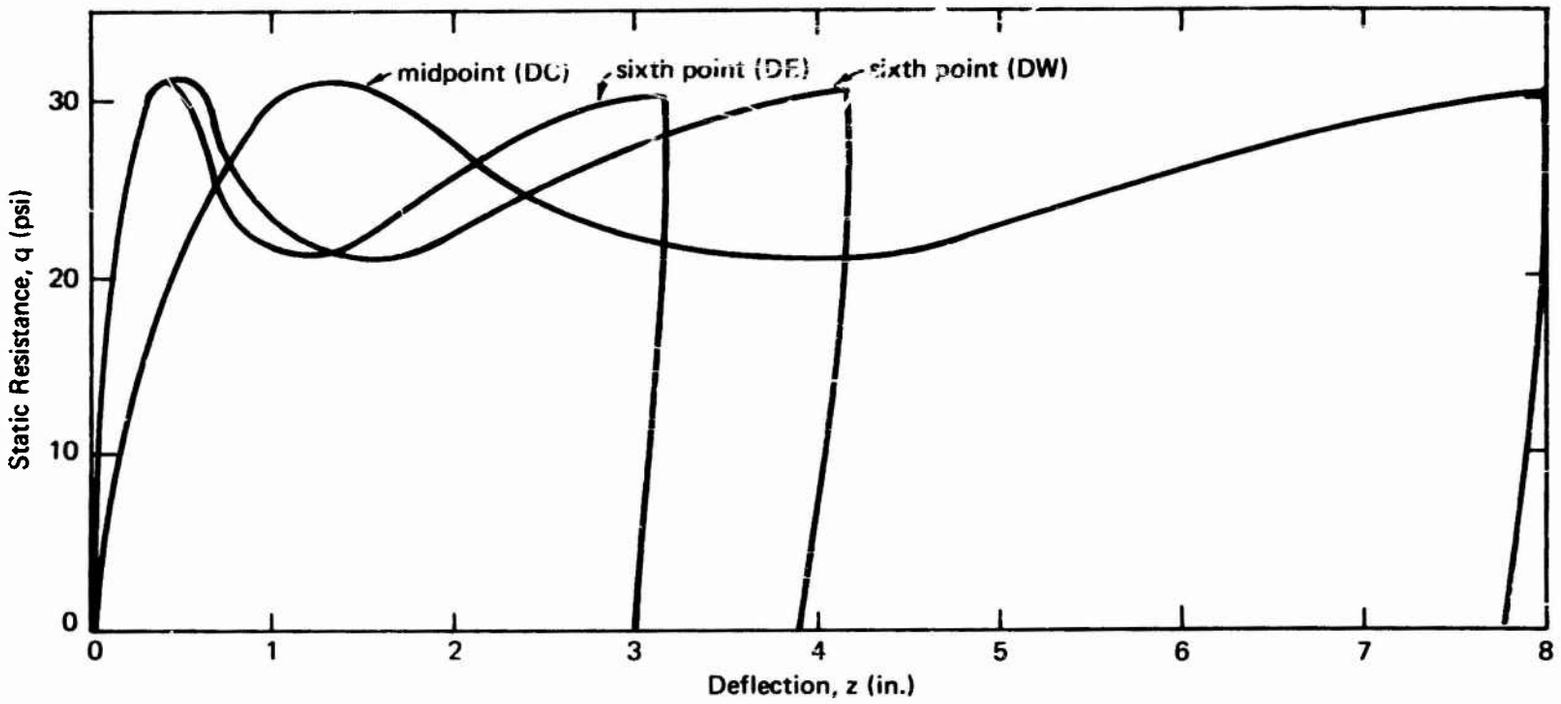

Figure D-4. Static resistance diagram at sixth point of span for slab 3S4.

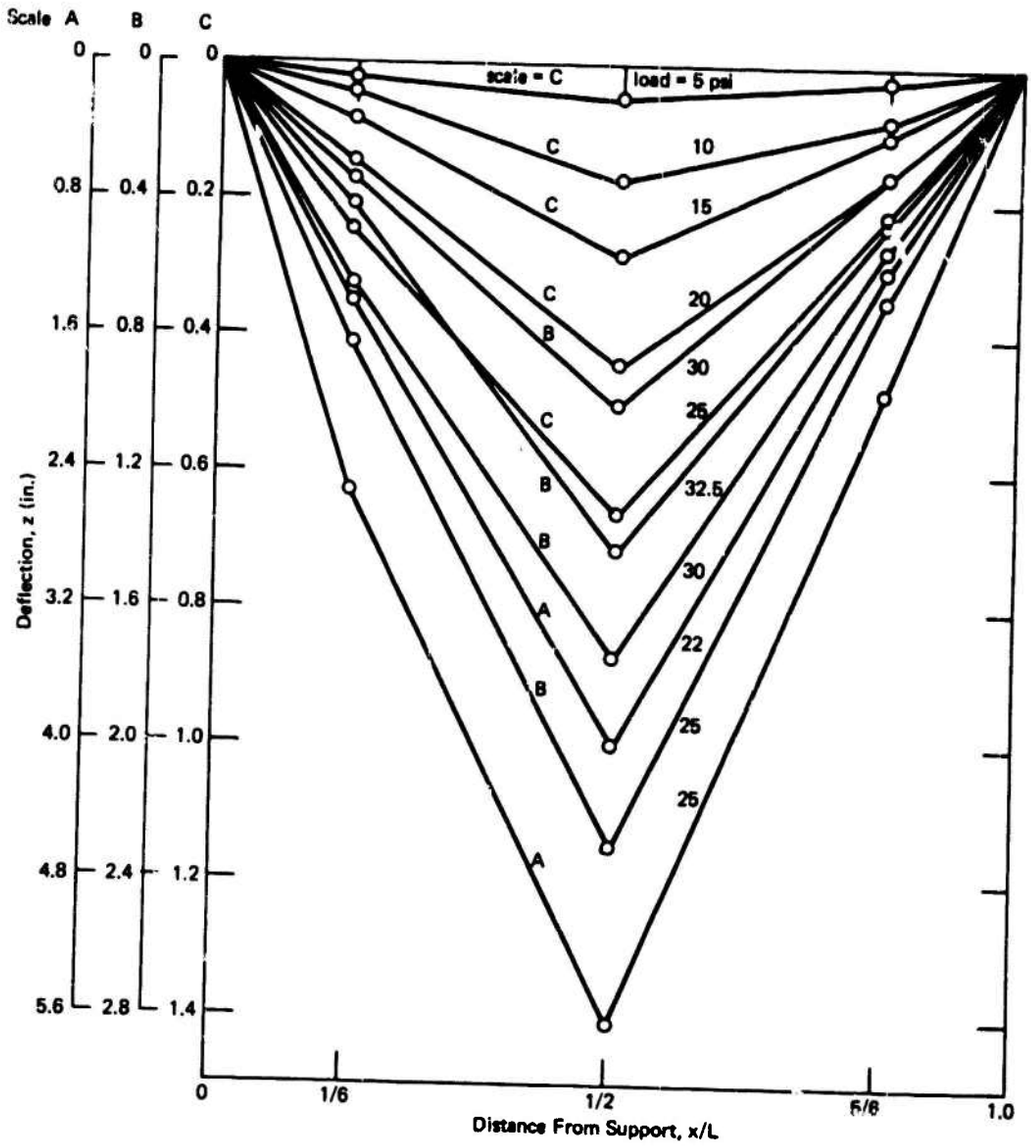

Figure D-5. Deflection profile at various loads for slab 3S4.

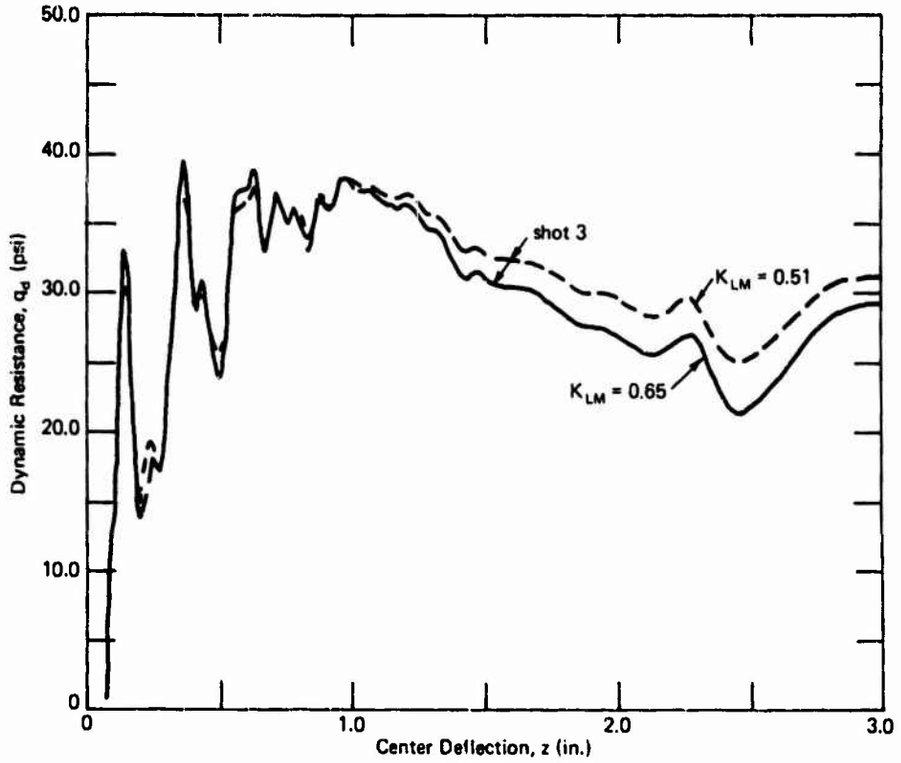

Figure D-6. Dynamic resistance function for slab 3D1.

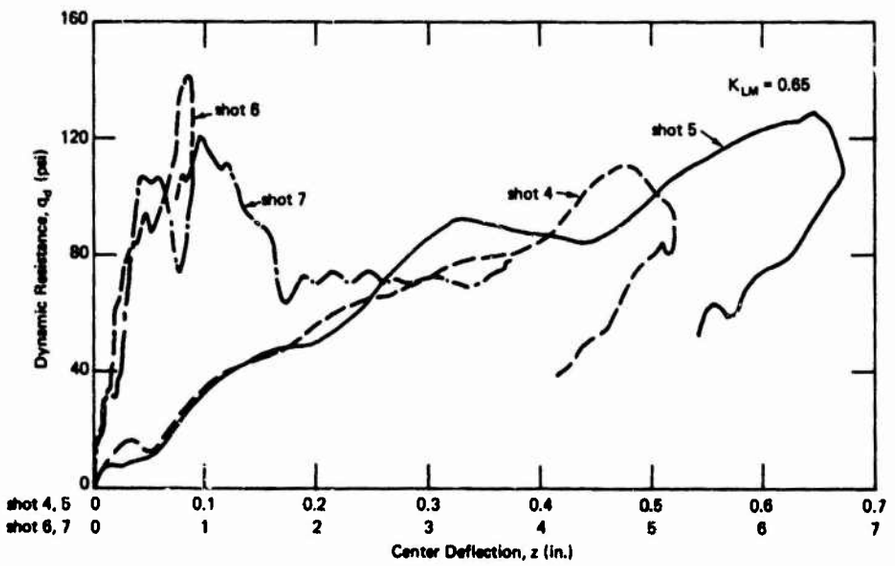

Figure D-7. Dynamic resistance function for slab 4.75D1.

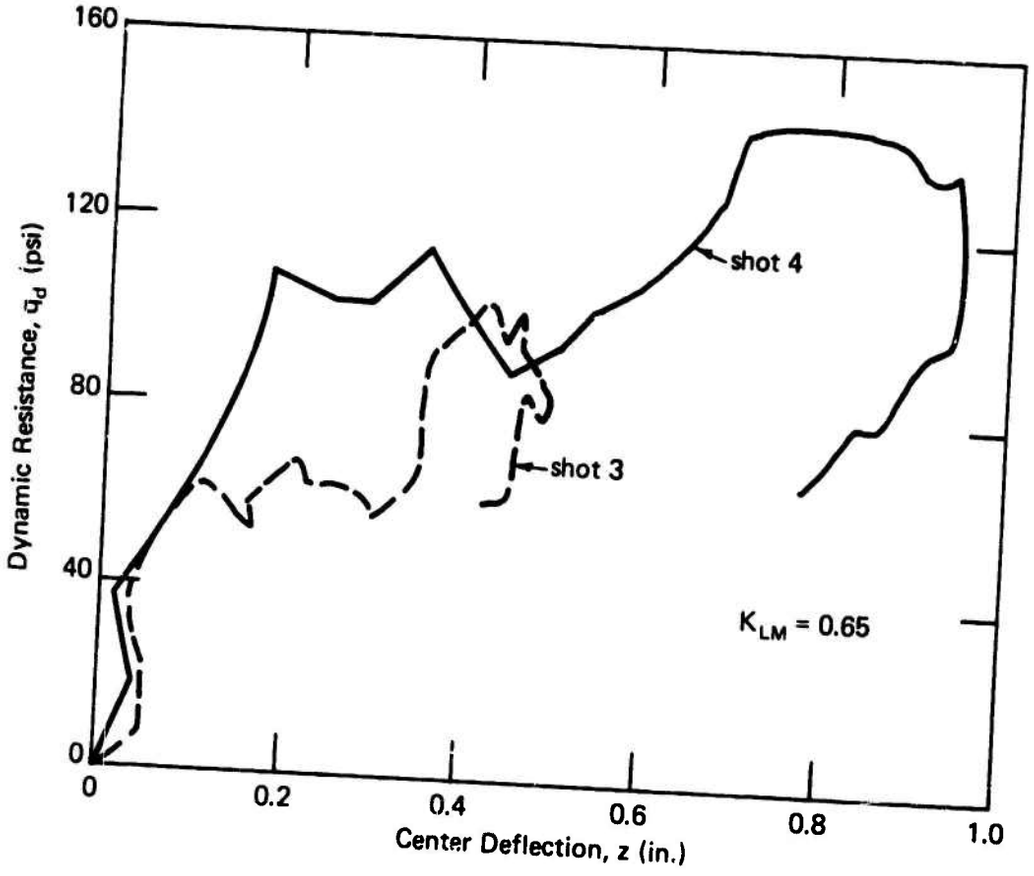

Figure D-8. Dynamic resistance function for slab 4.75D2.

Appendix E

PHOTOGRAPHS OF SLABS TESTED TO FAILURE

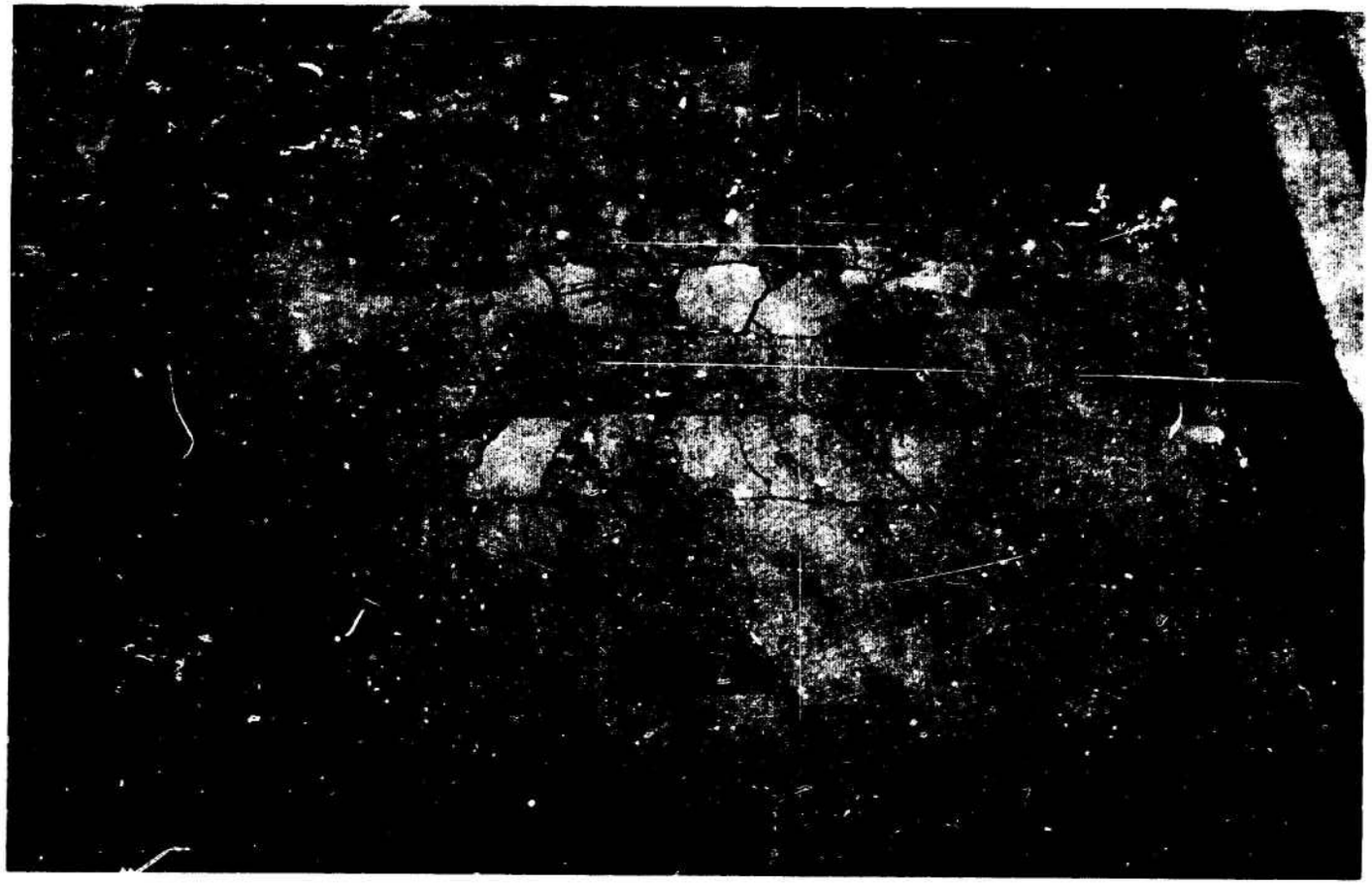

Figure E-1. Unloaded face of slab 3S1 after static test.

Loaded Face

Unloaded Face

Figure E-2. Views of slab 3S2 after test.

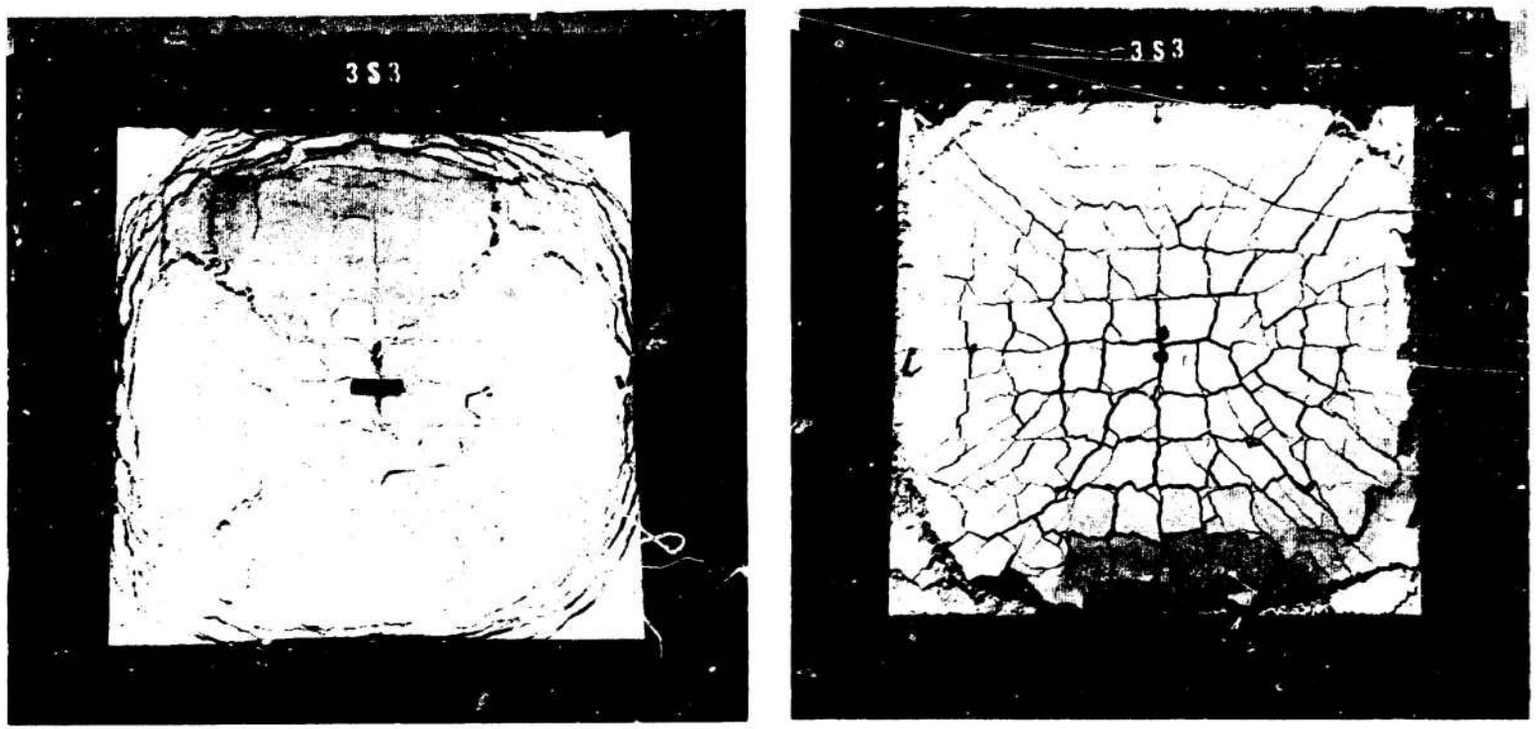

Loaded Face

Unloaded Face

Figure E-3. Views of slab 3S3 after test.

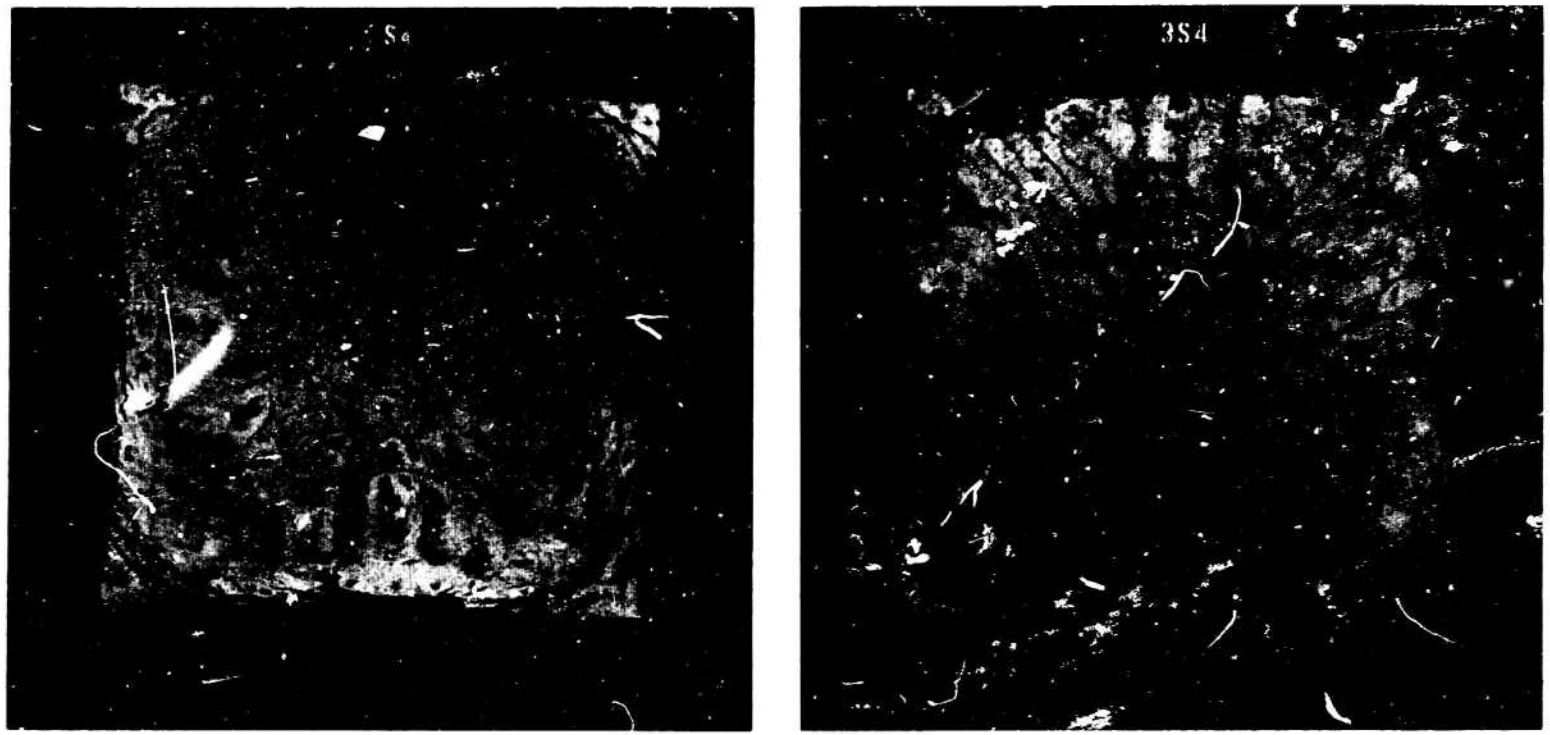

Loaded Face

Unloaded Face

Figure E-4. Views of slab 3S4 after test.

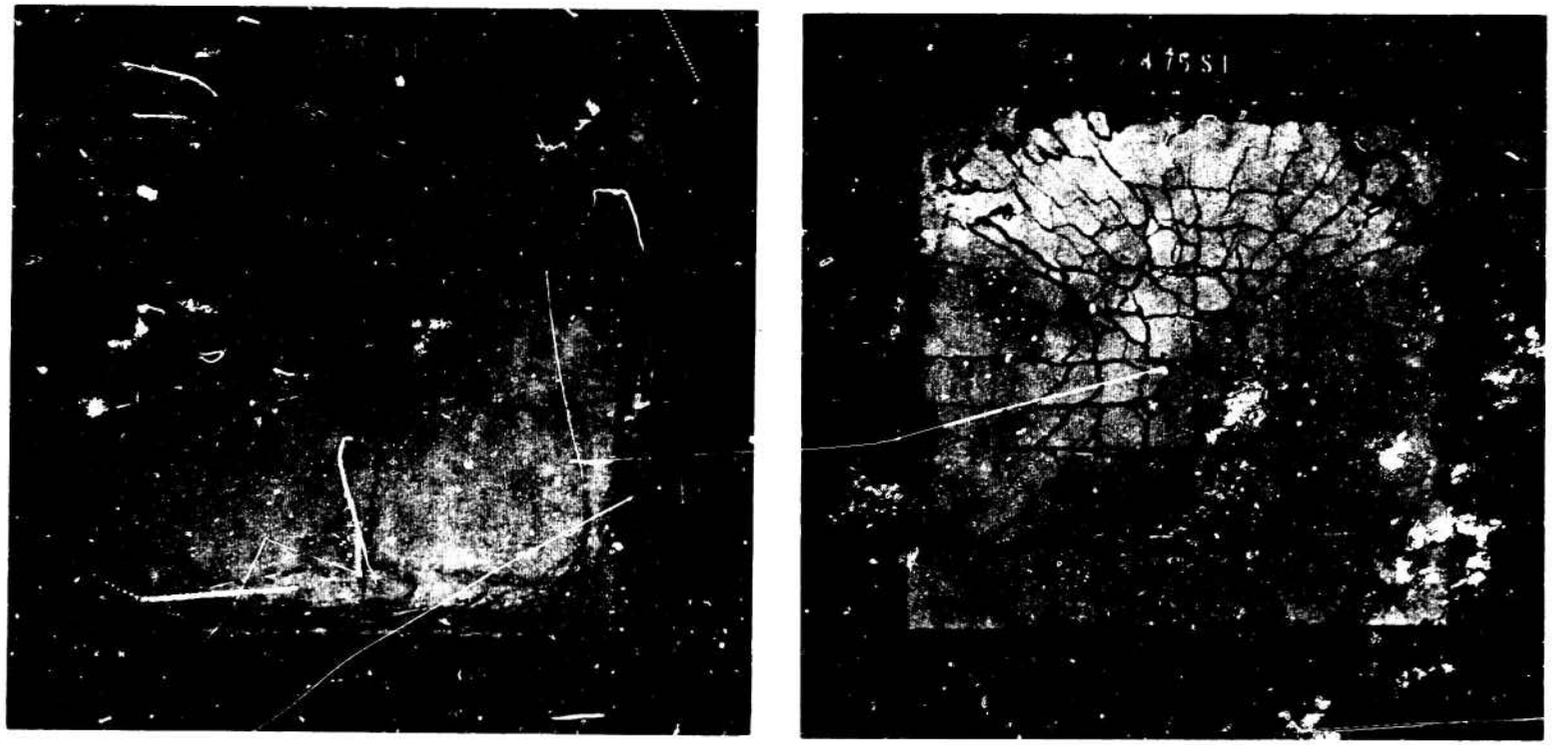

Loaded Face

Unloaded Face

Figure E-5. Views of slab 4.75S1 after test.

Figure E-6. Displacement of slab 4.75S1 near support at large center deflections

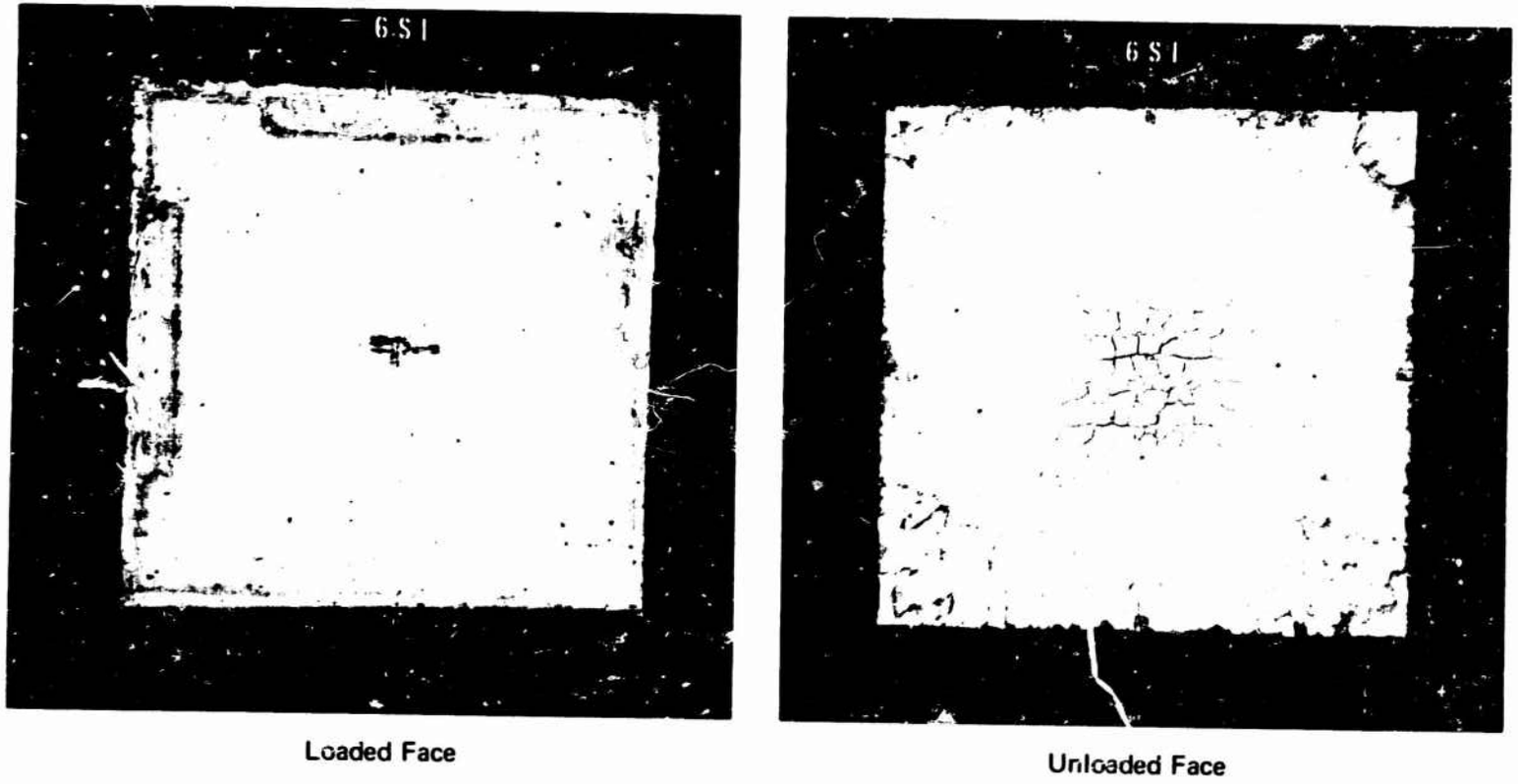

Loaded Face

Unloaded Face

Figure E-7. Slab 6S1-9 after test.

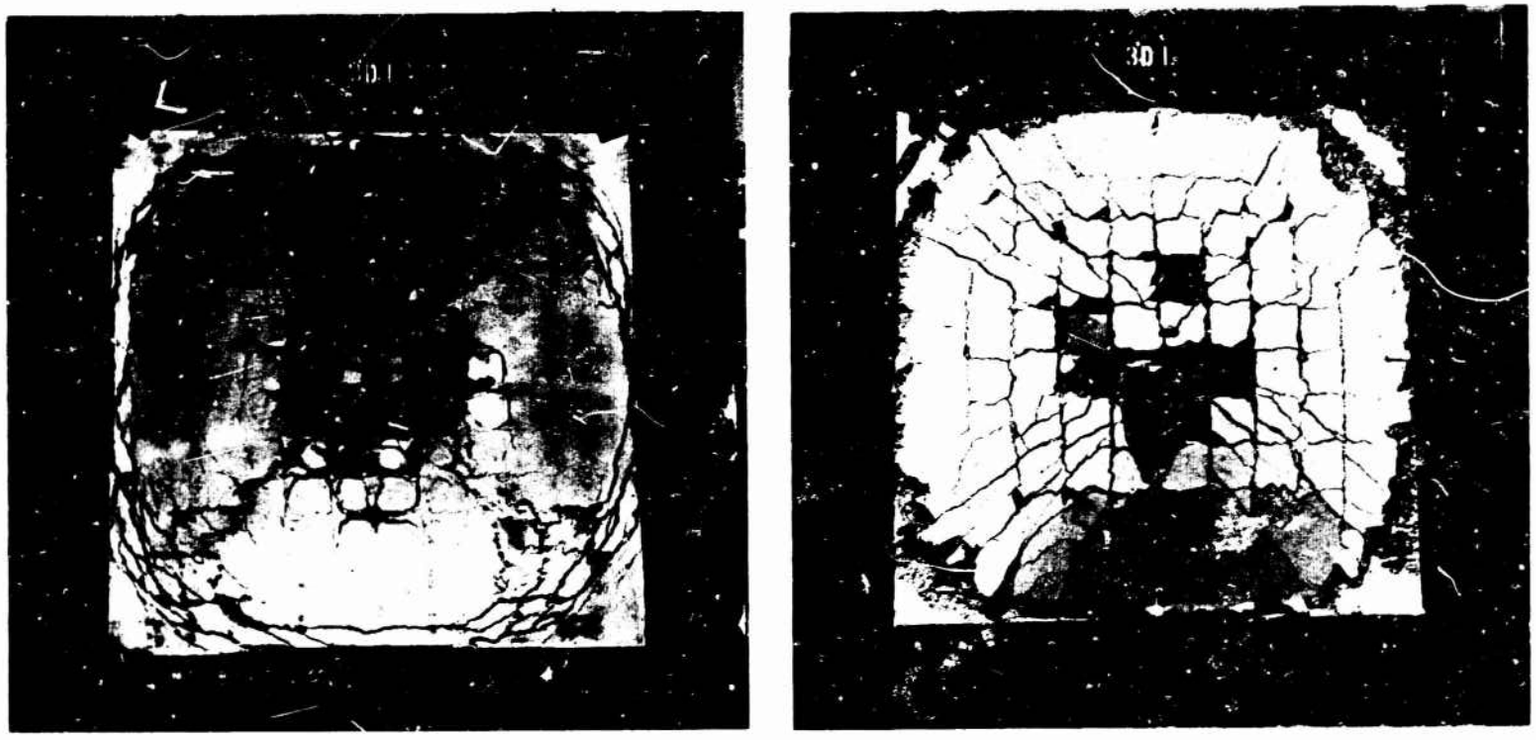

Loaded Face

Unloaded Face

Figure E-8. Slab 3D1-3 after test.

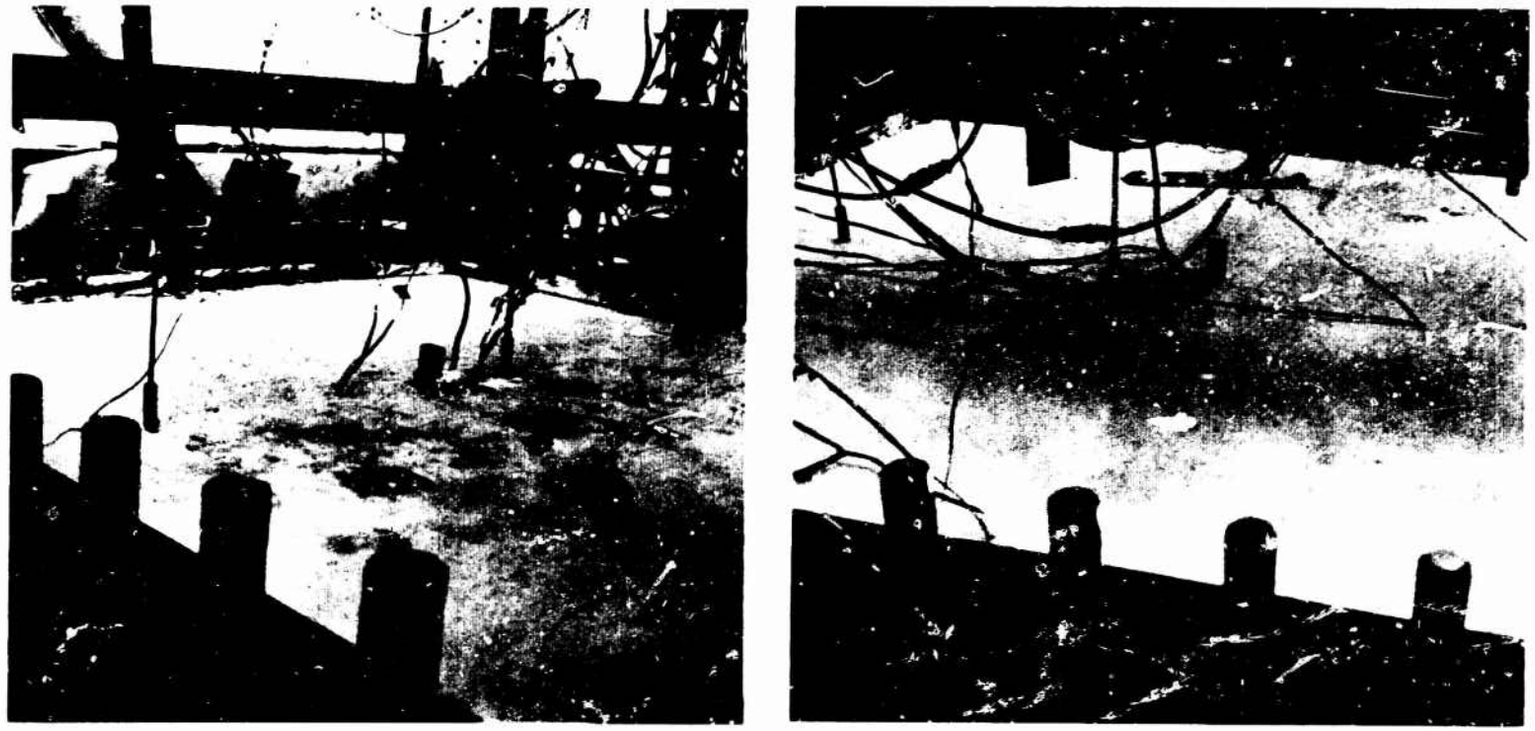

Slab 4.75D1-6

Slab 4.75D2-4

Figure E-9. Unloaded face of slabs 4.75D1 and 4.75D2 before last cycle of loading.

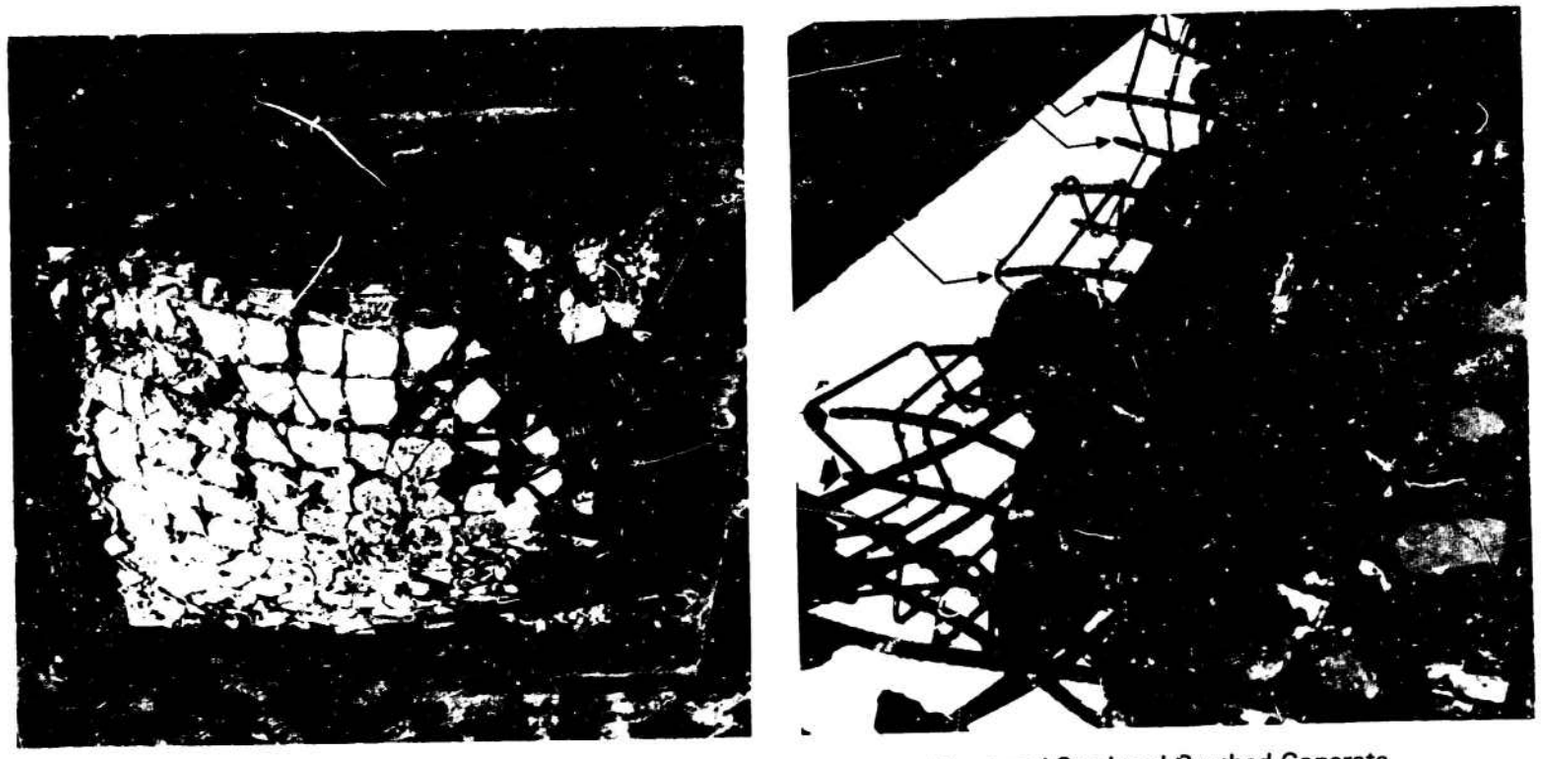

Unloaded Face

Ruptured Steel and Crushed Concrete

Figure E-10. Slab 4.75D1-7 after test.

Figure E-11. Fragmentation of slab 4.75D2-5 after test.

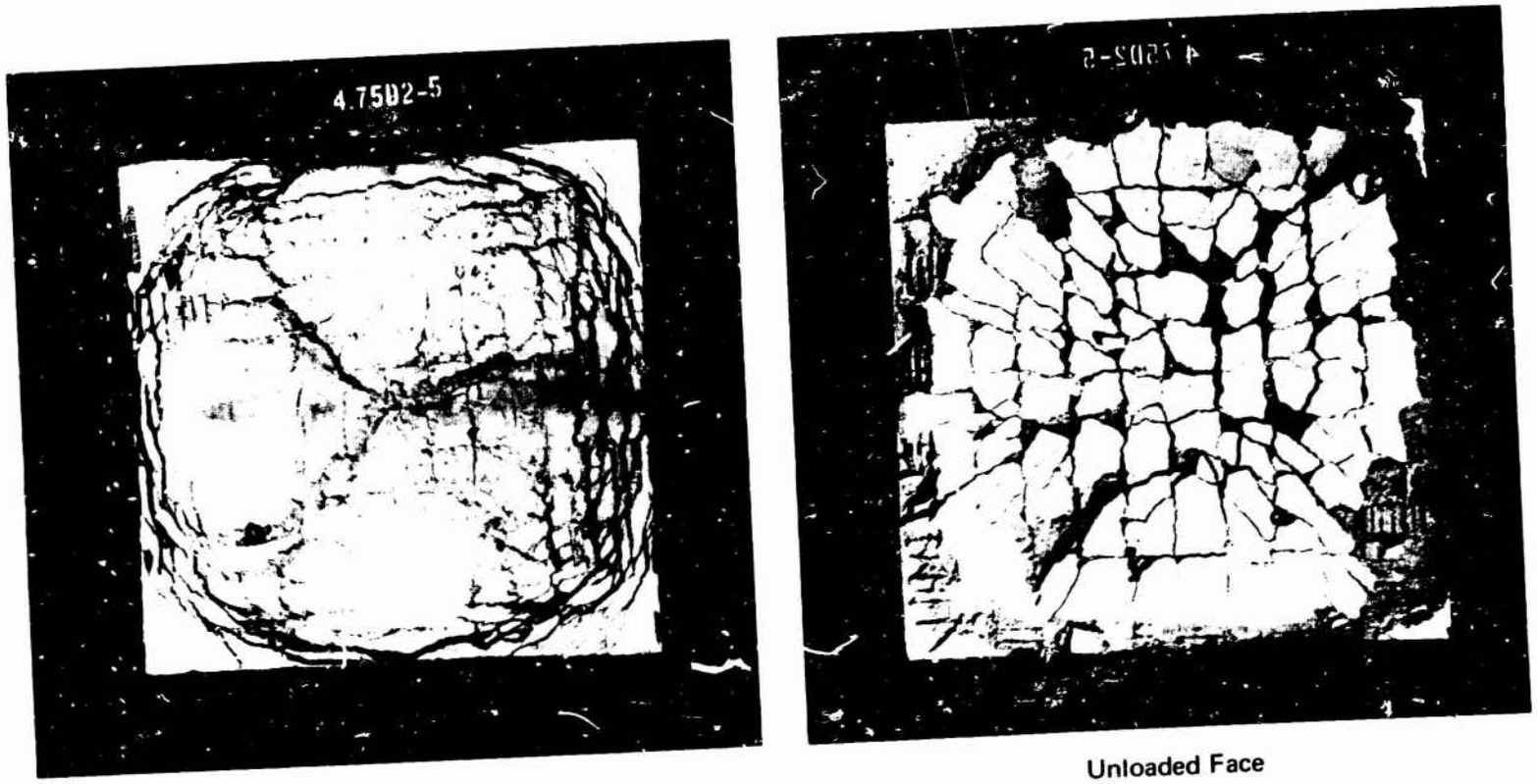

Loaded Face

Unloaded Face

Figure E-12. Slab 4.75D2-5 after test.

Table 8. Measured and Computed Maximum Dynamic Deflection

Slab No.	Measured Peak Load, p_o (psi)	Theoretical Ultimate				Maximum Dynamic Deflection			
		Resistance		Deflection, z_{ud} (in.)	Load Ratio, p_o/q_{ud}	Theory		Measured, z_M (in.)	Measured / Theory
		q_u (psi)	q_{ud} (psi)			z_M/z_{ud}	z_M (in.)		
		Column 1*	Column 2†	Column 3‡	Column 4§	Column 5¶	Column 6**		
3D1-1	3.5	31.8	44.5	1.26	0.08	0.02	0.03	0.05	1.66
3D1-2	10.5				0.23	0.09	0.11	0.09	0.82
4.75D1-1	10.5	90.9	127.0	1.18	0.08	0.02	0.02	0.03	1.50
4.75D1-2	18.0				0.14	0.04	0.05	0.05	1.00
4.75D1-3	50.0				0.39	0.25	0.30	0.37	1.23
4.75D1-4	62.0				0.49	0.37	0.44	0.46	1.04
4.75D1-5	77.0				0.60	0.57	0.67	0.60	0.90
4.75D1-6	87.0				0.68	0.77	0.91	0.76	0.84
4.75D2-1	11.0	95.0	133.0	1.18	0.09	0.02	0.03	0.04	1.33
4.75D2-2	91.0				0.68	0.77	0.91	0.77	0.85
4.75D2-3	55.0				0.41	0.27	0.32	0.50	1.56
4.75D2-4	91.0				0.68	0.77	0.91	0.96	1.05

* From Equation 17.
† From Equation 26 with DIF = 1.40.
‡ From Equations 16 and 27.
§ Measured peak load divided by Column 2.
¶ From Figure 36.
** Column 5 x Column 3.

Table 9. Measured and Computed Dynamic Load Capacity

Slab No.	Dynamic Resistance			Dynamic Load Capacity, $(p_o)_{max}$ (psi)		
	q_u (psi)*	DIF†	q_{ud} (psi)‡	Theory§	Measured¶	$\frac{\text{Measured}}{\text{Theory}}$
3D1	31.8	1.40	44.5	36.8	< 39	< 1.08
4.75D1	90.9	1.40	127.0	103.0	< 98	< 0.95
4.75D2	95.0	1.40	133.0	108.0	< 110	< 1.02

* From Equation 17.

† Average value based on measured strain rates in steel and concrete.

‡ From Equation 26.

§ From Equation 33.

¶ From Table 7.

What is the effect of longitudinal edge restraint on the dynamic load capacity of a slab? First consider an unrestrained slab with a resistance function described by Equation 31. Assume that the permissible maximum deflection is four times the effective yield-point deflection (ductility factor = 4). For this case, the peak dynamic load capacity is[18] $(p_o)_{max} = 0.88\, q_{dy}$ or $(p_o)_{max} = 1.10\, q_y$, with DIF = 1.25. Comparing the above expression with Equation 35,

$$\frac{(p_o)_{max} \text{ of slab with longitudinal restraint}}{(p_o)_{max} \text{ of slab without longitudinal restraint}} = \frac{1.14}{1.10}\left(\frac{q_u}{q_y}\right) \cong \frac{q_u}{q_y} \qquad (36)$$

Therefore, for a step pulse, the dynamic load capacity increases approximately in direct proportion to the enhancement factor, q_u/q_y. The material and geometric properties of the slab which affect this factor were discussed in a previous section.

The point where line B is tangent to curve A in Figure 23 defines the maximum allowable deflection and maximum useful strain energy which can be absorbed by the slab under a step pulse. Note that the useful strain energy capacity is approximately 25% of the total energy capacity of the slab. Also, the maximum allowable deflection is 1.4 times the dynamic ultimate deflection based on the resistance function defined by Equation 28 or

$$\left(\frac{z_m}{z_{ud}}\right)_{allowable} < 1.4 \quad \text{for } T/T_n > 10 \qquad (37)$$

Equation 37 limits the acceptable failure criteria for a longitudinally restrained slab under a step pulse of infinite duration. For example, even if either leakage of air overpressure through the slab ($z_m/z_s \approx 1$) or rupture of reinforcement ($z_m/z_t \approx 1$) are acceptable modes of failure, the maximum deflection must be limited to $z_m/z_{ud} = 1.4$. Otherwise, any long-duration load which produces deflection greater than $1.4\,z_{ud}$ will totally collapse the slab.

Period of Vibration. By equating the strain energy and kinetic energy of the slab to that of an equivalent spring-mass system, the period of vibration can be approximated as

$$T_n = 2\pi \sqrt{K_{LM}\left(\frac{m}{k_{fc}}\right)} \qquad (38)$$

where K_{LM} = load-mass factor = 0.63 (Reference 8).

m = $\gamma t/g$ = mass of slab per unit of surface area, psi-sec^2/in.

k_{fc} = stiffness of a "fixed" slab relative to the deflection at midspan based on a "cracked" transformed section, psi/in

The expression for the slab stiffness, k_{fc}, is given in Table 3. This value was shown to correlate best with the measured stiffness shown in Figure 26.

The period of vibration computed from Equation 38 is compared with measured values in Table 10. The difference between measured and computed values increases with the level of loading, which is natural to expect. However, the measured and computed values are the same order of magnitude for the range of loadings.

Concrete Missile Fragments

Under certain conditions, concrete fragments are torn free from a slab under blast loading. These fragments act as missiles which could jeopardize the functional integrity of the slab. For such cases, ejection of concrete missile fragments is a failure criterion for design.

Three sources of concrete missile fragments are illustrated in Figure 38. Fragments can be caused by stress wave propagation through the slab, dynamic deflections in the tensile membrane region of behavior, and loads greater than the dynamic load capacity of the slab.

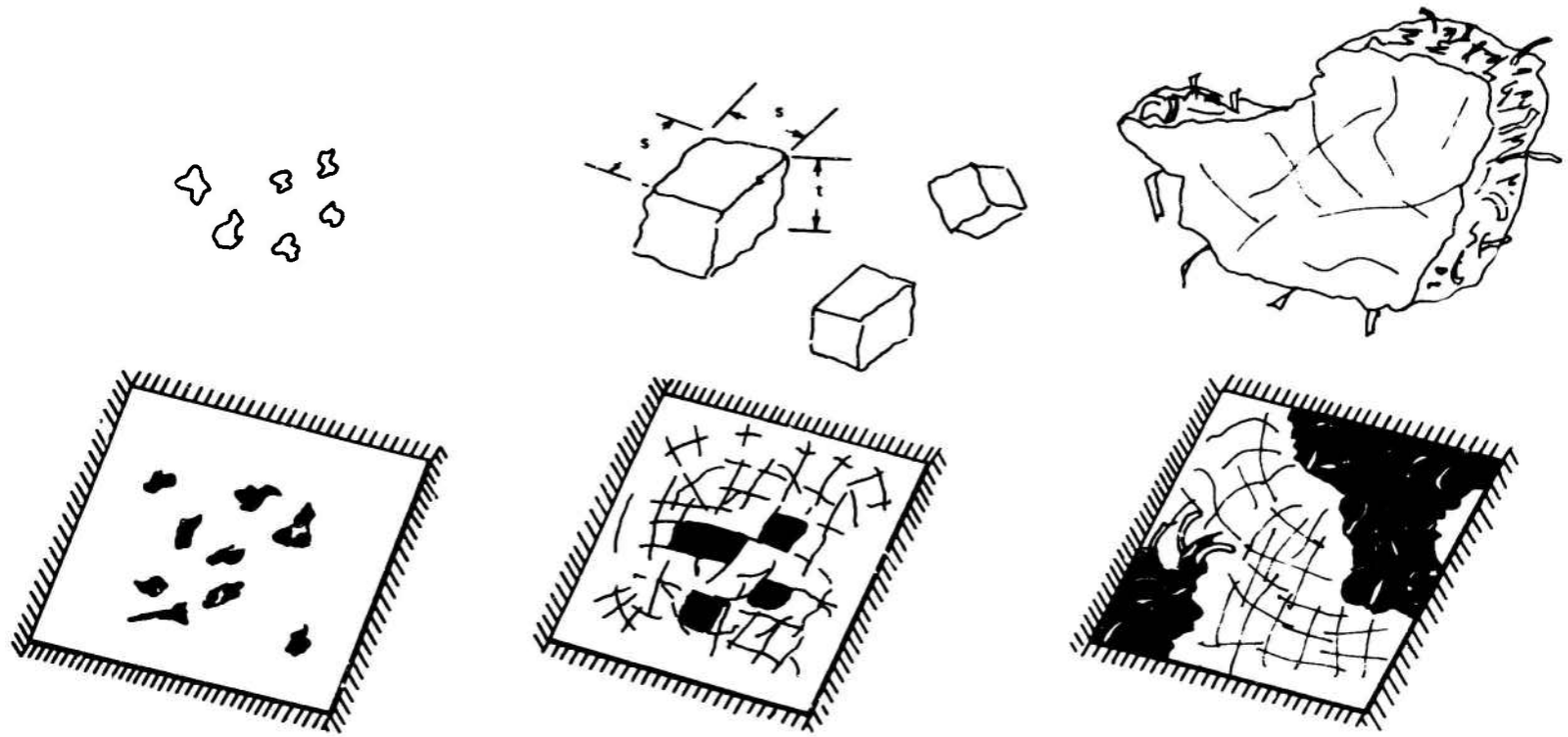

Figure 38. Three causes of concrete missile fragments.

Table 10. Measured and Computed Period of Vibration

Slab No.	Period of Vibration, T_n (msec)			
	Computed*	Measured		Measured/Computed
		Tested Value†	Average‡	
3D1	17.4	10.0, 12.5, 14.2	12.3	0.58-0.82 (0.71)
4.75D1	10.1	6.9, 7.0, 9.6, 10.0, 10.5, 10.5	9.1	0.69-1.04 (0.90)
4.75D2	10.0	6.9, 10.1, 11.5, 11.9	10.1	0.69-1.19 (1.01)

* From Equation 38.

† Values listed in order of increasing maximum dynamic deflections.

‡ Average values taken from acceleration-time and strain-time curves.

A blast wave striking the face of a slab will cause a stress wave to travel through the depth of the slab and reflect from the opposite face. The reflected wave will result in tensile stresses. Takahashi and Allgood[21] have shown that under certain conditions these stresses are sufficient to spall concrete from the unloaded face of the slab. The critical load duration, T_{cr}, corresponding to a peak load, p_o, that will initiate spalling of concrete at a distance h from the unloaded face of the slab is[21]

$$T_{cr} = \frac{2 p_o h}{c f_t'} \tag{39}$$

where c = velocity of shock wave

f_t' = tensile strength of concrete

It was concluded from Equation 39 that spalling could be a problem for high overpressures (several thousand psi) and very short load durations (less than about one msec). This explains why concrete did not spall from the unloaded face of the NCEL slabs (see Figure E-9); all slabs were subjected to long-duration loads of less than 100 psi.

Concrete missile fragments resulted from dynamic loads which deflected the slab into the tensile membrane mode of behavior. As the tensile membrane region spread outward from the center of the slab, the main reinforcement yielded, causing concrete blocks the size of the reinforcing mesh (s x s x t) to break loose from the slab. This type of missile fragment was apparent in slab 3D1-3 (Figure E-8). This source of missile fragments can be avoided by using either smaller-size bars closely spaced or lacing bars between the main reinforcement. The effectiveness of lacing bars was demonstrated by the behavior of slabs 4.75D1 and 4.75D2 (see Figures E-10 through E-12). These slabs underwent large tensile membrane deflections, but the lacing bars (see slab details in Figure 21) prevented this type of missile fragment. However, the lacing bars did not prevent severe spalling of concrete to the level of the reinforcement as shown in Figures E-11 and E-12.

Large missile fragments (Figure 38) resulted when deflections exceeded that corresponding to the capacity of the slab as a tensile membrane ($z_m > z_t$). Whole sections of the slab were torn loose from its support line where reinforcement yielded, necked down, and ruptured in tension (see Figure F-10). It would appear that the failure modes of either slab 3D1-3 (Figure E-8) or slab 4.75D1-7 (Figure E-10) are typical for slabs under long-duration loads greater than the value given by Equation 35. If the pressure on the slab is not relieved by blocks of concrete being freed from the reinforcing mesh, the pressure will deflect the slab until whole portions of the slab are eventually torn loose. Thus, closely spaced longitudinal bars and lacing bars can prevent intermediate-size missile fragments but will precipitate a much more violent and destructive mode of failure under long-duration loads.

FINDINGS AND CONCLUSIONS

The following findings and conclusions apply only to a uniformly loaded, square slab with edges fully restrained against rotation and partially restrained against translation. Unless otherwise noted, reference to dynamic load implies a step pulse.

1. The ultimate flexural resistance is increased by full or partial restraint against outward movement of the edges. The enhancement factor, q_u/q_y, can be several hundred percent. The exact magnitude depends primarily upon the cross-sectional properties of the slab, crushing strain of the concrete, span-thickness ratio, and degree of longitudinal restraint.

a. Steel Ratio. The enhancement factor increases with a decrease in the tensile steel ratio, p; the factor is infinite for $p = 0$ and approaches unity as p approaches the balanced steel ratio, p_b. In general, the effect of

compression steel depends on the ratio p'/p. For p greater than some critical value (0.6 to 0.8%), the enhancement factor increases with p'/p. For p less than the critical steel ratio, the factor decreases with p'/p (see Figure 19).

b. **Crushing Strain of Concrete.** The enhancement factor increases with the crushing strain of the concrete. Disintegration of the concrete limits the maximum in-plane thrust and moment resistance of the slab cross section and, therefore, the ultimate flexural resistance of the slab. An average crushing strain of 0.0038 in./in. gave the best correlation between theory and tests, although higher and lower strains were recorded in the tests.

c. **Span-Thickness Ratio.** For span-thickness ratios less than 18, material instability (concrete crushing) limits the enhancement factor which decreases with increasing span-thickness ratios. For span-thickness ratios greater than 18, geometric instability (similar to the snap-through deflection of a linkage) limits the enhancement factor which is independent of L/t (see Figure 19).

d. **Degree of Longitudinal Restraint.** The enhancement factor decreases with increasing amounts of longitudinal edge movement. The effect of edge movement on enhancement factor increases with span-thickness ratio; for a given span, the thicker the slab the more edge movement which can be tolerated without significantly reducing the ultimate flexural resistance (see Figure 18).

2. The flexural ultimate deflection *directly* depends upon the properties of the cross section, crushing strain of concrete, span-thickness ratio, and degree of longitudinal edge restraint (see Equation 15). For span-thickness ratios less than 18, this critical deflection is controlled by material instability; the latter is very sensitive to the parameters just cited (see Figures 15, 16, and 27). For span-thickness ratios greater than 18, the critical deflection is controlled by geometric instability which occurs at a center deflection equal to 0.42 t. This value is based on test data (see Figure 27).

3. The induced compressive thrust is a maximum when the midspan deflection reaches the critical deflection. Based on a collapse mechanism consisting of four plane quadrants, the thrust (theoretical) is maximum at the corners and minimum at midspan. At the corners, the maximum thrust is 80 to 100% of the balanced thrust, N_b, for $30{,}000 < f_y < 50{,}000$ psi and $p - p' < 2.5\%$. The balanced thrust is the thrust on the cross section, which would produce simultaneous yielding of tension steel and crushing of concrete at the extreme fiber. At midspan, the maximum thrust is 60 to 100% of the balanced thrust for $30{,}000 < f_y < 60{,}000$ psi, $p - p' < 1.5\%$; and $10 < L/t < 20$ (see Figures 12 and 13).

4. Cracking was first visible in the unloaded face of the slab at a static resistance ranging from 67 to 96% of the flexural resistance based on simple yield-line theory (Table 6).

5. The strength and behavior of longitudinally restrained slabs are deflection-sensitive. Initial slab deflections induce increasing compressive forces in the plane of the slab. These forces significantly enhance the stiffness, cracking resistance, and ultimate flexural resistance of the slab. However, strength and behavior rapidly deteriorate beyond a critical deflection. Cracking increases and the resistance decreases to a level very near that indicated by simple yield-line theory. Thereafter, resistance increases with deflection as the in-plane forces change from compression to tension near the central region of the slab. This deterioration in strength and behavior should not prohibit the initial strength and behavior from being utilized to resist a one-time dynamic load. Neither should it prohibit the entire strain energy capacity of the slab from being utilized to resist short-duration loads.

6. Air pressure leaked through the slab at center deflections slightly less than the secondary deflection, z_s, which corresponds to the valley in the static resistance function. The value of z_s can be approximated from Equation 21.

7. Any increase in static ultimate flexural resistance from longitudinal edge restraint provides an equivalent increase in the dynamic load capacity of the slab. For example, a slab with an enhancement factor of 2.5 can safely resist a peak dynamic load which is 2.5 times greater than the dynamic load capacity of the same slab with no longitudinal restraint. If this additional load carrying capacity is available, it can be utilized in the design of slabs to resist a one-time dynamic load. Utilizing the effects of longitudinal restraint could prove very economical in blast resistant design, particularly for large ratios of peak dynamic load to static working load.

8. The flexural resistance function can be calculated from the expressions summarized in Figure 39.

9 The response chart in Figure 36 will predict with reasonable accuracy the peak dynamic load required to produce a given dynamic deflection at the center of a longitudinally restrained slab.

10. A longitudinally restrained slab will collapse under a peak dynamic load greater than approximately 81% of the *dynamic* ultimate flexural resistance. If the dynamic increase factor (DIF) is 1.40, the required peak dynamic load to cause failure is 14% greater than the *static* ultimate flexural resistance.

Ruptured Bars at Support (Typical)

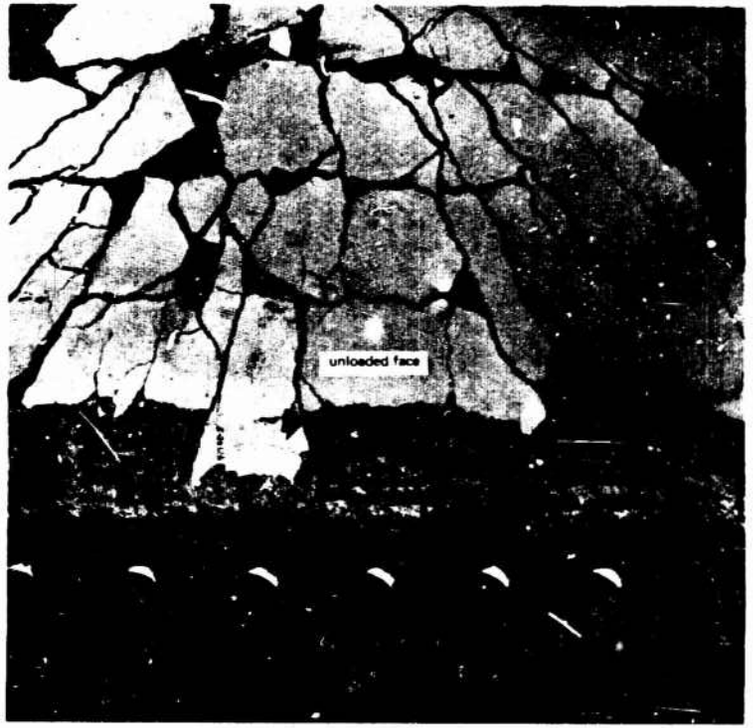

Disintegrated Concrete at Support (Typical)

Figure F-13. Slab 4.75D2-5 with ruptured bars and disintegrated concrete at supports.

LIST OF SYMBOLS

Note: When the letter **d** is added as a subscript to a symbol it refers to a section on the diagonal of the slab; the letter **e** as a subscript refers to a section on the edge of the slab.

A_s — Area of tension reinforcement per unit width of slab (in.^{2}/in.)

A_s' — Area of compression reinforcement per unit width of slab (in.^{2}/in.)

A_v — Area of shear reinforcement per unit width of slab (in.^{2}/in.)

a — Acceleration (in./msec^2)

a_m — Maximum acceleration (in./msec^2)

c — Distance from compression edge of slab to neutral axis (in.)

c_b — Distance from compression edge of slab to neutral axis at simultaneous yielding of tension steel and crushing of concrete (in.)

DIF — q_{ud}/q_u, dynamic increase factor

d — Distance from compression edge of slab to centroid of tension reinforcement (in.)

d' — Distance from compression edge of slab to centroid of compression reinforcement (in.)

E — Strain energy (in. lb/in.^{2})

E_c — Tangent modulus of elasticity of concrete (psi)

E_s — Modulus of elasticity of reinforcing steel (psi)

f_c — Stress in concrete (psi)

f_c' — Static compressive strength of 6 x 12-inch concrete cylinder (psi)

f_c'' — $0.85 f_c'$ = compressive strength of concrete in flexure[3] (psi)

f_{cd}' — Dynamic compressive strength of [illegible] concrete cylinder (psi)

f_s — Stress in tension reinforcement (ps

f_s' — Stress in compression reinforcemer

f_t' — Tensile strength of concrete (psi)

f_u — Static ultimate strength of reinforc

f_y — Static yield strength of reinforcem

f_{yd} — Dynamic yield strength of reinforc

g — Gravitational acceleration, 32.16 f

h — Distance from extreme fiber to pla tensile stress in concrete equals f_t' (

I_c — Moment of inertia of a cracked rei concrete section per unit width of

I_g — Moment of inertia of an uncracked unit width of slab (in.^{4}/in.)

K_{LM} — Load-mass factor

k — Constant

k_1 — Ratio of average compressive stress (f_c'') in concrete

k_2 — Coefficient defining fraction of th from the extreme fiber to the resul the concrete

k_{fc} — Elastic stiffness at center of square edges and cracked section (psi/in.)

k_{fg} — Elastic stiffness at center of square edges and uncracked section (psi/i

k_{sc} — Elastic stiffness at center of square simple edges and cracked section (p

k_{sg} — Elastic stiffness at center of square simple edges and uncracked sectior

f'_{cd} Dynamic compressive strength of 6 x 12 inch concrete cylinder (psi)

f_s Stress in tension reinforcement (psi)

f'_s Stress in compression reinforcement (psi)

f'_t Tensile strength of concrete (psi)

f_u Static ultimate strength of reinforcement (psi)

f_y Static yield strength of reinforcement (psi)

f_{yd} Dynamic yield strength of reinforcement (psi)

g Gravitational acceleration, 32.16 ft/sec^2

h Distance from extreme fiber to plane where tensile stress in concrete equals f'_t (in.)

I_c Moment of inertia of a cracked reinforced concrete section per unit width of slab (in.^{4}/in.)

I_g Moment of inertia of an uncracked section per unit width of slab (in.^{4}/in.)

K_{LM} Load-mass factor

k Constant

k_1 Ratio of average compressive stress to peak stress (f''_c) in concrete

k_2 Coefficient defining fraction of the depth measured from the extreme fiber to the resultant force in the concrete

k_{fc} Elastic stiffness at center of square slab with fixed edges and cracked section (psi/in.)

k_{fg} Elastic stiffness at center of square slab with fixed edges and uncracked section (psi/in.)

k_{sc} Elastic stiffness at center of square slab with simple edges and cracked section (psi/in.)

k_{sg} Elastic stiffness at center of square slab with simple edges and uncracked section (psi/in.)

L Clear span of slab (in.)

M Bending moment per unit width of slab (in.-lb/in.)

M_b Ultimate moment of all internal forces about mid-thickness of section at simultaneous yielding of tension reinforcement and crushing of concrete (lb/in.)

M_u Ultimate moment of all internal forces about mid-thickness of section (in.-lb/in.)

$\bar{M}_u$ Ultimate moment of all internal forces about mid-thickness of section under the average thrust acting along the span (in.-lb/in.)

M_y Ultimate moment of all internal forces about mid-thickness of section under zero thrust (in.-lb/in.)

m Unit mass (psi-msec^2/in.)

N Horizontal thrust per unit width of slab (lb/in.)

N_b Sum of all internal forces on section at simultaneous yielding of tension reinforcement and crushing of concrete (lb/in.)

N_u Sum of all internal forces on section at ultimate (lb/in.)

p A_s/d, ratio of tension reinforcement per unit width of slab (in.$^{-1}$); dynamic pressure (psi)

p' A'_s/d, ratio of compression reinforcement per unit width of slab (in.$^{-1}$)

p_b Ratio of tension reinforcement corresponding to $N_b = 0$ (in.$^{-1}$)

p_o Peak dynamic pressure (psi)

$(p_o)_{max}$ Peak dynamic load capacity (psi)

p_v A_v/s, ratio of vertical shear reinforcement per unit width of slab (in.$^{-1}$)

q $(p - p')\, f_y/f''_c$, reinforcing index, static flexural resistance of slab (psi)

$\bar{q}$	$(p f_s - p' f'_s)/f''_c$
q_c	Static flexural resistance of slab corresponding to first visible cracking in unloaded face (psi)
q_d	Dynamic flexural resistance of slab (psi)
q_s	Secondary resistance of slab (psi)
q_t	Tensile membrane resistance of slab (psi)
q_u	Static flexural resistance of slab at ultimate (psi)
q_{ud}	Dynamic flexural resistance of slab at ultimate (psi)
q_y	Static flexural resistance of slab for zero thrust (psi)
r	A_v/d, ratio shear reinforcement
s	Distance between reinforcing bars (in.); ratio of total horizontal edge movement to clear span
T	Duration of dynamic load (msec)
T_n	Effective natural period of vibration (msec)
T_{cr}	Critical load duration (msec)
t	Thickness of slab (in.); time (msec)
t_m	Time to maximum deflection (msec)
u	Deflection of slab along diagonal (in.)
v	Unit shear stress (psi)
v_u	Shear stress at ultimate (psi)
x	Length of slab strip measured from edge to diagonal of slab (in.)
y	Distance along slab edge measured from corner (in.)
z	Deflection at center of slab (in.)
z_m	Maximum deflection at center of slab (in.)
z_c	Deflection at center of slab corresponding to first visible cracking of concrete (in.)
z_s	Deflection at center of slab at secondary resistance (in.)
z_t	Deflection at center of slab at collapse of slab as a tensile membrane (in.)
z_u	Deflection at center of slab at ultimate (in.)
γ	Unit weight (lb/ft^3)
ϵ	Strain
$\dot{\epsilon}$	Strain rate (in./in./sec)
ϵ_c	Strain in concrete
ϵ_m	Maximum strain
ϵ_o	$2 f''_c/E_c$
ϵ_s	Strain in tension reinforcement
ϵ'_s	Strain in compression reinforcement
ϵ_u	Concrete crushing strain in flexure; ultimate strain of reinforcement
ϵ_y	Yield strain of reinforcement
μ	Poisson's ratio
ϕ	Slope of end portion of a slab strip (radians)

REFERENCES

1. E. Hognestad. "Yield-line theory for the ultimate flexural strength of reinforced concrete slabs," American Concrete Institute, Journal, Proceedings, vol. 49, no. 7, Mar. 1953, pp. 637-656.

2. K. W. Johansen. Yield-line theory. London, Cement and Concrete Association 1962.

3. A. Sawczuk. "Membrane action in flexure of rectangular plates with restrained edges," in Flexural mechanics of reinforced concrete; proceedings of the international symposium, Miami, Florida, Nov. 10-12, 1964. New York, American Society of Civil Engineers, 1965, pp. 347-358.

4. R. H. Wood. Plastic and elastic design of slabs and plates; with particular reference to reinforced concrete floor slabs. New York, Ronald Press, 1961.

5. R. Park. "Ultimate strength of rectangular concrete slabs under short-term uniform loading with edges restrained against lateral movement," Institution of Civil Engineers, Proceedings, vol. 28, June 1964, pp. 125-150. (Paper no. 6705)

6. Massachusetts Institute of Technology. School of Engineering. Technical Report R-65-25: Effect of membrance action on slab behavior, by J. F. Brotchie, A. Jacobson, and S. Okubo. Cambridge, Mass., Aug. 1965. (Contract NBy-32243) (AD 470747)

7. Newmark, Hansen and Associates. Report N596: Resistance and behavior of thick reinforced concrete slabs under static and dynamic loads (U), by W. L. Gamble, et al. Urbana, Ill., Feb. 1968. CONFIDENTIAL. (DASA 2061) (Contract DASA 01-67-C-0061) (AD 387433L)

8. C. H. Norris, et al. Structural design for dynamic loads. New York, McGraw-Hill, 1959.

9. Army Engineer Waterways Experiment Station. Technical Report no. 1-789: A dynamic ultimate strength study of simply supported two-way reinforced concrete slabs, by D. R. Denton. Vicksburg, Miss., July 1967. (Contract OCD-PS-65-44) (AD 658749)

10. A. Ingerslev. "The strength of rectangular slabs," Institution of Structural Engineers, Journal, vol. 1, 1923.

11. E. O. Pfrang, C. P. Siess and M. A. Sozen. "Load-moment-curvature characteristics of reinforced concrete cross sections," American Concrete Institute, Journal, Proceedings, vol. 61, no. 7, July 1964, pp. 763-778.

12. E. Hognestad. "Inelastic behavior in tests of eccentrically loaded short reinforced concrete columns," American Concrete Institute, Journal, Proceedings, vol. 49, no. 2, Oct. 1952, pp. 117-139.

13. American Concrete Institute. Committee 318. Building code requirements for reinforced concrete (ACI 318-63). Detroit, Mich., June 1963.

14. ACI-ASCE Committee 326. "Shear and diagonal tension," pts 1-3. American Concrete Institute, Journal, Proceedings, vol. 59, no. 1, Jan. 1962, pp. 1-30; no. 2, Feb. 1962, pp. 277-333; no. 3, Mar. 1962, pp. 353-395.

15. Naval Civil Engineering Laboratory. Technical Note 941: A versatile data tape system for static and dynamic tests, by R. H. Seabold. Port Hueneme, Calif., Jan. 1968.

16. S. Timoshenko and S. Woinowsky-Krieger. Theory of plates and shells, 2d ed. New York McGraw-Hill, 1959.

17. R. Park. "Tensile membrane behaviour of uniformly loaded rectangular reinforced concrete slabs with fully restrained edges," Magazine of Concrete Research, vol. 16, no. 46, Mar. 1964, pp. 39-44.

18. American Society of Civil Engineers. Committee on Structural Dynamics. Design of structures to resist nuclear weapons effects. New York, 1961. (ASCE manuals of engineering practice no. 42)

19. Naval Civil Engineering Laboratory. Technical Report R-395: Dynamic shear strength of reinforced concrete beams--Part I, by W. A. Keenan. Port Hueneme, Calif., Dec. 1965. (AD 627661)

20.————. Technical Report R-502: Dynamic shear strength of reinforced concrete beams—Part II, by R. H. Seabold. Port Hueneme, Calif., Jan. 1967. (AD 644823)

21.————. Technical Note N-905: Static versus dynamic testing of deep slabs (U), by S. K. Takahashi and J. R. Allgood. Port Hueneme, Calif., Aug. 1967. CONFIDENTIAL. (AD 383822L)

DISTRIBUTION LIST

SNDL Code	No. of Activities	Total Copies	
–	1	20	Defense Documentation Center
FKAIC	1	10	Naval Facilities Engineering Command
FKNI	13	13	NAVFAC Engineering Field Divisions
FKN5	9	9	Public Works Centers
FA25	1	1	Public Works Center
–	15	15	RDT&E Liaison Officers at NAVFAC Engineering Field Divisions and Construction Battalion Centers
–	295	295	NCEL Special Distribution List No. 2 for persons and government activities interested in reports on Atomic, Biological, and Chemical Defense

Unclassified
Security Classification

DOCUMENT CONTROL DATA - R & D

(Security classification of title, body of abstract and indexing annotation must be entered when the overall report is classified)

1. ORIGINATING ACTIVITY (Corporate author) Naval Civil Engineering Laboratory Port Hueneme, California 93041	2a. REPORT SECURITY CLASSIFICATION Unclassified 2b. GROUP

3. REPORT TITLE

STRENGTH AND BEHAVIOR OF RESTRAINED REINFORCED CONCRETE SLABS UNDER STATIC AND DYNAMIC LOADINGS

4. DESCRIPTIVE NOTES (Type of report and inclusive dates)
Final; July 1964—March 1967

5. AUTHOR(S) (First name, middle initial, last name)
W. A. Keenan

6. REPORT DATE	7a. TOTAL NO. OF PAGES	7b. NO. OF REFS
April 1969	131	21

8a. CONTRACT OR GRANT NO. DASA-RSS3318 b. PROJECT NO. Y-F008-08-02-123 c. d.	9a. ORIGINATOR'S REPORT NUMBER(S) R-621 9b. OTHER REPORT NO(S) (Any other numbers that may be assigned this report)

10. DISTRIBUTION STATEMENT

This document has been approved for public release and sale; its distribution is unlimited.

11. SUPPLEMENTARY NOTES	12. SPONSORING MILITARY ACTIVITY
	Defense Atomic Support Agency Washington, D. C.

13. ABSTRACT

Two studies, one theoretical, the other experimental are reported. The strength and behavior of restrained reinforced concrete slabs were investigated under both static and dynamic loads. Nine 6-foot-square slabs were tested: six under uniform static pressure and three under long-duration dynamic loads. Steel reinforcement ranged from zero to 1.33 percent. The slabs failed initially in a flexural mode, followed by total collapse at a much greater deflection. The thinner slabs deflected more than 2.5 times their thickness under both types of loading.

The theoretical study deals with a square slab, restrained against rotation and longitudinal movement at the edges. The study covers static resistance, failure criteria, size and extent of fragments, and design recommendations. An analytical method is developed to predict the static resistance, deflection, and longitudinal restraining thrust at ultimate failure.

The resistance and behavior of longitudinally restrained square slabs are predictable, and if properly designed can resist dynamic loads effectively and more economically than those with no longitudinal edge restraint.

DD FORM 1 NOV 65 1473 (PAGE 1)
S/N 0101-807-6801

Unclassified
Security Classification

14 KEY WORDS	LINK A		LINK B		LINK C	
	ROLE	WT	ROLE	WT	ROLE	WT
Concrete						
Slabs						
Longitudinal edge restraints						
Flexural strength						
Static resistance						
Dynamic resistance						
Deflection						
Analytical prediction method						
Design recommendations						